Chromatic detection from cone photoreceptors to individual V1 neurons to behavior in macaque monkeys

Charles A Hass

A dissertation
Submitted in partial fulfillment of the
Requirements of the degree of

Doctor of philosophy

University of Washington 2013

Reading committee:
Gregory D Horwitz, Chair
Fred Rieke
Anitha Pasupathy

Program authorized to offer degree:
Neurobiology and Behavior

Abstract

Chromatic detection from cone photoreceptors to individual V1 neurons to behavior in macaque monkeys

Charles A Hass

Gregory D Horwitz, Chair

Vision is the culmination of countless biophysical events from the initial stages of sensory transduction to conscious perception. Despite the complexity of this process, our brains encode the visual world effortlessly in only a few hundred milliseconds. Color is a particularly salient visual cue yet we know relatively little about how color is encoded by neurons in the neocortex. Using a combination of neurophysiological, psychophysical, and theoretical approaches we investigated the role of neurons in the primary visual cortex (V1) in chromatic contrast detection in macaque monkeys. We recorded extracellularly from individual V1 neurons and tested the hypothesis that V1 neurons behave as the linear cardinal mechanisms at the observer's detection threshold. Although many neurons in V1 were active at detection threshold, we found that their responses were inconsistent with the cardinal mechanisms model. A subset of these neurons were responsive to both cardinal colors at detection threshold indicating that some V1 neurons are very broadly tuned to color even in response to low-contrast stimuli. Next, we investigated two sources of noise that affect the detectability of chromatic stimuli: eye-movements and noise in the phototransduction cascade. Monkeys made low amplitude (<1º) saccades (microsaccades) while performing a detection task that suppressed their ability to see low spatial frequency achromatic (but not red-green isoluminant) stimuli. An analysis of saccade-triggered responses revealed that cone-opponent and non-opponent V1 neurons are both modulated by microsaccades, suggesting the the locus of the differential behavioral effect on achromatic and isoluminant stimuli is downstream of V1. Lastly, we created a model of stimulus transduction in the cone outer segments to

compare the sensitivity of individual V1 neurons and behaving monkeys to the limits imposed by phototransduction in the cones. We found that the temporal frequency dependence of the monkey's contrast sensitivity to red-green isoluminant (but not luminance) modulations followed closely the frequency dependence of signal processing in the cones. The shape of the temporal contrast sensitivity function can be explained almost entirely by the deterministic component of the modeled cone responses; noise in the phototransduction cascade made only minor contributions.

Table of Contents

Acknowledgements

This dissertation reflects the work of many people. The experiments were conducted in collaboration with my advisor, Greg Horwitz, and my colleagues, Juan Anguyera and Zack Lindbloom-Brown. Elise Grover and Leah Tait provided countless hours of technical expertise and experimental assistance throughout my tenure as a graduate student. This work was financially supported by a variety of sources including the UW's Neurobiology Training Grant and by the ARCS foundation, whose commitment to funding graduate student research was a key factor to my progress at UW.

I am particularly grateful to my committee members – Fred Rieke, Anitha Pasupathy, Mike Shadlen, and Geoff Boynton – for their efforts in developing my intellectual capacities as a neurophysiologist. At times, their efforts served to expose my weaknesses and challenge my assumptions. On other occasions, they provided invaluable feedback on project ideas and preliminary drafts of manuscripts. Regardless of the circumstance, their efforts were directed towards the goal of improving my capacities as a scientist, and I hope that this dialog can continue in the future.

I would also like to thank the friends I have made during my time at UW: Stephanie Furrer, Mike Famulare, Melissa Caras, Shin Kira, Kevin Oishi, Adrienne Mueller, Grant Storey, and many others. Our conversations have pushed me to be more rigorous in my own work while expanding my understanding of neurobiology well beyond the cortical mechanisms underlying color vision.

Lastly, I would like to thank my advisor, Greg Horwitz. His commitment to well crafted arguments, his knack for thoughtful quantitative analyses, and his dedication to the members of his lab have been truly impressive. I have tried my best to emulate these skills while in his lab, and I will continue this endeavor in the future.

Introduction

An enduring goal of neurophysiological research is to understand how physical stimuli in the environment are transduced into neural signals and how these signals are related to the behavior of the observer. Vision remains a premiere model system in this endeavor for several reasons: light is easy to control in experimental settings, many of the neuronal structures responsible for vision are accessible to experimentation, and countless behaviors depend on the visual system. Modern investigations typically follow one of two complementary approaches: psychophysics and neurophysiology. Psychophysicists infer a set of theoretical "mechanisms" that parsimoniously explain a body of behavioral data, whereas neurophysiologists measure the neuronal responses that are presumably the biological basis of these mechanisms. Forging links between these two bodies of work has greatly improved our understanding of signal processing for several sensory modalities (Britten et al. 1992; Geisler and Albrecht 1997; Palmer et al. 2007; Yang and Shadlen 2007; Rinberg et al. 2006; Romo et al. 2002)

Our understanding of visual perception has also benefited from theoretical studies that seek to explain perceptual phenomena in terms of the underlying neurophysiology using a concise mathematical framework. Quantitative models can make predictions that are experimentally testable, and thus provide an important intermediary between psychophysical and neurophysiological studies. Moreover, theoretical studies have the ability to investigate the relationships among biophysical phenomena that would be impossible to dissociate in a real experiment (Soltani and Wang 2009; Wright and Calabrese 2011; Rule et al. 2011).

Research on chromatic contrast detection actively engages all three of these disciplines. Chromatic detection has a rich history of psychophysical investigations (Andersen and Finlayson 2010), and color vision was among the first visual submodalities studied neurophysiologically (Svaetichin 1956; Motokawa et al. 1962; Hubel and Wiesel 1968). This dissertation uses a combination of neurophysiological, psychophysical, and theoretical approaches to investigate chromatic detection in the primate visual system. The principal aims of this research are to:

1. To test the hypothesis that individual V1 neurons act as the neural substrate for the cardinal mechanisms of chromatic detection.
2. Understand behavioral and neuronal sensitivity in terms of the limits of performance set by signal transduction in the cone photoreceptors.
3. Understand how behavioral and neuronal sensitivity to chromatic stimuli are affected by fixational eye movements

Behavioral measurements as a method to understand visual signal processing

Sensory signals are transduced by the primary receptors and are transmitted to the brain, which acts on these signals to guide behavior. Despite this multistep process, a careful analysis of certain behaviors can provide a window into the computations performed at different levels of the neural circuit. Perhaps the best example of this comes from Maxwell's use of the color matching task to prove trichromacy in humans. At the time of Maxwell's experiment, it was well understood that light could be subdivided into different components each associated with a different hue, but it was unknown how light is transduced by the eye and how many transduction elements are required. Thomas Young (1802) and Herman von Helmholtz (1852) had both hypothesized that normal human vision requires three transducers, but neither accounts provided direct quantitative evidence.

Maxwell's approach combined careful empirical observations grounded in a quantitative theoretical framework to prove the trichromatic theory. His subjects viewed an apparatus that produced a bipartite field: half of the field was illuminated by a "test" stimulus, and the other half was illuminated by the superposition of a set of "primary" lights. The subject's task was to adjust the radiance of the primary lights such that the two halves of the bipartite field appeared identical. Maxwell's critical observation was that, for color-normal subjects, any monochromatic test light could be matched in appearance by a linear combination of exactly three primary lights (Maxwell 1860). This suggested that three broadly tuned transduction elements were sufficient to mediate color vision: subjects with four transduction elements would have required an additional primary light to accomplish the task, and subjects with two transduction elements would have reported multiple combinations of three primaries that all produce matches to the test.

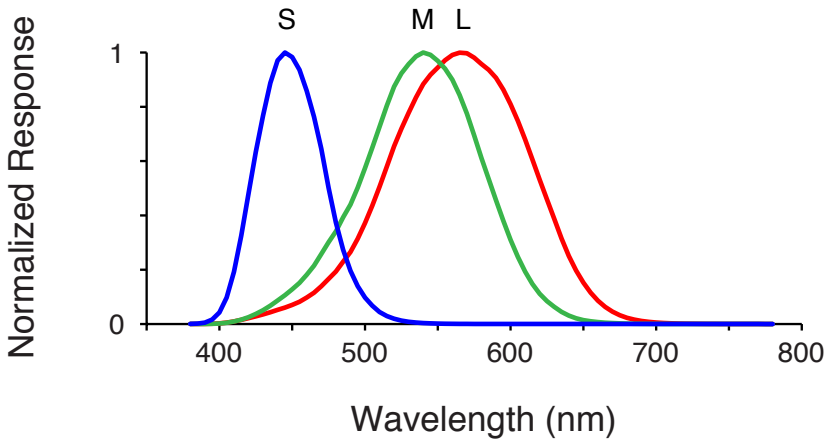

Figure 1.1 Corneal cone fundamentals for the cone photoreceptors as derived by Stockman et al. (1993).

We now know that the three transduction elements correspond to the cone photoreceptors of the retina. The cone photoreceptors convert light into neural signals by virtue of a light sensitive pigment, and the spectral sensitivity of the photopigments are unique to each cone type. By combining color-matching data from color-normal and color-blind subjects, various estimates of the cone spectral sensitivities have been developed (De Vries 1948; Vos and Walraven 1971; Smith and Pokorny 1975; Stockman et al. 1993). The spectral sensitivities of the cone photopigments peak at different locations in the visible spectrum (Figure 1.1), and the three cone types are named for the portion of the spectrum to which they are maximally sensitive: the short- middle-, and long-wavelength sensitive cones (L-, M-, and S-cones for short). Electrophysiological measurements from cone photoreceptors in macaque monkeys (Baylor et al. 1987) confirm the cone sensitivity functions measured psychophysically in humans.

The fact that color-matching functions can be linearly transformed into the spectral sensitivities of the cone photoreceptors (Andersen and Finlayson 2010) remains an impressive accomplishment that lends credibility to the use of behavioral measurements in elucidating the function of neural circuits. On the other hand, neither the color-matching functions nor the cone fundamentals are sufficient to explain all aspects of color perception. For example the color-matching functions only tell you when two lights are indistinguishable – not what they look like or how easily they are detected. Likewise, the

'principle of univariance' states that the response of a cone depends on the number of photons absorbed but not on the type of photon (Rushton 1972). The consequence of univariance is that signals from different cone types must be compared for an observer to distinguish lights on the basis of their spectra. The number and physiological properties of the post-receptoral mechanisms that implement this cone signal comparison remains a focal point of color vision research.

Psychophysical investigations of post-receptoral color mechanisms

Psychophysical experiments, which attempt to quantify the limits of perception, have been instrumental in developing mechanistic theories of the post-receptoral signal processing involved in color vision. Of all the psychophysical methods, detection tasks have been particularly useful. In a typical experiment, observers are asked to detect a visual stimulus amidst an otherwise neutral background. For example, in a spatial two alternative forced choice (2AFC) detection task, a visual stimulus is presented in one of two locations on a visual display and the observer's task is to determine which location contains the stimulus. The intensity of the stimulus necessary to support a criterion level of performance is taken as an estimate of the observer's threshold for detection.

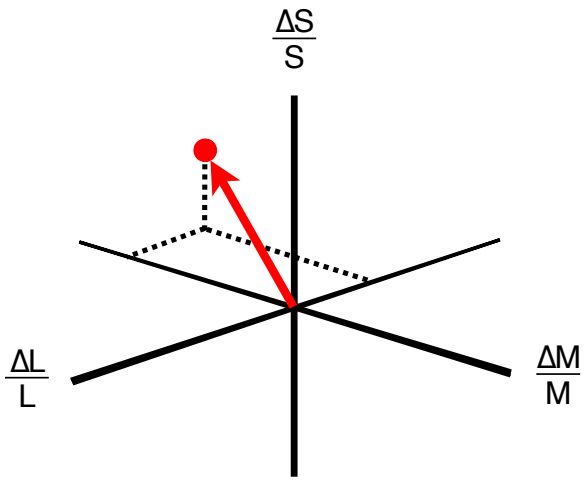

Figure 1.2 L, M, S-cone contrast space. The origin of the space corresponds to the adapting field of the visual display. The chromaticity of a stimulus can be represented a point in the space or as vector.

The utility of chromatic detection tasks is multifaceted. First, performance on detection tasks is consistent from session to session, which is important for investigations that rely on data collected over the course of several months. Second, detection psychophysics is affiliated with the strong theoretical framework of signal processing (Green and Swets 1966). Third, the hallmark of color vision – the ability to distinguish lights on the basis of their spectra – is conserved at detection threshold (Rollman and Nachmias 1972; Mullen and Kulikowski 1990).

Chromatic stimuli used in detection experiments can be defined by their effects on the cone photoreceptors. Defining stimuli in terms of 'cone contrast' is currently common practice due to the fact that cone photoreceptors exhibit Weber adaptation at high background intensities (Schneeweis and Schnapf 1999). A consequence of Weber adaptation is that inputs to cone photoreceptors are normalized by the mean light intensity. Thus, the output of cone photoreceptors encodes contrast rather than absolute light level. Psychophysical detection thresholds (in units of cone excitation) depend on the intensity and spectral characteristics of the background (Whittle and Challands 1969; Sigel and Pugh Jr 1980) but are less dependent on these factors when stimulus intensity is defined in contrast units.

A color space defined by cone contrast is illustrated by Figure 1.2. The origin of this space represents the adapting field of the display, and the three basis vectors represents modulations of the three cone types. Individual stimuli can be represented as points or equivalently, as vectors emanating from the origin. The distance of a point from the origin (or the length of the vector) represents the stimulus intensity. The position of the point (or the orientation of the vector) specifies the relative amounts with which the stimulus affects the three different cone types. For example, a point that lies on one of the axes corresponds to a light that modulates one of the cone types but does not affect the others, whereas a point in the interior of one of the octants corresponds to a stimulus that affects all three cone types.

If stimulus detection occurs when the activity in any of the three cone types exceeds a threshold, then the locus of points that are equally detectable should lie on a surface whose principal axes are aligned to the cone isolating color directions. If signals from the cone photoreceptors are processed independently, then the isodetection surface will be a

rectangular prism. If the cone signals interact via probability summation prior to the decision stage (Graham 1977), then the isodetection surface can take on the more rounded appearance of a superquadratic surface. If the signal-to-noise properties of the three cone types are identical, then the distention of the isodetection surface should be predicted by the relative proportions of each cone type on the retinal mosaic.

Detection experiments in humans, however, do not support this prediction. Figure 1.3 A shows detection thresholds for a human observer in response to stimuli that lie in a plane spanned by the L- and M-cone isolating axes. The isodetection contour is maximally distended in the L+M direction and minimally distended in the L–M direction. Similarly, for stimuli in the plane spanned by the S-cone and L+M color directions, the isodetection contour is maximally distended in the L+M+S color direction (Figure 1.3 B). These data suggest that signals from the cone photoreceptors do not form the signal-processing bottleneck for visual detection under these spatiotemporal conditions. Nevertheless, the shape of the detection contours provide clues to the identity and number of the post-receptoral mechanisms that are important for color vision.

If a group of stimuli are detected by the same visual mechanism, then there should exist a scaling of their intensities such that they are equally detectable. This hypothesis predicts that detection contours can be decomposed into groups of stimuli detected by the same mechanism. For example, a linear mechanism responds identically to stimuli that lie on a line perpendicular to the mechanism vector: these stimuli all have the same projection onto the mechanism vector.

Several experiments demonstrate that detection contours for stimuli of low spatial and temporal frequencies are approximately piecewise linear (Cole et al. 1993; Sankeralli and Mullen 1996). These experiments suggest the existence of three post-receptoral visual mechanisms, and the slope of each segment of the detection contour was used to estimate the cone inputs to each of the three mechanisms (Figure 1.3). One mechanism receives opposed inputs from the L- and M-cones. The second receives strong inputs from the S-cones opposed to the sum of L- and M-cones (S–[L+M]). The third receives summed input from the L- and M-cones (L+M). By convention, these three mechanisms are referred to as the Red-Green (RG), Blue-Yellow (BY), and Luminance (LUM) mechanisms respectively.

Isodetection surfaces in 3D space can be used to estimate the cone inputs to the post-receptoral detection mechanisms, but the strength of this approach depends on the functional form of the best fitting isodetection surface. When ellipsoids are used to fit the data, their principal axes are taken as estimates of the cone inputs to the detection mechanisms. But because ellipsoids can be transformed into spheres (by linear transformations of the cone contrast axes), identifying the post-receptoral mechanisms using this approach can be problematic (Poirson et al. 1990). Discriminating an ellipsoid from a superquadratic on the basis of noisy data can be challenging, and the best-fitting isodetection surface is still a matter of debate (Cole et al. 1993; Sankeralli and Mullen 1996; Poirson et al. 1990).

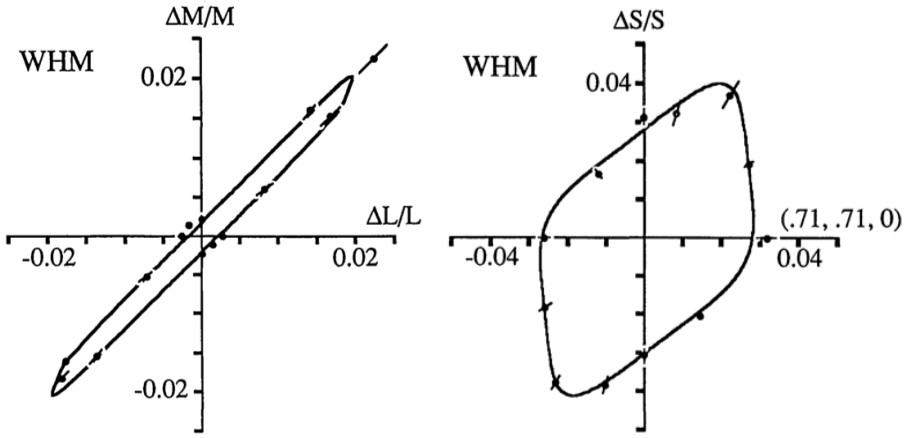

Figure 1.3 Isodetection contours in the L/M plane (left) and in the S vs. L+M plane (right). Detection thresholds (black points) were fit with an isodetection surface that assumes 3 statistically independent visual mechanisms that interact via probability summation. Used with permission from Cole et al. (1993).

The importance of RG and BY post-receptoral channels is supported by a seminal experiment by Krauskopf et al., (1982), who used a habituation technique to probe the identity of the post-receptoral mechanisms. Their experiment considered test stimuli that lie in the plane spanned by the S-cone isolating, and the L–M color directions (Figure 1.4). They hypothesized that detection of stimuli in this subspace is mediated by the RG and BY mechanisms exclusively, and they tested this hypothesis by habituating the observer using high contrast stimuli. Their critical finding was that a habituating stimulus

modulating along the L–M color direction increased thresholds for stimuli near the L–M axis but did not change thresholds for stimuli near the S-cone isolating axis. The reverse held true for a habituating stimuli modulated along the S-cone isolating axis. Habituating stimuli modulated along intermediate color directions affected both the RG and BY mechanisms and raised thresholds for all stimuli in this space. This suggested that the RG and BY mechanisms were independent of each other. Importantly, the effect of habituation was not due to adaptation in the cone photoreceptors: a habituating stimulus along the L+M color direction did not elevate thresholds for L–M test stimuli despite the fact that the habituator and the test stimulus both modulate the same cone types.

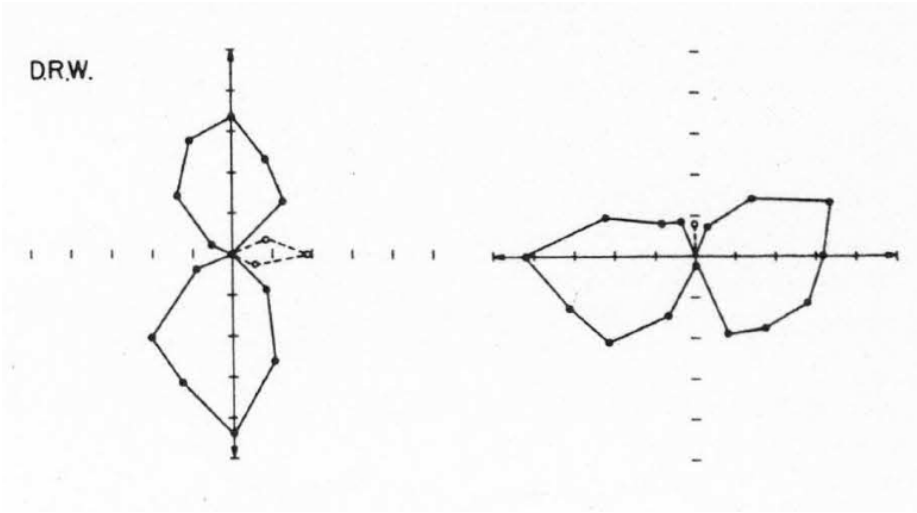

Figure 1.4 Habituation reveals the cardinal color mechanisms. Black points represent the elevation in threshold following habituation to the color direction indicated by the solid arrow. Notice that habituation does not increase thresholds for the orthogonal color directions. Used with permission from Krauskopf et al. (1982).

In summary, psychophysical detection tasks suggest the existence of three post-receptoral visual mechanisms that combine signals from the cone photoreceptors. The RG and BY mechanisms receive antagonistic inputs from different cone types and are thus chromatically selective. The RG and BY mechanisms are known as the 'cardinal mechanisms' and their hypothesized afferent inputs are illustrated in Figure 1.5. This wiring scheme is supported by several other psychophysical studies: Color matching ellipses in CIE space are distended maximally along the S-cone axis and minimally along the L–M color direction (LeGrand 1949; Nagy et al. 1987). Thresholds measured in the

context of noise masking along a cardinal direction are elevated for stimuli near the habituating stimulus but not for the stimuli near the orthogonal cardinal color direction. For non-cardinal habituating lights, thresholds are elevated for all test directions (Eskew et al. 2001; Giulianini and Eskew 1998; Sankeralli and Mullen 1997). Motion coherence experiments (Krauskopf and Farell 1990) demonstrate that the superposition of two drifting sinusoids appear to combine into a coherent percept when the component sinusoids are each a cardinal color, but do not cohere when the component sinusoids are each an intermediate color. How these post-receptoral mechanisms may be instantiated by neural circuits is an issue I turn to next.

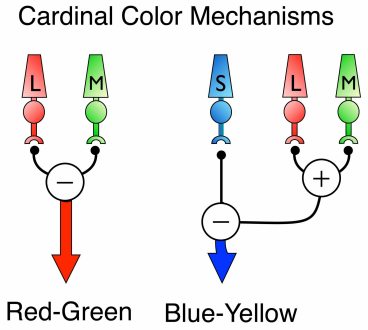

Figure 1.5 The presumed cone inputs to the RG and BY cardinal color mechanisms.

Visual stimulus tuning of neurons in the retina and thalamus

Electrophysiological recordings from individual cone photoreceptors from monkeys have largely confirmed the spectral sensitivities derived psychophysically in humans (Baylor et al. 1987). The photocurrent induced by a visual stimulus is related to the number of photons absorbed and not strictly to the type of photon (Baylor et al. 1987), confirming the principle of univariance. Although signals in the cone outer segments are considered independent from cone to cone, the signals are mixed beginning at the cone pedicles via gap junctions (Hornstein et al. 2004) and synapses with horizontal cells (Verweij et al. 2003), which form a substrate for center surround inhibition characteristic of retinal ganglion cell (RGC) receptive fields.

The lateral connectivity that gives rise to center surround spatial antagonism can also give rise to the *spectral* opponency critical for color perception. Retinal ganglion cells, whose axons form the efferent projection of the retina, receive inputs from the cone

photoreceptors via the circuitry of the inner and outer plexiform layers. If the net effect of this circuitry is to excite the RGC when one type cone photoreceptor is activated and to suppress the RGC when a different type of cone is activated, then the RGC will be spectrally opponent. Interestingly, the color-tuning of spectrally opponent RGCs is consistent with cardinal mechanisms: midget retinal ganglion cells receive antagonist inputs from the L- and M-cones (Sun et al. 2006; Field et al. 2010) via horizontal-cell inhibitory feedback (Crook et al. 2011). Red-green opponency among midget RGCs need not require spectrally pure center or surround components: mismatches in the L:M cone ratio between center and surround confers red-green spectral opponency (Crook et al. 2011). Small-bistratified ganglion cells receive strong S-cone inputs in opposition to the the L- and M-cones (Dacey and Lee 1994; Field et al. 2007). Cone opponency in small-bistratified cells appears to be mediated in part by horizontal cell inputs to S-cones, and in part by LM OFF diffuse cone bipolar cells (Crook et al. 2009).

Axons from RGCs travel to the lateral geniculate nucleus (LGN) of the thalamus where they synapse in specific laminae. Parasol RGCs primarily project to the magnocellular layers of the LGN (layers 1 & 2). Midget RGCs synapse in the parvocelluar layers (layers 3 to 6). Small-bistratified RGCs project primarily to the inter-laminar zones but also to the parvocellular and magnocellular layers (Wiesel and Hubel 1966; Kaas et al. 1978; Schiller and Malpeli 1978; Hubel and Livingstone 1990; Martin et al. 1997; Hendry and Reid 2000). The receptive field substructure for LGN cells is similar to their RGC inputs: many LGN cells have a center surround organization (Reid and Shapley 2002), although some cells types exhibit other types of substructure (Wiesel and Hubel 1966; De Monasterio and Gouras 1975) and the degree of spatial antagonism can depend on the color of the stimulus (Derrington et al. 1984). Like RGCs, LGN neurons appear to respond maximally in either the L–M (parvocellular) or S-cone (koniocellular) color directions (Derrington et al. 1984; De Valois et al. 2000; Reid and Shapley 2002; but seeTailby et al. 2008b). Contrast adaptation among parvocellular and koniocellular LGN cells appears to be minimal (Solomon et al. 2004a; Tailby et al. 2008b), and the color tuning of these neurons in response to low-spatial frequency drifting sinusoidal gratings is well predicted by a linear combination of cone inputs (Derrington et al. 1984; De Valois et al. 2000).

Stimulus tuning of neurons in the primary visual cortex

Neurons in the LGN project their axons to the thamo-recipient layers of the primary visual cortex in a cell-type specific manner: magnocellular neurons project to layer 4Cα, parvocellular neurons project to layer 4Cβ, and koniocellular neurons project to the upper layers of 4A and the lower portions of layer 2/3 (Hendry and Yoshioka 1994; Chatterjee and Callaway 2003). Signals from distinct LGN channels converge onto individual V1 neurons (Malpeli et al. 1981) and transform the spatial representation of visual stimuli. V1 neurons can be tightly tuned to orientation and spatial frequency (Hubel and Wiesel 1962; Hubel and Wiesel 1968), and some neurons elicit responses that are invariant to the spatial phase of a sinusoidal grating (Hubel and Wiesel 1962; Johnson et al. 2001). V1 neurons thus appear to act as localized spatio-temporal contrast filters (Movshon et al. 1978b; Movshon et al. 1978a; Rust et al. 2005; Touryan et al. 2002). On the other hand, V1 neurons receive modulatory inputs that often affect the responses to stimuli presented in the classical receptive field (Cavanaugh et al. 2002; Shushruth et al. 2012; Henry et al. 2013).

The spectral sensitivity of V1 neurons have been actively investigated starting with the first recordings from primate visual cortex (Motokawa et al. 1962; Hubel and Wiesel 1968). These initial experiments focused on measuring the responses of V1 neurons to monochromatic stimuli and compared color tuning, orientation tuning, and laminar position. These studies suggested that chromatically selective V1 neurons are rare outside the central 2º of vision (Zeki 1983), that the majority of neurons in layer 4Cβ are poorly tuned for orientation but exhibit center surround color antagonism (Gouras 1974; Zeki 1983; Hubel and Wiesel 1968; Livingstone and Hubel 1984) and that the majority of neurons in the cytochrome oxidase (CO) blobs of layer 2/3 are non-orientation tuned, double-opponent neurons with little response to diffuse white light (Livingstone and Hubel 1984).

Cytochrome oxidase blobs are anatomical sub-compartments within V1 that are thought to be specialized for color vision, but their importance in this regard remains contentious. Livingstone and Hubel (1988) contended, that because depth perception and motion discrimination are poor for isoluminant stimuli, color is processed independently

of other visual sub-modalities. The idea that color is processed in the blobs was supported by observations that CO blobs contain neurons that are selective to particular color directions (Ts'o and Gilbert 1988; Chatterjee et al. 2008) but are poorly orientation tuned (Livingstone and Hubel 1984; Ts'o and Gilbert 1988; Yoshioka and Dow 1996). Moreover, CO blobs receive cone opponent inputs from parvocellular (via layer 4Cβ) and koniocellular LGN (Hendry and Yoshioka 1994). Other studies dispute the functional specificity of neurons in the CO blobs: Neurons in CO blob and inter-blob regions have similar spatial frequency selectivities (Edwards et al. 1995; Engbert and Kliegl 2003) and orientation tuning bandwidths (Economides et al. 2011; O'Keefe et al. 1998) but may differ in their contrast sensitivity (Edwards et al. 1995; Economides et al. 2011).

The relationship between color and orientation tuning is also contentious. Lennie et al., (1990), like Livingstone and Hubel (1984), found that the few neurons that were responsive to color were often poorly tuned to orientation. On the other hand, many investigations find clear evidence for chromatically selective neurons that are also orientation and spatial frequency tuned (Johnson et al. 2001; Johnson et al. 2008; Conway 2001; Conway and Livingstone 2006). These experiments suggest that roughly 10-20% of V1 neurons respond preferentially to color (Johnson et al. 2001; Conway 2001; Solomon and Lennie 2005). These cells tend not to be orientation tuned. 30-40% of neurons respond roughly equivalently to color and achromatic stimuli (Johnson et al. 2001; Solomon and Lennie 2005), and the remainder of neurons prefer achromatic modulations. Neurons in these two categories are usually orientation tuned (Johnson et al. 2008).

Discrepancies between V1 color tuning and the cardinal mechanisms

The color-tuning of neurons in the early visual system is consistent with the cone inputs to the psychophysically identified cardinal mechanisms. The midget type retinal ganglion cells and the parvocellular LGN neurons have the same cone inputs as the Red-Green cardinal mechanism, whereas the small-bistratified type retinal ganglion cells and the koniocellular LGN neurons have the same cone-inputs as the Blue-Yellow cardinal mechanism (Figure 1.6). The cone inputs to neurons in the front end of the visual system are thus consistent with the orientation of detection contours measured behaviorally.

Despite this consistency, V1 neurons do *not* exhibit color tuning functions that segregate naturally into RG and BY categories (Figure 1.6) (Lennie et al. 1990; Johnson et al. 2004; Horwitz et al. 2007; Solomon and Lennie 2005). This suggests that the cardinal-color framework is an inadequate descriptor of V1 color preferences. There thus appears to be a transformation of color representation from the LGN to the cortex which can be summarized by stating that the RG and BY pathways are segregated anatomically through the LGN but converge on to single neurons in the V1 such that their preferred colors do not conform to the cardinal mechanisms model.

This discrepancy presents a conundrum: if the color tuning of neurons in the early stages of the visual system are consistent with the behavioral output of the observer, why is the color tuning of V1 neurons inconstant with both? A major caveat to this discrepancy is that the majority of neurophysiological investigations of color in V1 have been conducted in anesthetized monkeys using high contrast stimuli whereas the psychophysical experiments that defined the cardinal mechanisms were conducted in awake humans using low contrast stimuli. This gives rise to the possibility that V1 neurons are tuned to the cardinal color directions at detection threshold but exhibit different color-tuning profiles at higher contrast. This is supported by the observation that color tuning in V1 is not strictly separable with contrast (Solomon and Lennie 2005), and various non-linearities in V1 color tuning to high contrast stimuli (Hanazawa et al. 2000; De Valois et al. 2000; Horwitz et al. 2005; Horwitz and Hass 2012) complicate extrapolations low contrast stimuli.

There are at least two possible explanations for how V1 neurons could be tuned to the cardinal colors at detection threshold but exhibit non-cardinal color tuning when tested with high contrast stimuli. The first possibility is that the subset of V1 neurons that are active at detection threshold are those that are tuned to the cardinal-color directions. Not all V1 neurons are active at detection threshold, and those that receive convergent input from parvo- and koniocellular LGN channels may be inactive at detection threshold. Another possibility is that, despite the convergence of parvo- and koniocellular inputs onto single V1 cells, only one of the thalamic inputs is active at detection threshold. This might be the case, for example, if the synaptic input from one thalamic source were weaker than the other. In summary, the color tuning of individual V1 neurons

appears inconsistent with the cardinal mechanisms model, but this inconsistency could be reconciled by measuring the color tuning of V1 neurons in the regime originally used to define the cardinal-mechanisms.

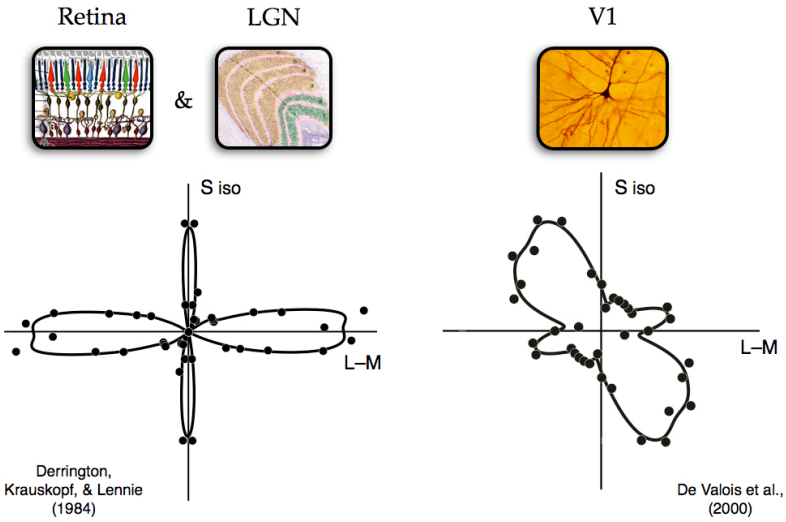

Figure 1.6 Color tuning of neurons in the retina, LGN, and V1 as assessed using high contrast stimuli. The lower panels are a population histogram of preferred color directions for the LGN (left) and V1 (right). Angle in this histogram signifies color and the eccentricity of each dot from the origin signifies the number of neurons tuned to that color. Retinal ganglion cells are not depicted but show a similar population color tuning as the LGN. The LGN data were replotted with permission from Derrington et al., (1984). V1 data were replotted with permission from De Valois et al., (2000).

Research aims

Aim 1: To determine if individual V1 neurons behave as the cardinal mechanisms at detection threshold by testing a specific prediction of the cardinal model. Chapter 2 will be devoted to this aim.

Aim 2: To determine how on-going motor commands (microsaccades) influence the stimulus-driven responses of V1 neurons, and influence the detectability of a chromatic stimulus. Chapter 3 will be devoted to this aim.

Aim 3: To determine the relationship between signal processing in the cone outer segments, the sensitivity of individual V1 neurons, and the sensitivity of macaque monkeys. Chapter 4 will be devoted to this aim.

V1 mechanisms underlying chromatic contrast detection

Understanding vision requires understanding the signal processing that supports visual detection. Visual detection is often investigated with two complementary approaches: psychophysics and neurophysiology. Psychophysicists infer a set of theoretical visual "mechanisms" that parsimoniously explain a body of behavioral data, whereas neurophysiologists measure the neuronal responses that are presumably the biological basis of these mechanisms. Forging links between these two bodies of work has greatly improved our understanding of signal processing in the visual system. For example, many aspects of achromatic contrast detection can be explained by the spatiotemporal contrast sensitivity of neurons in the primary visual cortex (V1) (Tolhurst et al. 1983; Geisler and Albrecht 1997; Boynton et al. 1999; Hawken and Parker 1990; Palmer et al. 2007). Whether the same is true for chromatic contrast detection is unknown.

Substantial psychophysical evidence supports the idea that chromatic detection is mediated by two cardinal mechanisms: a red-green mechanism that receives antagonistic signals from L- and M-cones, and a blue-yellow mechanism that receives strong S-cone input opposed to a combination of L- and M-cones (Cole et al. 1993; Sankeralli and Mullen 1996; Sankeralli and Mullen 1997; Krauskopf et al. 1982; LeGrand 1949; Nagy et al. 1987). Under the cardinal mechanisms model (Figure 2.1), stimulus modulations in the two mechanism-isolating directions are detected by distinct populations of neurons. Stimuli in intermediate color directions are detected by both populations, and could be detectable via probability summation even if neither population reaches detection threshold individually (Sachs et al. 1971; Graham 1977).

This chapter was published in The Journal of Neurophysiology, which maintains copyrights for this material, and has been reprinted with permission. The full citation for this publication is:
Hass, C.A., & Horwitz G.D. (2013). *V1 mechanisms underlying chromatic contrast detection.* The Journal of Neurophysiology. 109: 2483-94, 2013.

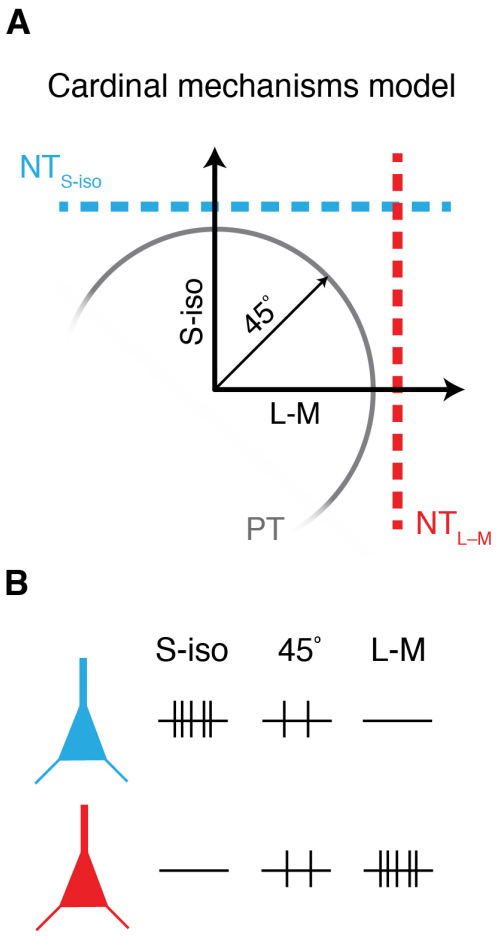

Figure 2.1 Relationship between neuronal and psychophysical detection thresholds under the cardinal mechanisms model. A: Under the cardinal mechanisms model, V1 neurons are tuned to either the L–M or S-cone isolating color direction. The response of a neuron to intermediate stimuli is determined by the projection of the stimulus onto its preferred cardinal color direction. Thus, neuronal detection thresholds (NT) can be represented by lines in the isoluminant plane (red and blue dashed lines for an L–M and S-cone tuned neuron, respectively). Psychophysical threshold (PT) is assumed to result from pooling across all responding neurons, and is lower than the neurometric threshold in either of the cardinal color directions. Due to probability summation, psychophysical thresholds trace out an arc in the interior of the square formed by the cardinal neurometric thresholds. B: Under the cardinal model, individual V1 neurons respond robustly to one of the two cardinal color directions but weakly to the intermediate color directions.

We asked whether signals measured in V1 at psychophysical detection threshold are consistent with the cardinal mechanisms model. Although V1 neurons are not tuned to the cardinal color directions when tested with high contrast stimuli (Lennie et al. 1990; Johnson et al. 2004; Krauskopf et al. 1996; Horwitz et al. 2007), the responses of V1 neurons have not previously been measured at chromatic detection threshold, and

nonlinearities in neuronal responses to high contrast stimuli complicate extrapolations to a low-contrast regime (Conway and Livingstone 2006; D'Zmura and Knoblauch 1998; Hanazawa et al. 2000; Solomon and Lennie 2005; Horwitz et al. 2005; Rucci and Desbordes 2003). The possibility remains that, near detection threshold, individual V1 neurons are preferentially sensitive to modulations in the cardinal color directions, as would be the case if only L–M or S-cone dominated LGN afferents were active at threshold. Such a result would indicate that chromatic detection is mediated by distinct populations of red-green and blue-yellow V1 neurons.

We recorded the responses of V1 neurons to near-threshold chromatic stimuli in awake behaving monkeys to test a prediction of the cardinal mechanisms model: responses of individual neurons to intermediate colors should be determined by the magnitude of the stimulus component in the preferred cardinal color direction. This was the case for only the minority of the V1 neurons we tested. Instead, we found a close relationship between the sensitivity of individual V1 neurons and the monkeys' behavioral sensitivity that generalized across cardinal and intermediate color directions. Additionally, using high contrast stimuli, we identified a population of neurons that responded preferentially to chromatic modulations and a population that was equally responsive to chromatic and luminance modulations. These populations were similarly sensitive to near-threshold chromatic modulations, a result that supports a role for jointly color-luminance tuned neurons in chromatic detection. We conclude that the chromatic contrast sensitivity of individual V1 neurons is well matched to that of the monkey, and that even at low contrasts, a privileged status for a set of cardinal color directions is not evident.

Materials and Methods

Animal preparation

Two female Macaca mullata participated in this study. Each monkey was surgically implanted with a stabilization head-post and scleral search coil. Neuronal recordings were obtained via surgically implanted recording chambers (Crist Instruments, MD) which were centered over the posterior occipital cortex adjacent to the longitudinal fissure.

Surgical procedures were performed under sterile conditions using isoflurane or sevoflurane anesthesia. Following surgery, monkeys were administered the following analgesics: buprenorphine (0.01-0.03 mg/kg BID for 2 days) and ketoprofen (5 mg/kg BID for 3 days). All animal procedures, including those related to surgery, housing, and behavioral training, were conducted in accordance with the National Institute of Health's Guide for Care and Use of Laboratory Animals as well as the University of Washington's Institutional Animal Care and Use Committee.

Behavioral task and stimuli

Monkeys were trained to perform the spatial two alternative forced choice (2AFC) detection task illustrated in Figure 2.2A. Monkeys viewed a computer monitor at a distance of 100 cm while seated in a primate chair in an otherwise dark room. Each trial began when the monkey fixed its gaze on a 0.1º black square located at the center of the monitor. Five hundred milliseconds later, a Gabor stimulus appeared in one of two mirror symmetric locations about the fixation point and disappeared after 666 ms. Following a brief delay (100 to 600 ms), the fixation point disappeared and two choice targets appeared. Choice targets were 0.2º black squares positioned between the fixation point and the two possible stimulus locations. Monkeys were given juice rewards for making an eye movement to the choice target located in the direction of the Gabor stimulus. No feedback was given for incorrect choices. All stimuli were presented binocularly. Trials were aborted if, at any time before the onset of the choice targets, the monkey's gaze deviated from an electronically defined 1º square window centered on the fixation point. Event timing and eye position monitoring was controlled by routines written in REX (Laboratory of Sensorimotor Research, National Eye Institute). Stimuli were generated using custom software written in Matlab (The MathWorks, MA) that used routines from the Psychophysics Toolbox (Brainard 1997).

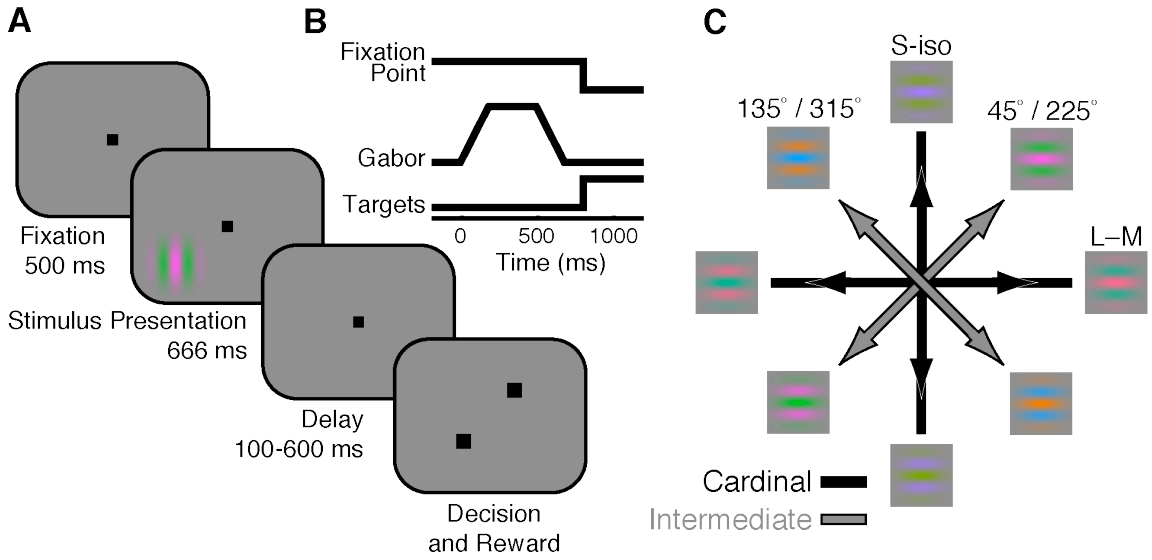

Figure 2.2. A: Display geometry B: Event timing of the chromatic contrast detection task. C: The four color directions represented as vectors in the isoluminant plane. For each neuron, only two color directions were tested during the detection task: the neuron's preferred cardinal and intermediate colors as identified during an initial characterization procedure.

To avoid high temporal-frequency cues, which might favor detection via luminance-tuned mechanisms, stimulus contrast ramped up and down smoothly (Wandell 1985). Contrast increased linearly for 167 ms, remained constant for 332 ms, and then decreased linearly for 167 ms (Figure 2.2B). The sinusoidal component of the Gabor stimulus drifted at 3 Hz, and the Gaussian envelope had a standard deviation of 0.4°. The orientation and spatial frequency of the Gabor stimulus were optimized for each neuron as described previously (Horwitz and Hass 2012). The time course, Gaussian envelope, and drift rate of the Gabor stimulus were held constant across all psychophysical and neurophysiological experiments.

Stimuli were displayed on a cathode ray tube computer monitor (Sony Trinitron, 760x1400 pixels, 75 Hz refresh rate) whose phosphor emission spectra were characterized with a spectroradiometer (PR650, Photo Research Inc, CA). The color depth of each channel of the monitor was increased from 8 to 14 bits using a digital video signal processor (Bits++, Cambridge Research) at the expense of spatial resolution: each pixel was twice as wide as it was tall. Gamma correction was performed in software. All stimuli were presented on a uniform gray background (CIE coordinates: x = 0.33, y = 0.33, Y = 100 cd/m2).

Stimuli were generated using the method of silent substitution (Estévez and Spekreijse 1982) and were based on the Stockman, McLeod, and Johnson 1993 cone fundamentals (Stockman et al. 1993). For 78 neurons, stimuli were based on the 2° fundamentals, and for 30 neurons, stimuli were based on the 10° fundamentals. Results from these two sets of experiments were similar and thus have been pooled together in this report. Most importantly, the main conclusion of this study – that the signal-to-noise ratio of individual V1 neurons at psychophysical detection threshold does not depend on color direction – was unaffected by this manipulation. A more thorough analysis of the differences between the two stimulus sets and their impact on our results can be found in the Discussion. Unless otherwise stated, contrast was defined as the vector norm of the stimulus in L, M, S cone-contrast space:

$$\text{Contrast} = \sqrt{\left(\frac{\Delta L}{L}\right)^2 + \left(\frac{\Delta M}{M}\right)^2 + \left(\frac{\Delta S}{S}\right)^2} \qquad \text{Eq. 2.1}$$

Recording procedures

Recordings from individual V1 neurons were attained via glass-tipped transdural tungsten microelectrodes (FHC Inc.) with impedances of 1 to 2 MΩ measured at 1000 Hz. The raw voltage signal was amplified, bandpass filtered (100 Hz to 8 kHz), and digitized at 40 kHz using the Multichannel Acquisition Processor (Plexon Inc.). Single unit isolation was assessed by stability in the action potential waveform over the duration of the recording and the absence of inter-spike-intervals < 1 ms.

During an initial characterization procedure, we estimated each neuron's color tuning using circularly apertured drifting sinusoidal gratings of a preferred orientation, size, and spatial frequency. Chromaticities were selected from in an isoluminant plane defined by two axes (Figure 2.2C): one in which L- and M-cones modulated out of phase (L–M or 0°), and one the modulates only the S-cones (S-cone isolating or 90º). The plane spanned by L–M and S-cone axes consists of stimuli that are isoluminant for the Stockman-MacLeod-Johnson standard observer. Stimuli in this plane are not perfectly isoluminant for the monkeys, but are expected to be approximately so. During the initial neuronal characterization procedure, stimulus contrasts in the L–M and S-cone isolating color directions were roughly matched for detectability (~13x threshold) and presented in

four color directions (two cardinal and two intermediate). Thus, modulations in the intermediate color directions (45º and 135º) produced roughly equal changes in the detectability of their S- and L–M components. Had we equated the S and L–M components for cone contrast, the S-cone component would have been sub-threshold when the L–M component was clearly visible. The suprathreshold appearance of intermediate colors was distinct from that of the cardinal colors. The 45°/225° intermediate appeared lime/magenta and the 135°/315° intermediate appeared orange/cyan.

During the detection task, behavioral performance and neuronal responses were measured simultaneously in the preferred cardinal and intermediate color directions using the method of constant stimuli. We identified each neuron's preferred cardinal and intermediate color direction on the basis of mean firing rates to the suprathreshold sinusoidal gratings used during the initial characterization procedure. Gabor stimuli were presented at 7 contrasts spanning the monkey's psychophysical detection threshold. Presentations of 15 stimuli were randomly interleaved across trials: 2 color directions x 7 contrasts + 1 zero contrast (blank).

Contrast selection procedure

Measuring psychometric functions via the method of constant stimuli required a judiciously selected range of contrasts. If contrasts were too high or too low, or the contrast range too wide, then the informative (steep) portion of the psychometric function would have been poorly sampled. This problem was exacerbated by the fact that we tailored the spatial frequency and color direction of the stimuli to maximize each neuron's response and thus presumably their relevance to behavioral performance. Because psychophysical thresholds vary by as much as 2 orders of magnitude across the color directions and spatial frequencies we tested (Mullen 1985; Burr et al. 1994), using the same contrast range for each neuron would have undoubtedly led to poor sampling of the psychometric function.

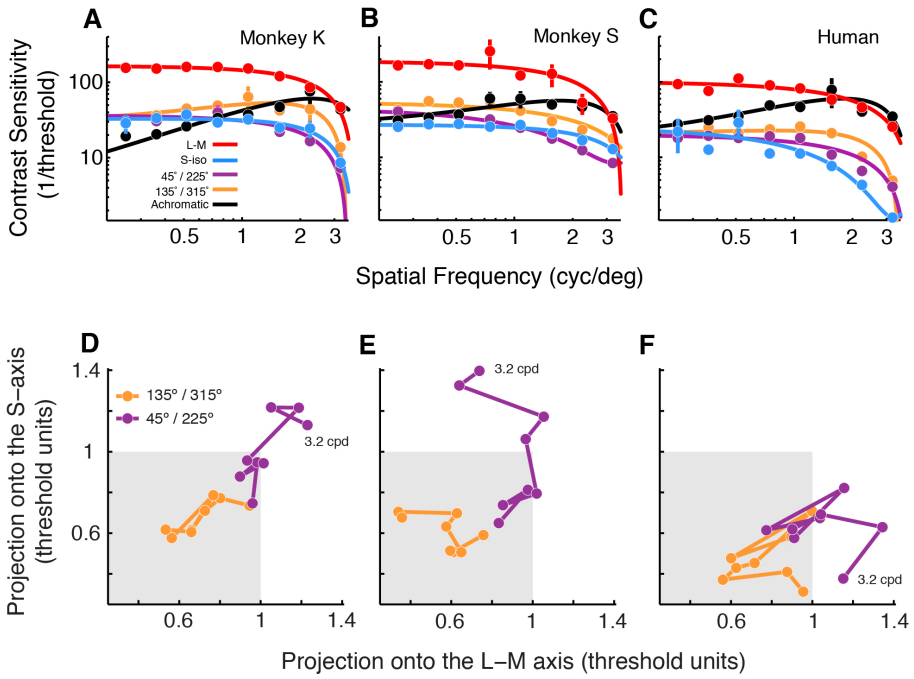

Figure 2.3 A, B, and C: Spatial contrast sensitivity functions for two monkeys and one human subject in the four isoluminant color directions shown in Figure 2.2C and the achromatic color direction. Data points represent the average sensitivity (1/threshold) estimated with the QUEST adaptive procedure. Curves are the best fitting 2nd order polynomials. Error bars represent ±1 s.e.m. D, E, and F: Data from A, B, and C replotted in terms of the cardinal mechanisms model. Detection thresholds for intermediate colors (points) are represented in threshold units along the L–M (abscissa) or S-cone isolating (ordinate) cardinal color directions. Points that lie on the interior of the gray shaded square are qualitatively consistent with the cardinal mechanisms model (i.e., probability summation among the cardinal mechanisms). Individual points are color coded according to color direction, and are joined together in ascending order of spatial frequency. The point corresponding to the highest spatial frequency stimulus in the 45º/225º color direction is labeled in each panel.

To facilitate selecting appropriate contrast ranges for the detection task, we first measured behavioral detection threshold for 32 Gabor stimuli (each combination of 4 color directions and 8 spatial frequencies). Thresholds were determined using the QUEST adaptive procedure for each subject (Watson and Pelli 1983). Contrast sensitivity functions in each color direction were fit independently with a second order polynomial (Figure 2.3). The fits were then used to determine the contrasts used during neuronal recordings. Contrasts were typically chosen to span a range from 0.25 to 2x the detection threshold estimated by the fit, but in rare cases were adjusted manually to ensure adequate sampling.

To confirm that the monkeys were performing the task near threshold difficulty levels for humans, the first author performed the QUEST version of the 2AFC detection task using the same display that was used in the monkey experiments. Eye position was not measured in these experiments and psychophysical reports were indicated with button presses. Written, informed consent was obtained from the human observer, and the experimental procedures conformed to the policies of the University of Washington Human Subjects Division.

Fitting contrast-response functions

A linear neuron tuned to a cardinal color direction will respond to modulations in intermediate color directions simply by virtue of the fact that intermediate colors have a component in the preferred cardinal direction. Expressed rigorously, the response of such a neuron depends on the projection of a stimulus onto its preferred cardinal color direction. To ask whether V1 neurons behave this way, we measured contrast-response functions (CRFs) in each neuron's preferred cardinal and intermediate color directions and fit them simultaneously with the following model:

$$\text{Spike counts}_{(\text{card})} = \beta_0 + \beta_1 * \max[\text{Contrast} - \beta_2, 0]^2 \quad \text{(Eq. 2.2)}$$

$$\text{Spike counts}_{(\text{int})} = \beta_0 + \beta_1 * \max[(\text{Contrast} * \beta_3) - \beta_2, 0]^2 \quad \text{(Eq. 2.3)}$$

In this model, CRFs in the two color directions are modeled as horizontally-scaled versions of each other. β0, β1, and β2 are fitted parameters that represent the background discharge, contrast gain, and spike threshold, respectively. β3 is a fitted parameter that determines the scaling between the cardinal and intermediate CRFs. If the CRF in the cardinal direction is steeper than in the intermediate direction, β3 is < 1. If the CRF in the intermediate color direction is steeper than in the cardinal color direction, β3 is > 1. Parameters were fit using maximum likelihood estimation assuming Poisson error. Contrast was defined as the projection of each stimulus onto the preferred cardinal color direction for Figure 2.4C&D, and defined as multiples of psychophysical threshold in Figure 2.4F&G.

The basis of the fit, half-squaring, has been used to describe the contrast-response functions of V1 neurons before (Anzai et al. 1999; Heeger 1992), but we found that the

addition of a non-zero baseline firing rate (β0) and a contrast threshold (β2) improved the quality of many fits. The β3 parameter was included to allow us to test the hypothesis that contrast-response functions in the cardinal and intermediate directions were horizontally scaled versions of each other (that is, β3 = 1). The model does not include response saturation because none of the neurons showed signs of saturation over the contrasts we tested.

We considered quantifying neuronal activity differently for simple and complex V1 neurons (viz. F1 and F0 components of the response, respectively), but results obtained this way were nearly identical to those obtained using raw spike counts. Although we encountered simple cells with robust F1 components during our initial characterization procedure, the time course of the Gabor stimulus in the 2AFC task often dominated the neural response more so than the F1 component of the drifting Gabor. We thus quantified neuronal activity as spike counts during the stimulus interval for all analyses.

Quantification of psychometric and neurometric sensitivity

A primary objective of this study was to quantify the signals present in V1 at chromatic detection threshold and to relate these signals to behavioral sensitivity. We quantified behavioral sensitivity by fitting a cumulative Weibull function to the psychophysical data:

$$p(correct) = 1 - 0.5e^{-(\frac{x}{\alpha})^{\beta}} \qquad \text{(Eq. 2.4)}$$

where P(correct) is the probability of a correct detection and x is the stimulus contrast. The fitted parameters, α and β, correspond to the threshold (i.e., the contrast necessary to support 82% correct detection) and slope of the psychometric function, respectively.

To quantify the reliability of neuronal signals in a way that is directly comparable to behavioral thresholds, we used an ideal observer analysis based on the responses of each neuron (Tolhurst et al. 1983; Newton and Eskew 2003; Palmer et al. 2007). For each color direction and contrast, we calculated an ROC curve based on the distribution of spike rates in response to a stimulus inside the RF (signal) and no stimulus presented (noise). The performance of the ideal observer was calculated as the area under the ROC curve, which gave rise to a single point on a neurometric function (e.g., Figure 2.5A&B).

This method assumes a model of detection in which, on each trial, the ideal observer receives a draw from a signal distribution (which represents the information available from the neuron at the tip of the electrode) and a draw from the noise distribution (which represents the information available from a theoretical but identical neuron whose receptive field is in the mirror symmetric location opposite the fixation point) (Britten et al. 1992). The ideal observer's choice is based on whichever draw is larger, and is correct when the larger draw came from the signal distribution. We quantified the performance of the ideal observer by fitting equation 4 to the raw neurometric data, where the fitted parameters α and β describe the neurometric threshold (NT) and slope, respectively. To compare neuronal and behavioral thresholds directly, we calculated the neurometric to psychometric threshold ratio (TR) separately for each color direction. Although we routinely tested only contrasts within 0.25 to 2 times the QUEST estimate of detection threshold, threshold ratios varied over a wider range because psychometric and neurometric thresholds were occasionally at the upper and lower ends of this range.

To assess differences in neuronal sensitivity across color direction statistically, we performed a permutation test based on an F-statistic:

$$\mathrm{F} = \frac{\sum_{i} n_i \frac{(\overline{Y}_i - \overline{Y})^2}{k-1}}{\sum_{ij} \frac{(Y_{ij} - \overline{Y}_i)^2}{(N-k)}} \qquad \text{(Eq. 2.5)}$$

where i is the mean neuronal sensitivity (NT or TR) for the i_{th} color direction, $\overline{\mathrm{Y}}$ is the mean across all color directions and neurons, k is the number of color directions, n_i is the number of observations for the i_{th} color direction, Y_{ij} is the sensitivity of the j_{th} neuron in the i_{th} color direction, and N is the total number of observations. Next, we calculated F-statistics for 5000 datasets that were permuted by randomly reassigning neuronal sensitivity values (NT or TR) to color directions subject to two constraints: 1) the two values for any given neuron were reassigned to a cardinal direction and an intermediate direction (consistent with our experimental design) and 2) the number of values within each color direction was the same as in the original dataset. The permuted data sets thus

maintained the statistical dependence within-cells that was observed in the real dataset but randomly shuffled the association between neural sensitivity values and color. The p-value was calculated as the percentage of permuted F-statistics that exceeded the observed F-statistic.

Choice probability

For each neuron, we converted firing rates to z-scores within each stimulus condition (color direction x contrast x stimulus location), and then pooled z-scores according to the choice the monkey expressed at the end of the trial. We calculated an ROC curve from these two distributions of z-scores, and defined choice probability as the area beneath the curve (Britten et al. 1996). Choice probability equals 0.5 when the monkey's choice is unrelated to the variations in the neuronal response. Choice probability > 0.5 indicates that the monkey more often reported the stimulus to be inside the RF on trials in which the firing rate was unusually high. Firing rates were z-scored to remove effects of the color direction and contrast of the stimulus in the RF.

Inclusion criteria

We recorded from 96 V1 neurons in two monkeys performing the 2AFC chromatic detection task (51 from monkey K, 45 from monkey S). Receptive fields were located between 3º and 8° from the fovea (mean ± SD: 5.14 ± 0.88º). A minimum of 16 trials per color contrast condition was collected from each neuron. For the purposes of fitting contrast-response functions, we included neurons for which one or more ROC areas exceeded 0.8 (n= 67). We used the same inclusion criteria for the analysis of threshold ratios. For the analysis of choice probability, we included only those color/contrast conditions in which the monkey made ≥ 5 choices to each target.

Results

Preliminary psychophysical results

In order to test the appropriate contrast ranges during our neurophysiology experiments it was critical that we first measure psychophysical detection thresholds in the cardinal and intermediate color directions and across the range of spatial frequencies

preferred by parafoveal V1 neurons. In these preliminary measurements, psychophysical thresholds were estimated using the QUEST adaptive procedure (Watson and Pelli 1983). Stimuli were centered at [-5º, -3.5º] or [5º, 3.5º] with respect to the fixation point. Consistent with psychophysical results from humans, contrast sensitivity functions for isoluminant stimuli were spatially lowpass (Figure 2.3 A-C) and sensitivity for achromatic stimuli was bandpass (Mullen 1985). Note that the Gaussian envelope (SD = 0.4°) renders stimuli of nominal spatial frequency < ~1 cycles/deg artifactually similar. Nevertheless, we were able to observe an attenuation of achromatic contrast sensitivity below this value. Spatial frequencies > 4 cycles/deg were not tested to avoid complexities introduced by chromatic aberrations. The qualitative and quantitative similarities between the human (Figure 2.3C) and monkey observers demonstrate that the monkeys were under behavioral control.

Under the cardinal mechanisms model, stimulus modulations in intermediate color directions are detected on the basis of pooled signals from the cardinal mechanisms. As shown in Figure 2.1, this should cause detection thresholds in the intermediate directions to be lower than detection thresholds mediated by either of the cardinal mechanisms individually. We tested this prediction by plotting detection thresholds for intermediate colors in terms of threshold units along the cardinal color directions (Figure 2.3D-F). Points that lie on the interior of the gray shaded square are qualitatively consistent with the cardinal mechanisms model (i.e., probability summation among the cardinal mechanisms). This was the case for detection of the 135º/315º intermediate across all the spatial frequencies we tested, but not for the 45º/225º intermediate at > 1 cycle/degree. These psychophysical results are agnostic to the color tuning of individual neurons, an issue that we turn to next.

Testing the cardinal mechanisms model in V1

We asked whether individual V1 neurons were tuned to the cardinal directions at psychophysical detection threshold. For two example V1 neurons (Figure 2.4A&B) spike counts in response to the L–M cardinal color direction were greater than responses to the intermediate color direction at every contrast tested. This tuning is consistent with a preference for the cardinal direction, but this interpretation depends critically on how

stimulus contrast is defined. Implicit in our definition of contrast (Eq. 2.1) is the equality of contributions from the L-, M-, and S-cone types. Changing the relative weights on the three cone types changes the contrast values, which in turn can scale contrast-response functions along the contrast axis.

To determine whether V1 neurons conform to the cardinal mechanisms model, we tested a prediction that it makes: spike counts in intermediate color directions should be determined by the projection of the stimulus onto the neuron's preferred cardinal axis. For example, a neuron tuned to the L–M color direction would respond equally well to stimulus modulations in L–M+S and L–M–S color directions if their L–M components are equal. To test this prediction, we quantified stimulus contrast as the projection onto the preferred cardinal axis and fit CRFs using a model which represents the difference between the CRFs as a scaling of the contrast axis (Eqs. 2.2 and 2.3). If V1 neurons respond like the psychophysical cardinal mechanisms, the two contrast-response functions should overlay each other, and the scale factor that relates cardinal and intermediate CRFs ($\beta 3$ in Eq. 2.3) should equal one. The CRFs for some neurons were consistent with the linear cardinal model (Figure 2.4C), but the majority of neurons gave rise to CRFs that were inconsistent with the cardinal model (Figure 2.4D). $\beta 3$ was significantly > 1 for 82% of the neurons individually (Wald tests, $p < 0.05$) and across the population (geometric mean = 1.50; t-test on $\log(\beta 3)$, $p < 0.001$; Figure 2.4E).

As a control analysis, we randomly partitioned responses to cardinal colors into two groups and then fit them with Eqs. 2.1 and 2.2. The average $\beta 3$ parameter from this control analysis was not significantly different from one (t-test on $\log(\beta 3)$, $p = 0.24$), which demonstrates that the tendency we observed in the data for $\beta 3 > 1$ is not a trivial consequence of the model fitting procedure. We conclude that individual V1 neurons respond more strongly to modulations in intermediate color directions than predicted by the cardinal model.

Comparing contrast-response functions equated for stimulus detectability

The qualitative similarity between neuronal and behavioral chromatic sensitivity led us to ask whether CRFs in cardinal and intermediate color directions might match quantitatively if stimulus intensity were represented in units of detection threshold. We scaled the contrast values so that an intensity of "1" in any color direction was detectable

82% of the time, and then re-fit Eqs. 2 and 3 to the data. For the few neurons that were well described by the cardinal model, this rescaling necessarily forced a discrepancy between cardinal and intermediate CRFs (Figure 2.4F). For most neurons, however, this manipulation yielded a closer correspondence in the CRFs (e.g., Figure 2.4G). The average β3 (Eq. 2.3) for the entire population was not significantly different from 1 (geometric mean = 0.97, p = 0.59, t-test on log(β3), Figure 2.4H). We conclude that the CRFs of V1 neurons are more closely related to psychophysical detection thresholds than to the S and L–M components of cone contrast modulations.

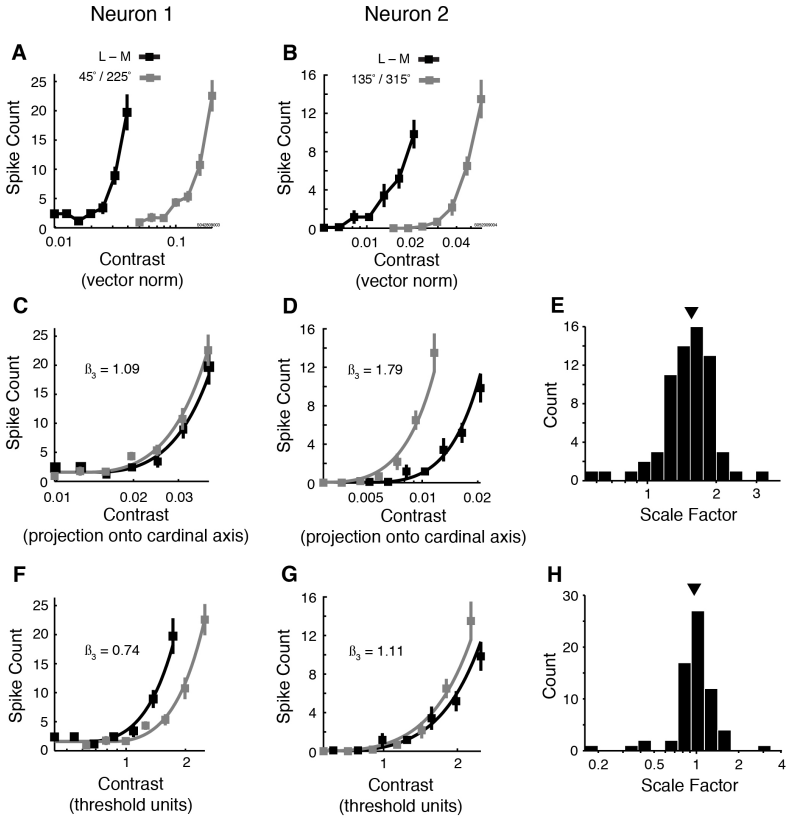

Figure 2.4 Analysis of contrast-response functions (CRFs) measured during the detection task. A and B: CRFs for two example neurons in response to stimulus modulations along their preferred cardinal (black) and intermediate color directions (gray). Contrast was quantified as the vector norm of the stimulus (Eq. 2.1). C and D: CRFs for the same neurons in A and B but recalculating contrast as a stimulus' projection onto the preferred cardinal axis. Fits are half-squaring functions (Eqs. 2 and 3). Under the linear cardinal mechanisms model, the two CRFs should be identical. E: Histogram of scale factors (β3 in Eq. 2.3) across the population of neurons tested (n = 67). F and G: CRFs for the neurons in A and B but quantifying contrast in units of psychophysical detection threshold. H: Histogram of scale factors (β3 in Eq. 2.3) after redefining contrast in units of psychophysical detection threshold. Error bars represent ±1 s.e.m.

Neurometric sensitivity

Chromatic detection depends on the amplitude and variability of neural responses to low-contrast chromatic stimulation. To compare neuronal sensitivity across colors, we performed an ideal observer analysis that incorporates measurements of neuronal signal and noise (see Methods). Specifically, neuronal sensitivity was quantified as the neurometric threshold (NT) derived by fitting a cumulative Weibull function to the performance of a theoretical ideal observer with access to neuronal responses (Figure 2.5A&B; see Methods). Every neuron was tested in two color directions during the detection task, and NTs were calculated for each color direction separately.

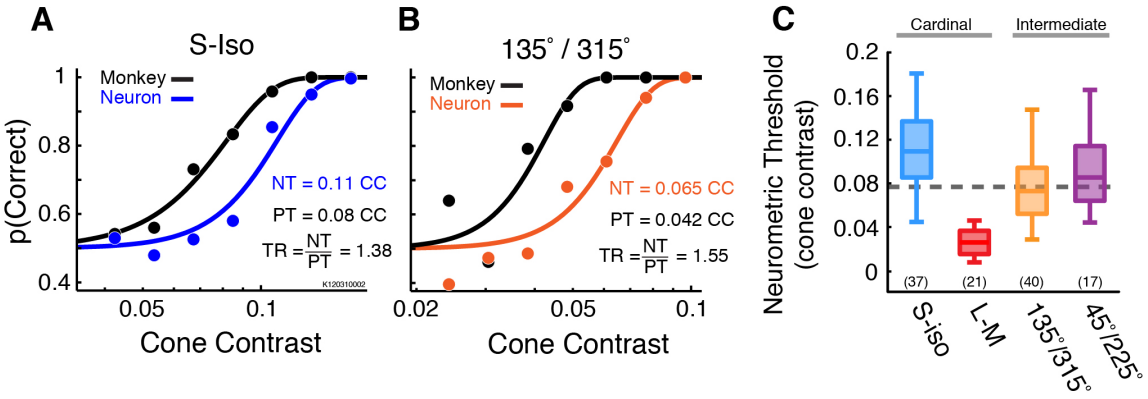

Figure 2.5 Ideal observer analysis of neuronal responses. A and B: Example psychometric (black) and neurometric (blue and orange) functions from a single neuron in response to modulations in the preferred cardinal (A) and intermediate (B) color directions. Black points represent the raw psychophysical data. Blue and orange points represent the performance of an ideal observer with access to the neuronal responses (i.e., area under the ROC curve). Neurometric thresholds (NT) and psychometric thresholds (PT) were obtained from the best fitting cumulative Weibull distribution (curves). C: Distributions of neurometric thresholds for each color direction. The top and bottom of each box represent upper and lower quartiles respectively, and the horizontal line inside each box represents the median. Vertical lines indicate the range. The dashed gray line represents the median neurometric threshold calculated across cells and color directions. The number of neurons measured in each color direction is indicated in parentheses. The total number of cells included in the analysis was 67 (each neuron contributes a TR to one cardinal and/or one intermediate color direction).

An analysis of neurometric thresholds showed that V1 neurons were preferentially sensitive to some colors directions relative to others (permutation test on NTs $p < 0.001$; Figure 2.5C). Neurometric thresholds in the L–M color direction were lower than in any other color direction, and were 4.1 times smaller than for the S-cone isolating color

direction (unpaired t-test $t(56) = 5.5$, $p < 0.001$; mean for L–M = 0.029, mean for S-cone isolating = 0.12). This analysis demonstrates that individual neurons are capable of producing reliable signals to near-threshold chromatic stimuli, and that the contrast (as defined by Eq. 2.1) necessary to evoke a reliable response depends on color direction.

Neurometric-to-psychometric threshold ratios

To quantify the relationship between neuronal sensitivity and behavioral performance we calculated neurometric-to-psychometric threshold ratios (TR) for each neuron in both color directions tested. A TR of 1 means that the neuron and monkey are equally sensitive. A TR > 1 means that that the monkey is more sensitive than the neuron. On average, monkeys were 1.5 times more sensitive than V1 neurons (geometric mean TR = 1.5, 95% CI [1.38, 1.63]; Figure 2.6A). 30% of the neurons in our sample did not respond above baseline over the range of contrasts tested (i.e., at psychophysical detection threshold), and their threshold ratios were undefined. These neurons are unlikely to contribute to processing chromatic signals at detection threshold.

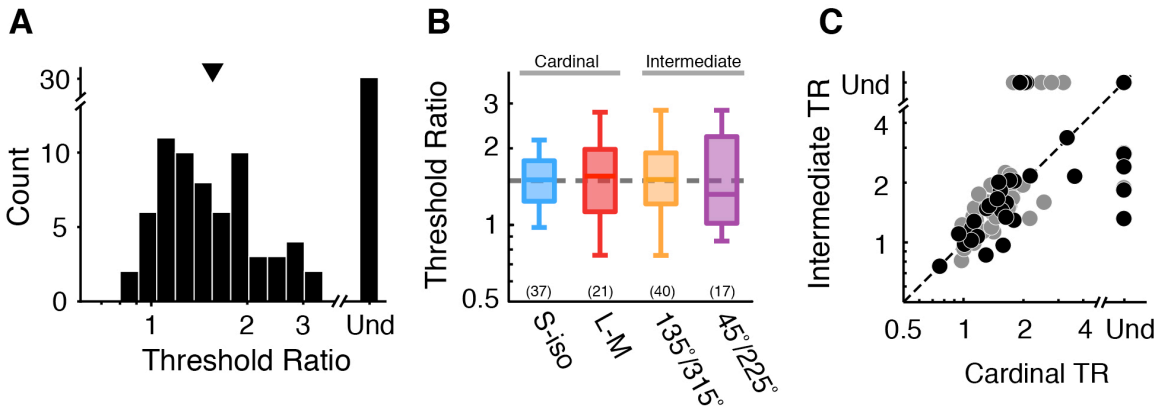

Figure 2.6 Comparison of threshold ratios within and between cells. A: Neurometric to psychometric threshold ratios (TR) across the population of neurons (n = 96) combined across color directions. Neurons were tested in two color directions, but only contribute a single TR to the population histogram (i.e., the minimum of the two). Threshold ratios were considered undefined (Und) when the neurometric threshold could not be measured (no points on the neurometric function > 0.8). Triangle represents the geometric mean. B: Distributions of threshold ratios for each color direction across neurons that were responsive at psychophysical threshold. The number of neurons measured in each color direction is indicated in parentheses. The total number of cells included in the analysis was 67 (each neuron contributes a TR to one cardinal and/or one intermediate color direction). C: Threshold ratios measured in each neuron's preferred cardinal and intermediate color direction (black: monkey K, gray: monkey S).

To determine if the relationship between neurometric and psychometric sensitivity depended on color direction, we compared TRs across the four color directions tested. This analysis was necessarily limited to those neurons for which neurometric thresholds were measureable given the contrast range that we used (see Methods). For this sub-population of neurons, the distributions of TRs were highly overlapping (Figure 2.6B) and the geometric mean threshold ratio did not differ significantly across color direction (permutation test on log(TRs) $p = 0.42$; see Methods). Note that under the cardinal mechanisms model we would expect TRs to be higher in the intermediate directions than in the cardinal directions (Figure 2.1), which we did not observe.

Consistency between neurometric and psychometric sensitivity was also observed within cells. Threshold ratios measured in each neuron's preferred cardinal and intermediate color directions were not significantly different (paired t-test, $p = 0.60$; Figure 2.6C). Moreover, the within-cells analysis demonstrated that TRs in the cardinal and intermediate color directions were well correlated (Spearman's $r = 0.84$, $p < 0.01$). We conclude that V1 neurons differ widely in their sensitivity relative to the monkey, but that the relationship between neuronal and psychophysical sensitivity does not depend on color direction.

A potential explanation for the consistency of TR across color directions is that we tested too narrow a range of color directions: each neuron was tested in only two neighboring color directions of the four we considered. To control for this possibility, we tested 11 neurons in two orthogonal color directions: L–M and S-cone isolating. Only 4 of these 11 neurons were sensitive to one of the cardinal color directions and insensitive to the other. The remaining 7 neurons were sensitive to both color directions and were often more sensitive than the monkey (Figure 2.7A). For these neurons, TRs in response to L–M were slightly smaller than in response to S-cone isolating stimuli (geometric mean TR for L–M = 0.8 and for S-cone isolating = 1.05, paired t-test, $p = 0.043$; Figure 2.7B). Thus, S-cone isolating and L–M stimuli produce similarly reliable signals in V1 at the monkeys' detection threshold, both across neurons and within the subpopulation that are sensitive in both color directions.

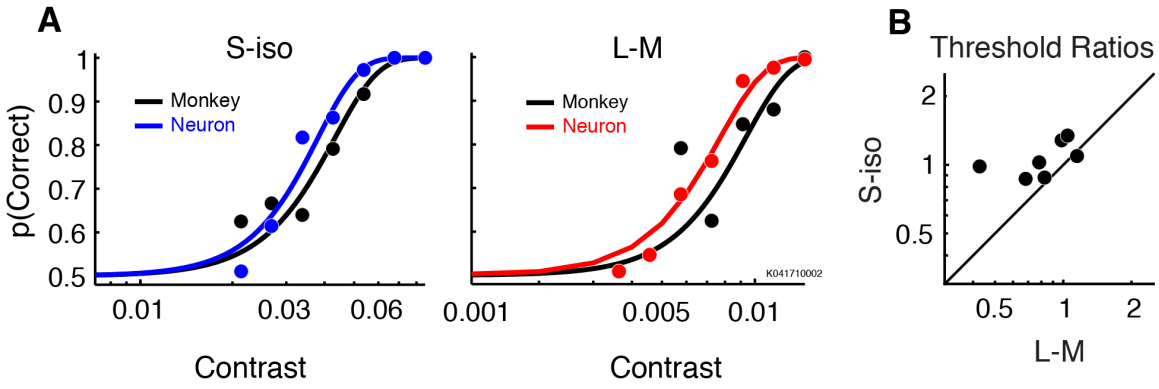

Figure 2.7 Sensitivity of individual neurons to modulations in the L–M and S-cone isolating color directions. A: Example psychometric (black) and neurometric (blue or red) performance and the best fitting cumulative Weibull distributions (solid curves). This neuron was slightly more sensitive than the monkey in response to modulations in either of the cardinal color directions. B: Threshold ratios of the subset of neurons that were tested in the L–M and S-cone isolating color directions and were responsive at psychophysical threshold to both colors.

Choice probability

V1 neurons that contribute to chromatic detection must be responsive at the monkey's chromatic detection threshold, however the converse is not true: not all chromatically sensitive neurons must contribute to psychophysical contrast detection. To identify V1 neurons that are most likely to contribute to the monkey's psychophysical judgments, we performed an analysis of choice probability (CP). This analysis hinges on the logic that neurons that are causally linked to behavior may produce responses that are correlated with the monkey's behavior on a trial by trial basis (Britten et al. 1996; Palmer et al. 2007; but see Nienborg and Cumming 2009).

By this analysis, neuronal responses were correlated with the monkeys' choices only weakly. The average choice probability was 0.52 ± 0.008 s.e.m., which is slightly but significantly greater than 0.5 (t-test, $p < 0.05$). Very few individual V1 neurons had significant choice probabilities ($n = 4$ of 67, Wilcoxon, $p < 0.05$), and those that did were not obviously unusual in any other way. Specifically, they were not unusually sensitive compared to neurons with insignificant CP (t-test on log(TR), $p = 0.44$). Nevertheless, to designate a population of V1 neurons that were the best candidates for contributing to task performance, we extracted the subset of 32 neurons that had a choice probability > 0.51 (the median value). This subpopulation was neither particularly sensitive (t-test on log(TR), $p = 0.71$) nor differentially sensitive across color direction (ANOVA on log(TR)

$F(3,27) = 0.84$, $p = 0.48$). Choice probability thus appears to provide little leverage into the question of which V1 neurons mediate performance on our task.

Suprathreshold response properties of chromatically sensitive V1 neurons

The degree to which a V1 neuron participates in color vision has traditionally been inferred from its responses to suprathreshold chromatic stimuli (Lennie et al. 1990; Johnson et al. 2001; Solomon and Lennie 2005), but the extent to which these suprathreshold measurements predict near-threshold sensitivity is unknown.

Following Johnson et al. (2001), we computed a color sensitivity index (CSI) based on responses to the high-contrast chromatic gratings used in our initial characterization procedure:

$$\mathrm{CSI} = \frac{\mathrm{FR}_{\,(\mathrm{Pref\ Isolum})}}{\mathrm{FR}_{\,(\mathrm{L+M})}} \qquad \text{(Eq. 2.6)}$$

where $FR_{(\mathrm{Pref\ Isolum})}$ is the average firing rate in response to the preferred isoluminant stimulus and $FR_{(\mathrm{L+M})}$ is the average rate in response to a 13% contrast L+M stimulus. Neurons with CSIs ≤ 0.5 were classified as luminance preferring ($n = 19$). Neurons with CSIs between 0.5 and 2 were classified as color-luminance cells ($n = 46$), and neurons with CSIs ≥ 2 were classified as color-preferring cells ($n = 31$). The prevalence of color-preferring neurons in our data set is higher than reported previously (32% vs. 11%; Johnson et al. 2001; Johnson et al. 2008; Conway 2001) and the prevalence of luminance-preferring neurons is lower (20% vs. 60%). This outcome likely reflects our use of 4 chromatic stimuli (three of which robustly modulate the S-cones) instead of a single red-green isoluminant stimulus. When we redefined color sensitivity as the ratio of responses to the L–M and L+M color directions, the proportion of color-preferring neurons (13%) was closer to those of previous studies (Johnson et al. 2001; Johnson et al. 2008; Conway 2001).

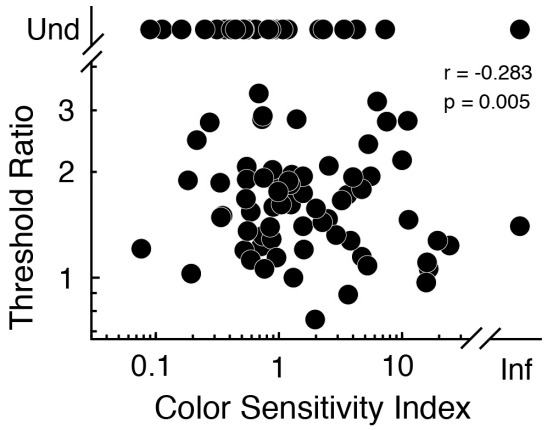

Figure 2.8 The relationship between color sensitivity index and threshold ratio. Color sensitivity indices were calculated on the basis of mean firing rates in response to suprathreshold sinusoidal gratings. Threshold ratios were calculated from responses in the chromatic detection task. The smaller of the two threshold ratios from each neuron is shown here, but results were qualitatively similar when we used the larger one (see Figure 2.6C).

A comparison of CSI and TR (Figure 2.8) showed a weak but significant relationship (Spearman's $r = -0.28$, $p = 0.005$); neurons that were particularly sensitive during our detection task (i.e., those with the lowest TRs) tended to be color-preferring whereas neurons that were insensitive tended to be color-luminance or luminance-preferring. As expected, luminance preferring neurons had higher TRs than color-luminance or color-only cells (Wilcoxon tests: $p < 0.05$), but many ($n = 8$ of 19) had TR $\leq$ 3, indicating non-negligible sensitivity to isoluminant modulations. Threshold ratios of color-luminance and color-only neurons were statistically indistinguishable (Wilcoxon test, $p = 0.17$). This result supports a role for color-luminance neurons in chromatic detection and argues against the idea that they can be considered "miscalibrated photometers" whose sensitivity to chromatic stimuli is small and has no behavioral significance (Gegenfurtner et al. 1994; Billock 1995).

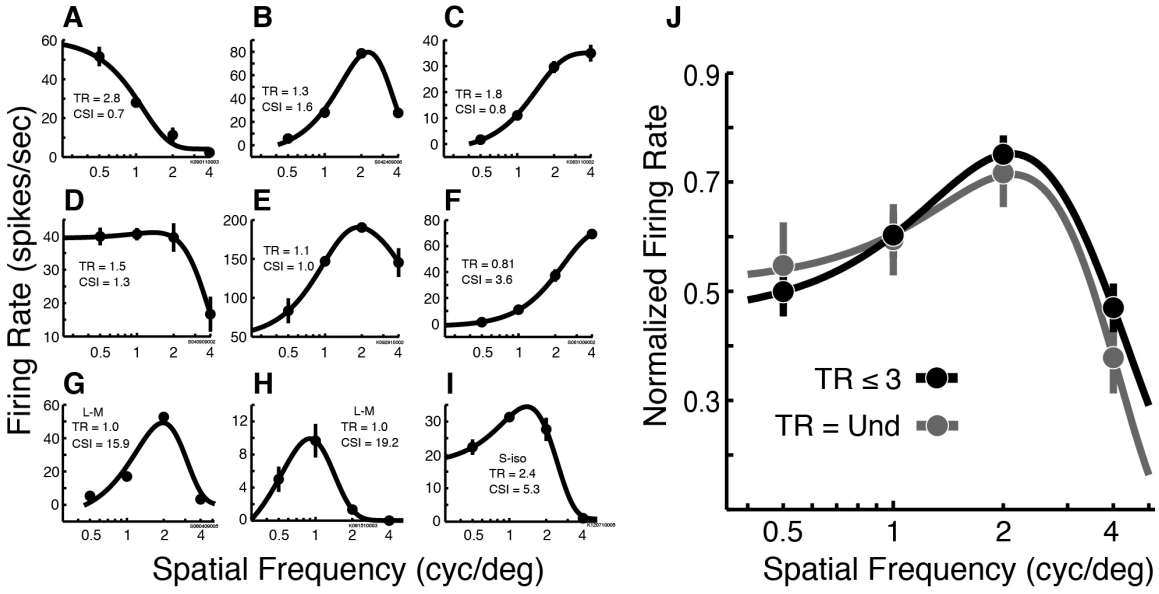

Figure 2.9 Spatial frequency tuning of neurons that were sensitive (i.e., threshold ratio ≤ 3) at the monkey's chromatic detection threshold. A–F: Data from six individual neurons illustrating low-pass (A and D) and band-pass (B,C,E,F) tuning in response to achromatic sinusoidal gratings. G–I: Data from three example neurons illustrating band-pass tuning in response to isoluminant sinusoidal gratings. Curves are the best fitting difference of Gaussians. The threshold ratio (TR) and color sensitivity index (CSI) are provided for each neuron. J: Population average spatial frequency tuning curve for neurons that were sensitive (black) and insensitive (gray) at chromatic detection threshold. Individual tuning functions were normalized by their maximum value and then averaged across neurons. Error bars represent ±1 s.e.m.

Color-luminance V1 neurons, unlike color-preferring neurons, tend to have bandpass spatial frequency tuning (Johnson et al. 2001). Our observation that color-luminance neurons are sensitive at chromatic detection threshold thus implies bandpass spatial frequency tuning among the most chromatically sensitive V1 neurons. Consistent with this prediction, neurons that were sensitive at the monkeys' detection threshold had a range of spatial frequency preferences and tuning bandwidths when measured with achromatic gratings (Figure 2.9A-F). Bandwidths calculated by fitting a difference of Gaussians model to the raw data (Johnson et al. 2001) were poorly correlated with threshold ratios (Spearman's $r = 0.14$, $p = 0.25$; data not shown), and the population spatial frequency tuning function of neurons sensitive at detection threshold (TR ≤ 3) was similar to the tuning function for insensitive neurons (Figure 2.9J). For most neurons, spatial frequency tuning was measured with achromatic gratings, but a similar result was obtained from a subset of neurons (n = 14) whose spatial frequency tuning was measured

using gratings of the preferred isoluminant color direction (Figure 2.9 G-I). The existence of chromatically sensitive, spatially bandpass V1 neurons is consistent with psychophysical observations (Bradley et al. 1988; Losada and Mullen 1994; Mullen and Losada 1999), and argues against the view that strongly color-opponent, lowpass, unoriented neurons are the sole mediators of color processing in V1 (Livingstone and Hubel 1984).

Discussion

Detection psychophysics has been instrumental in developing models of contrast sensitivity on the basis of neural detection mechanisms (Blakemore and Campbell 1969; Mullen 1985; Tolhurst et al. 1983; Boynton et al. 1999; Geisler and Albrecht 1997; Cole et al. 1993; Sankeralli and Mullen 1996). Simultaneous measurement of neuronal responses and psychophysical performance offers a powerful method of testing these models. Using this approach, we showed that individual V1 neurons are responsive at chromatic detection threshold but their tuning is inconsistent with the linear cardinal mechanisms model. Contrast-response functions did not match when contrast was defined as the projection of a stimulus onto the preferred cardinal axis but were better matched when contrast was defined in units of detection threshold. An ideal observer analysis showed that neurometric thresholds were on average 1.5 times greater than the monkeys' psychometric thresholds, and this result was consistent across the 4 color directions we tested. In contrast to the independence between the cardinal mechanisms demonstrated psychophysically (Krauskopf et al. 1982; Krauskopf and Farell 1990; Sankeralli and Mullen 1997) and supported by the physiology and anatomy of the visual system prior to V1 (De Valois et al. 1966; Derrington et al. 1984; Chatterjee and Callaway 2003), some V1 neurons were sensitive at detection threshold in both L–M and S-cone isolating color directions. Lastly, we found that many V1 neurons that responded to high contrast luminance stimuli were also well driven by isoluminant stimuli at the monkey's psychophysical threshold. This suggests a role for jointly color-luminance tuned neurons in chromatic detection.

Relationship to psychophysically defined detection mechanisms

Psychophysical experiments have demonstrated that chromatic detection is mediated by multiple visual mechanisms, but the tuning and number of these mechanisms is controversial (for review see: Eskew 2009; Stockman and Brainard 2009). Evidence in favor of the cardinal mechanisms model comes from a variety experimental techniques including color matching (LeGrand 1949), detection (Cole et al. 1993; Sankeralli and Mullen 1996), chromatic habituation (Krauskopf et al. 1982), noise masking (Sankeralli and Mullen 1997; Giulianini and Eskew 1998; Eskew et al. 2001), and motion coherence judgments (Krauskopf and Farell 1990). Using essentially the same techniques, other experiments have acknowledged a dominant role for the cardinal mechanisms in chromatic detection but suggest the existence of an unknown number "higher-order" mechanisms that also contribute to color vision (Krauskopf et al. 1986; Krauskopf and Gegenfurtner 1992; Webster and Mollon 1994; Krauskopf et al. 1996; Stoughton et al. 2012). A third group of experiments found evidence of higher-order mechanisms and argued against a dominant role for the cardinal mechanisms (Gegenfurtner and Kiper 1992; D'Zmura and Knoblauch 1998; Hansen and Gegenfurtner 2006).

The higher-order chromatic detection mechanisms revealed psychophysically may result, in part, from cone signal processing in V1. Many previous studies have documented non-cardinal color tuning in V1 (Lennie et al. 1990; Johnson et al. 2004; Horwitz et al. 2007). Our study confirms and extends these previous studies in three ways. First, we studied neurons in a low-contrast regime most appropriate for revealing detection mechanisms. Second, we analyzed the signal and noise components of neuronal responses in a way that is directly comparable to the psychophysical performance of the observer. Third, we measured neuronal responses directly, thereby obviating the need for stimulus manipulations to isolate detection mechanisms (e.g., habituation and noise masking) which can have complex effects on the responses of individual V1 neurons (Tailby et al. 2008a) and may affect task strategy (D'Zmura and Knoblauch 1998; Gegenfurtner and Kiper 1992). We conclude that even under these conditions, V1 neurons do not conform to the cardinal mechanisms model.

One potential concern with this conclusion is that detection might be mediated exclusively by the subset of neurons tuned to the cardinal color directions (e.g., those

with β3 near 1, see Eqs. 2.2 & 2.3). While this possibility is consistent with our data, it is not strongly supported by them: neurons tuned to the cardinal axes were uncommon and only moderately sensitive to chromatic contrast. TRs of neurons with β3 within ±1 SD of 1 were not significantly different than TRs of neurons with β3 outside of this range (t-test, $p = 0.78$). Similarly, β3s were not significantly correlated to TRs (Spearman's $r = 0.02$, $p = 0.85$). We thus find no evidence that V1 neurons tuned to the cardinal axes have a special role in chromatic detection.

An additional concern is that our main conclusion – that V1 neurons do not behave as the cardinal mechanisms at detection threshold – is dependent on the spatial properties of the stimulus we used. Indeed, color tuning is not, in general, separable from spatial tuning (Lennie et al. 1990; Johnson et al. 2001). For example, LGN neurons are tuned to the cardinal color directions when tested with full field stimuli but not when tested with stimuli that are spatially band-limited such as sinusoidal gratings (Lennie et al. 1990; De Valois et al. 2000). Although it is possible that we might have obtained a different result by using a different spatial stimulus, we found that restricting our analysis to neurons with a preferred spatial frequency < 1 cycle/deg did not change our main conclusion (data not shown).

Our use of spatially band-limited stimuli was motivated by two factors: First, neurophysiological investigations have shown that some V1 neurons are chromatically and spatially opponent. For example, Johnson, Hawken, & Shapley (2008) showed clear examples of double-opponent V1 neurons that appear to behave in accordance with the cardinal mechanisms model (e.g., Johnson et al. 2008, their Figure 1). Spatially band-limited stimuli drive these cells more strongly than full-field stimuli and are thus presumably a better choice for revealing the a contribution of these cells to visual processing. Second, we wanted to compare fairly the neurometric sensitivity of color-only and color-luminance V1 neurons. Neurons in these two groups tend to be tuned for different ranges of spatial frequency (Johnson et al. 2001), and their respective contribution to color vision is a matter of debate. Fixing the spatial frequency of the stimulus would likely have biased the result in favor of one group or the other (lower spatial frequencies favoring the color-only group). By tailoring the spatial frequency to the neuron under study, we found that neurons in both categories were approximately

equally sensitive. Our results suggest a role for band-pass V1 neurons in the detection of isoluminant stimuli and is consistent with psychophysical evidence postulating spatial frequency selective mechanisms for chromatic detection (Bradley et al. 1988; Losada and Mullen 1994; Mullen and Losada 1999; Webster et al. 1990).

We looked for trial-to-trial covariations between neuronal and psychophysical behavior (CP) but did not find compelling evidence for this relationship among the V1 neurons we studied. Although one study of V1 (Palmer et al. 2007) has reported significant CP for the population of V1 neurons taken as a whole, CP has not been solidly established as a characteristic of individual V1 neurons. Another notable study failed to find significant choice probability in V1 (Nienborg and Cumming 2006). Another reason that we may have failed to find significant CP in this study is that z-scoring distributions of low spike counts can corrupt CP measurements (Kang and Maunsell 2012). Improved methods of measuring weak relationships between neuronal responses and behavior might reveal such a pattern in our data, but for our purposes, such a method would have to be sufficiently sensitive at the level of individual neurons to be useful for identifying those that contribute to behavior (or those that are modulated by top-down signals).

Small signal linearity

A motivation to study color vision at detection threshold is that the complexities of adaptation and gain control are minimized, potentially leading to a closer-to-linear color vision system (Solomon and Lennie 2005; Solomon et al. 2004b; Tailby et al. 2008a). This is undoubtedly true at many levels of the visual system, but we were surprised by clear nonlinearities in V1 responses even in the low contrast regime.

One nonlinearity that all V1 neurons exhibit is a spike threshold which naturally exerts a strong effect at low contrasts. This nonlinearity was expected, and was thus included in the model we used to fit contrast-response functions (Eqs. 2.2 and 2.3). The model also assumes that CRFs in pairs of color directions can be equated by scaling the contrast axis. This would be the case for a linear neuron with a static output nonlinearity (e.g. spiking threshold), but was demonstrably untrue for 39% of the neurons we recorded. For these neurons, an analysis of deviance rejected the simple contrast scaling

model in favor of a more complex model in which the spiking threshold and contrast gain parameters were allowed to differ between color directions (data not shown).

An additional nonlinearity was the width of color tuning observed for some V1 neurons. 7 of the 11 neurons we tested in the L–M and S-cone isolating directions were sensitive to both color directions at detection threshold. A linear-model fit to the TRs for these neurons predicts an average intermediate color direction TR of 0.65, which is lower than any of the TRs we measured when we directly tested each neurons' preferred intermediate color direction.

We have previously shown that the responses of many V1 neurons to high chromatic contrast are poorly described by a linear model (Horwitz and Hass 2012), and the current data suggest that this observation extends to near-threshold contrasts. Some V1 neurons in the current study were sensitive at psychophysical threshold to both L–M and S-cone isolating color directions. These neurons may have had isoresponse surfaces that resemble ellipsoids or hyperboloids of one sheet. A few neurons (n = 17) were sensitive at psychophysical threshold to one of the colors we tested but not the neighboring color direction (45º away in the color space of Figure 2.2). These neurons may have had hyperbolic isoresponse surfaces. Unfortunately, we were unable to draw stronger connections between these two data sets despite the fact that we tested 20 neurons in both experimental paradigms. Isoresponse surfaces measured at near-threshold contrasts were too noisy to be interpreted, and isoresponse surfaces measured at higher contrasts (those described in Horwitz and Hass 2012) were insufficient to infer neural responses at detection threshold.

Effects of stimulus eccentricity

Most chromatic detection experiments in humans have been performed at the fovea, but our experiments were performed at ~5° eccentricity, where V1 neurons are easily accessed, exhibit cone opponency, and have RFs that are large with respect to fixational eye movements. The spatial distribution of cones and their convergence onto downstream neurons depends critically on eccentricity, leaving open the possibility that our results could change if we had performed our study at a different eccentricity. A decisive test of this idea would require repeating our experiment, recording from a different region of V1.

However, psychophysical evidence from humans suggests that the cone inputs to the detection mechanisms that operate 18° in the periphery are similar to those at the fovea (Newton and Eskew 2003) although the relative sensitivity of these mechanisms depends on eccentricity (Mullen and Kingdom 1996; Mullen and Kingdom 2002).

We controlled the activity of the L-, M-, and S-cones using the method of silent substitution. Our use of human cone fundamentals in the silent substitution calculations is justified by the similarity in photopigment absorption spectra between monkeys and humans (Baylor et al. 1987). Nevertheless, it is likely that the 2º cone fundamentals we used in the majority of our experiments resulted in incomplete cone-isolation due to the relatively large eccentricity of the neurons we recorded (mean RF eccentricity = 5.14º SD = 0.88º). The 10° fundamentals presumably provided better cone isolation.

The major difference between the 2° and 10° cone fundamentals is that the 2° fundamentals implicitly assume a higher density of macular pigment. Macular pigment is dense in the fovea but is largely absent > 5° from the fovea (Snodderly et al. 1984). Because it absorbs short wavelength light preferentially, macular pigment affects the shape of the S-cone fundamental. As a result, high-contrast nominally S-cone isolating stimuli based on the 2° fundamentals can have appreciable luminance artifacts when presented outside of the fovea (Cottaris 2003; Sun et al. 2006).

The impact of this error on the results of our experiments is minimal because stimulus contrasts were low. The highest psychometric threshold for S-cone isolating stimuli corresponded to the point [0, 0, 0.17] in L-, M-, S-cone contrast space when represented using the 2º fundamentals, but corresponds to the point [0.0029 0.0072 0.172] when calculated using the 10º fundamentals. This introduces an L+M artifact of 0.71% cone contrast and an L–M artifact of 0.30% cone contrast. These contrasts were below detection threshold for both monkeys across all spatial frequencies we tested (see Methods: Spatial contrast sensitivity, and Figure 2.3). Moreover, the error in S-cone contrast (0.20% cone contrast) is small relative to the standard deviation of detection thresholds for S-cone isolating lights based on 2º cone fundamentals (average SD across spatial frequencies and monkeys = 0.93% contrast). As an extra precaution, we used the 10º fundamentals (Stockman et al. 1993) in a subset of experiments. The data from these experiments (n = 30) were neither qualitatively nor quantitatively different than the data

collected using the 2º fundamentals. Future studies of color processing in the macaque cerebral cortex will benefit from accurate measurements of corneal cone fundamentals specifically for these animals.

Effects of microsaccades on contrast detection and responses of V1 neurons

During free viewing, and even nominal fixation, humans and monkeys make several saccades per second. Each saccade shifts the pattern of light falling on the retina, but the visual world remains perceptually stable. This stability is thought to be due in part to saccadic suppression, which is a reduction in visual sensitivity around the time of saccades (for a review see, Matin 1974).

Saccadic suppression is profound during large amplitude saccades but is subtle or absent during microsaccades, which are small, involuntary saccades that occur naturally during fixation. Depending on the stimulus conditions and behavioral task, microsaccades can decrease visual sensitivity (Riggs et al. 1953; Ditchburn 1955; Zuber and Stark 1966; Beeler 1967), increase visual sensitivity (Deubel and Elsner 1986; Kelly 1990; Rucci and Desbordes 2003; Martinez-Conde et al. 2006), or exert no effect (Krauskopf et al. 1966) in human observers. These disparate observations can be understood as combinations of top-down suppressive signals (related to corollary discharge), bottom-up suppressive signals (e.g. blur and visual masking) and bottom-up facilitatory signals (e.g. relief from image fading).

We know less about the effects of microsaccades on the vision of macaque monkeys, a popular animal model in studies of visual neurophysiology. Understanding how microsaccades affect the vision of this animal is important for interpreting the results of neurophysiological experiments (e.g. Harwerth et al. 1993; Geisler and Albrecht 1997; Chen et al. 2006; Palmer et al. 2007; Chen et al. 2008). For example, microsaccades made by monkeys performing visual motion detection tasks exert two (possibly related) effects: they increase thresholds for changes in visual motion and suppress the responses of visual motion-sensitive neurons (Herrington et al. 2009). Together, these effects contribute to a correlation between neural activity and behavioral responses. We sought to determine whether microsaccades also influence contrast detection.

This chapter was published in The Journal of Vision, which maintains copyrights for this material, and has been reprinted with permission. The full citation for this publication is:

Hass, C.A., & Horwitz G.D. (2010). *Effects of microsaccades on contrast detection and responses of V1 neurons.* The Journal of Vision. 11(3): 1–17, 2011.

Large amplitude saccades (~20°) increase detection thresholds in humans for luminance but not chromatic contrast (Burr et al. 1994; Uchikawa and Sato 1995; Burr and Morrone 1996; Diamond et al. 2000). This specificity has motivated the hypothesis that the magnocellular visual pathway is suppressed selectively during saccades. Electrophysiological tests of this hypothesis have yielded mixed results (Ramcharan et al. 2001; Reppas et al. 2002; Royal et al. 2006). An alternative possibility is that mechanisms responsible for the luminance specificity of saccadic suppression act on cone non-opponent neurons at a higher level of the visual system. To address this possibility, we asked whether cone-opponent and non-opponent neurons in area V1, the next stage of visual processing, are differentially modulated by microsaccades.

Methods

Two monkeys (M. mulatta) participated in the experiments. All procedures conformed to the guidelines provided by the NIH and the University of Washington Animal Care and Use Committee. Each monkey was implanted with a titanium headpost to eliminate head movements and a monocular scleral search coil to measure eye position (Judge et al. 1980). During experimental sessions, the monkey sat in a primate chair 100 cm from a cathode ray tube (CRT) monitor in an otherwise dark room. Eye position signals were low-pass filtered with an 8-pole Bessel filter (180 Hz high frequency cutoff), digitized at 1 kHz, and stored to disk at 500 Hz. Event timing and eye position monitoring were mediated by a PC running the REX software package (NIH). Data were acquired for offline analysis with a Plexon MAP system (Plexon, Inc.). Single unit recordings were made with extracellular glass-insulated transdural tungsten electrodes with impedances ranging from 1-2 MΩ (Frederick Haer, Inc.). Neural signals were amplified and filtered with standard techniques, and spikes were isolated offline on the basis of waveform timing, shape, and amplitude criteria.

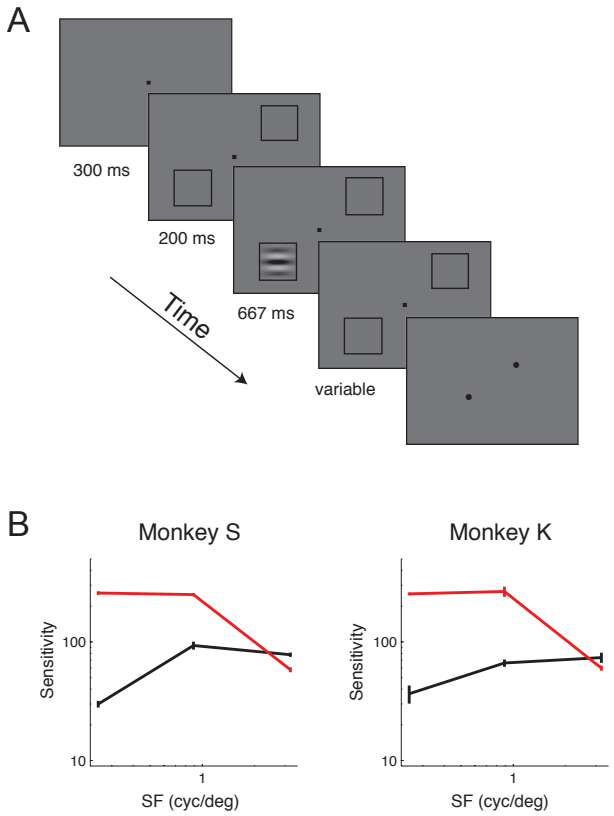

Figure 3.1 A: Ordered screenshots from the 2AFC contrast detection task. See text for details of the experimental methods. B: Contrast sensitivity of two monkeys as a function of color direction and spatial frequency. Stimuli varied in red-green contrast (red curve) and achromatic (luminance) contrast (black curve). Sensitivity is quantified as the reciprocal of the detection threshold, as estimated by the QUEST adaptive procedure (Watson and Pelli 1983). Throughout this report, contrast is represented in units of cone-contrast vector lengths $\text{Contrast} = \sqrt{\left(\frac{\Delta L}{L}\right)^2 + \left(\frac{\Delta M}{M}\right)^2 + \left(\frac{\Delta S}{S}\right)^2}$. A sensitivity of '1' thus represents a contrast of 0.58% to each cone type in the achromatic condition, and a contrast of 0.71% to the L and M cones in the red-green condition. Error bars are ±1 SEM.

Monkeys were trained to perform the two-alternative forced choice (2AFC) contrast detection task shown in Figure 3.1A. Each trial began when the monkey acquired a central fixation point. Three hundred milliseconds later, a pair of black 3.6 x 3.6° square frames appeared, one 5.0° to the right and 3.5° above the fixation point and the other 5.0° to the left and 3.5° below the fixation point. Two hundred milliseconds later, a horizontally oriented Gabor stimulus appeared inside one square for 667 ms. The monkeys' task was to identify the square in which the Gabor stimulus appeared.

Monkeys indicated the location of the stimulus by making a saccadic eye movement. At a random time 100-600 ms after the stimulus presentation, the fixation point disappeared and a pair of saccade targets appeared simultaneously. A saccade to the target in the direction of the Gabor stimulus was a correct response and was reinforced with a juice reward. Feedback was not provided following incorrect responses. In most experiments, saccade targets appeared 3° from the fixation point, but in a few experiments, they were positioned asymmetrically to mitigate choice biases. Trials were aborted whenever the monkey's eye position prematurely left a 1 x 1° electronically defined window around the fixation point.

Microsaccade detection

Microsaccades were detected using an algorithm used previously by Horwitz and Albright (2003). Eye velocity was computed by filtering horizontal and vertical eye position records with a smoothed differencing operator (a differencing operator convolved with a Gaussian of 4 ms standard deviation). A microsaccade was identified as a deflection of the eye during which eye speed (the vector norm of the horizontal and vertical velocities) exceeded 10°/sec for at least 8 consecutive ms. Pairs of microsaccades occurring within 40 ms of each other were considered a single movement. Visual inspection of eye position records confirmed that the movements identified by the algorithm appeared to be microsaccades.

Stimuli: Psychophysics

Stimuli were presented on a CRT monitor (Sony Trinitron) whose phosphor emission spectra and voltage-intensity relationships had been characterized with a spectroradiometer (PR650, PhotoResearch). A digital video signal processor (Bits++, Cambridge Research) increased the depth of each color channel from 8 to 14 bits. This increase was bought at the expense of spatial resolution; each pixel in the display was twice as wide as it was tall. Stimuli were generated using the Psychophysics Toolbox (Brainard 1997) for Matlab on a Mac Pro computer. The background of the screen was uniform gray (CIE coordinates: x = 0.33, y = 0.33, Y = 90 cd/m2).

The Gabor stimulus had a standard deviation of 0.8° and was truncated beyond 2 standard deviations. The sinusoidal component drifted upwards at 3 Hz and had a spatial frequency of 0.25, 0.89, or 3.22 cycles/degree. These spatial frequencies were selected to span the range over which saccadic suppression occurs (Burr et al. 1994) without extending to yet lower spatial frequencies that are unobtainable given the Gaussian envelope we used. To avoid detectable visual transients, the contrast of the Gabor was modulated according to a trapezoidal temporal envelope; the contrast ramped up linearly over the first half-cycle of the stimulus (167 ms), remained constant over the next cycle (333 ms), and ramped down linearly over the last half-cycle (167 ms).

The stimulus modulated in two color directions based on the Stockman, MacLeod, and Johnson 2° cone fundamentals (Stockman et al. 1993). The achromatic stimulus modulated each of the three cone types with identical cone contrast. The red-green stimulus modulated the L- and M-cones with identical contrast but in opposite phase. Stimulus contrast was determined on each trial by the QUEST adaptive staircase procedure (Watson and Pelli 1983). The QUEST procedure decrements the contrast following correct trials and increments the contrast following incorrect trials, thereby ensuring that the stimulus remains near detection threshold throughout the experiment. The first 10 trials of each staircase were omitted from the analysis. In each experimental session, at least six independent staircases were randomly interleaved: one for each combination of color and spatial frequency (except for 5 sessions with Monkey K in which the 0.89 cpd stimulus did not appear).

Stimuli: Neurophysiology

We stimulated most of the V1 neurons we studied with a dynamic white-noise stimulus. The stimulus was a 10 x 10 square grid of 0.1 x 0.1° elements whose colors changed synchronously and independently at 75 Hz. The color of each stimulus element was determined by independent Gaussian draws from red, green, and blue monitor phosphor intensity distributions. This stimulus modulates in chromaticity and luminance, and it modulates the spiking activity of cone-opponent and non-opponent neurons. The cone weights of V1 neurons stimulated in this way can be estimated through an analysis of the spike-triggered average stimulus (STA) (Horwitz et al. 2007). We studied the

responses of a smaller set of neurons to the Gabor stimulus during performance of the contrast detection task. In these experiments, the orientation and spatial frequency of the Gabor stimulus was tailored to the preferences of the neuron under study.

Statistics

Contrast detection thresholds in Figure 3.1B were obtained from the modal values of the QUEST function at the end of each session (Watson and Pelli 1983). This approach cannot be used to measure detection thresholds separately for trials on which a microsaccade occurred or did not occur during the stimulus presentation; QUEST does not maintain a separate staircase for these two types of trials. Instead, we quantified changes in detection threshold due to microsaccades by fitting the data from each stimulus condition with a cumulative Weibull function:

$$y = 1 - 0.5\ e^{-\left(\frac{x}{\beta_0 + \beta_1 \times I_{sac}}\right)^{\beta_2}} \quad \text{(Eq. 3.1)}$$

where y is a binary variable that equals 1 for correct trials and 0 for incorrect trials, x is cone-contrast of the stimulus (quantified as the length of the vector of cone contrasts), and Isac is a binary variable that equals 1 for saccade trials and 0 for no saccade trials. The β_i are parameters fitted by maximum likelihood assuming binomially distributed errors. β_o is the threshold on no saccade trials, $\beta_o+\beta_1$ is the threshold on saccade trials, and β_2 is a slope parameter. The change in threshold due to microsaccades in log units is:

$$\log_{10}\left(\frac{\beta_0 + \beta_1}{\beta_0}\right) \quad \text{(Eq. 3.2)}$$

Statistical significance of threshold changes was assessed by comparing the fit of the full model (Eq. 3.1) with the fit of the nested model in which β_1 was constrained to be 0 (analysis of deviance, McCullagh and Nelder 1989).

We used a non-parametric bootstrap procedure to test whether microsaccade vectors predicted task performance. Microsaccade vectors (direction and amplitude) preceding correct and incorrect responses were sorted into separate groups and the Euclidean distance between the centroids (mean vectors) of each group was recorded. Vectors were then resampled with replacement from the empirical distribution (the union of vectors

from correct and incorrect trials binned at 0.1 x 0.1˚), randomly reassigned to "correct" and "incorrect" groups, and the distance between centroids was recalculated. This procedure was repeated 10,000 times to estimate the distribution of intercentroid distances under the null hypothesis. The fraction of intercentroid distances from the resampled data sets that exceeded the intercentroid distance from the original data set is the p-value reported. The same procedure was used to test the hypothesis that microsaccade vectors depended on the target choice, but in this analysis vectors were grouped by which target the monkey chose at the end of the trial.

We calculated microsaccade-triggered spike-density functions for 21 V1 neurons during the detection of low contrast, red-green Gabor stimuli. These functions show changes in firing rate that are time-locked to microsaccades. To measure changes in firing rate that were not time-locked to microsaccades, we also performed a control version of this analysis in which we randomly permuted the association between the times of microsaccades and spikes across trials. These permutations preserve the temporal statistics of microsaccades and spikes but break any relationship between them. In this control analysis we constructed 200 randomly permuted data sets for each neuron, calculated a spike-density function from each data set, normalized each function by dividing it by its maximum, and averaged the 200 normalized spike-density functions together.

Results

Monkey K performed 14,577 trials of the contrast detection task and Monkey S performed 22,452 trials. Monkey K made 9,397 microsaccades during task performance and Monkey S made 35,996 microsaccades. Below, we summarize the metrics and timing of microsaccades and show that they are associated with increases in achromatic, but not red-green, detection thresholds. We then show that the responses of cone-opponent and non-opponent neurons in V1 are modulated similarly by microsaccades, suggesting that the color specificity of microsaccadic suppression originates downstream of V1.

Detection performance

Figure 3.1B shows contrast sensitivity for the 2 monkeys as a function of color direction and spatial frequency. The monkeys, like human observers, exhibited lowpass sensitivity for chromatic stimuli and attenuated sensitivity for low frequency, achromatic stimuli (Mullen 1985). The monkeys were slightly more sensitive than a human observer viewing the identical display (Hass and Horwitz 2010). These observations demonstrate that the monkeys' behavior was under stimulus control.

Microsaccades

Monkeys made frequent microsaccades while performing the 2AFC detection task. The movements we analyzed were necessarily small (mean amplitudes for Monkeys K and S were 0.34° and 0.25°, respectively; see Figures 3.2A and 3.2B) because eye movements that caused the eye to leave the fixation window aborted trials. The relationship between amplitude and speed shown in Figures 3.2C and 3.2D follows the "main sequence" and is consistent with the classification of these movements as saccades (Zuber et al. 1965). Monkey K tended to make saccades with a downward component (Figure 3.2E), whereas Monkey S tended to make saccades along the axis of the stimulus locations (Figure 3.2F).

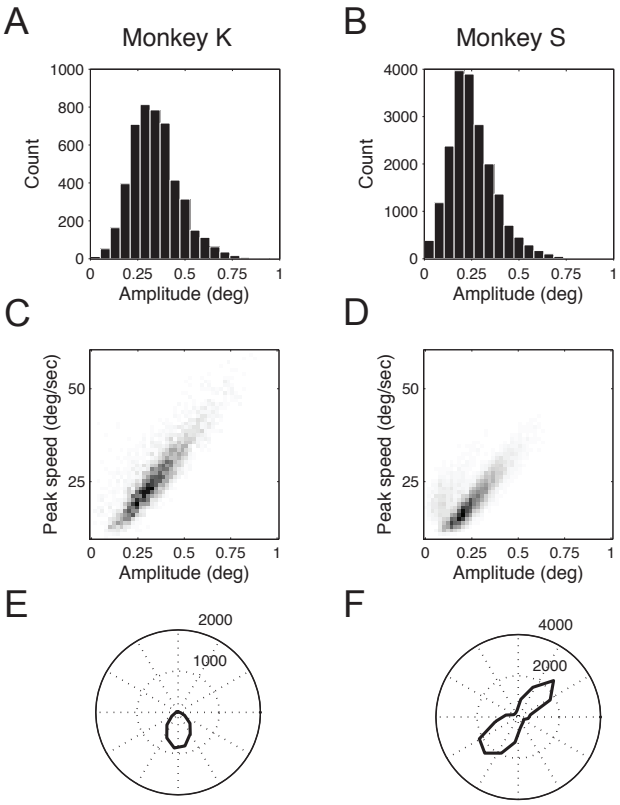

Figure 3.2 Metrics of microsaccades made during performance of the contrast detection task. A, B: Histogram of microsaccade amplitudes. C, D: Microsaccade peak speed vs. amplitude (saccadic main sequence). E, F: Polar histograms of saccade directions.

Figures 3.3A and 3.3B show the temporal distribution of microsaccades across the trial. For both monkeys, microsaccade rates peaked around the time of the onset of the Gabor stimulus. This peak is not due to any detectable visual event occurring at this time; the stimulus contrast ramped up gradually over the course of 167 ms and remained close to detection threshold. Omitting the square frames from the display eliminated these peaks (see dashed curves in Figure 3.3A&B) suggesting that they might represent a brief release from microsaccadic inhibition associated with the change in the visual display (Engbert and Kliegl 2003; Rolfs et al. 2008). Microsaccade rates during the stimulus presentation were low for both monkeys (Monkey K: 0.5 saccades/sec, Monkey S: 1.2 saccades/sec), suggesting that microsaccades are actively suppressed during this time.

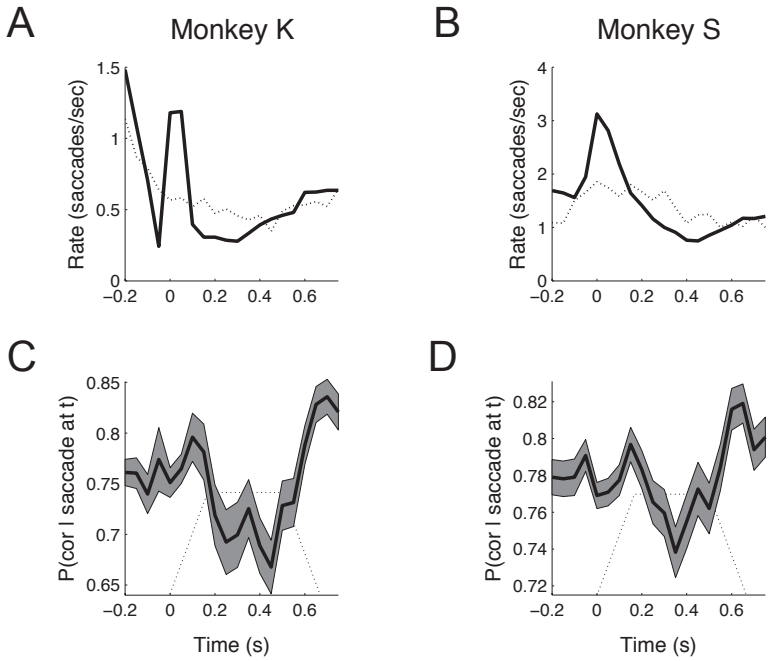

Figure 3.3 Time course of microsaccade occurrence and relationship to task performance. A, B: Peristimulus time histogram of microsaccade initiations. Data are aligned on stimulus onset (t = 0). Dotted curves shows microsaccade initiations in a set of control trials in which the frames did not appear. C, D: Proportion of correct choices as a function of when a microsaccade was made. Shaded area represents ±1 standard error of binomial proportion. Dotted line indicates time course of stimulus presentation. Y-axis position of dotted line in panels C and D is arbitrary. Note the different y-axis scales in A and B and in C and D.

Relationship between microsaccades and task performance

Suppressing microsaccades would be adaptive if they impair contrast detection. To explore this possibility, we compared performance on trials that had at least one microsaccade during the plateau phase of the stimulus (saccade trials) to those lacking microsaccades during this interval (no saccade trials). No saccade trials outnumbered saccade trials; the percentage of no saccade trials was 88% for Monkey K and 68% for Monkey S. Consistent with the idea that microsaccades impair contrast detection, the percentage of correct saccade trials was lower than the percentage of correct no saccade trials (Monkey K: 70 vs 76%, $p < 0.01$; Monkey S: 76 vs 78%, $p < 0.05$, z-tests of differences in binomial proportions). This result suggests that microsaccades impair contrast detection in monkeys. This result could be trivial if the monkeys made more microsaccades on low contrast trials than on high contrast trials, but this was not the case;

mean stimulus contrast was actually higher on saccade trials than on no saccade trials in 4 out of 6 conditions for monkey K and in 6 out of 6 conditions for monkey S.

The preceding analysis leaves open the possibility that microsaccades during trial epochs other than the stimulus plateau were also related to task performance. To measure the time course of the relationship between microsaccades and percent correct, we divided each trial into non-overlapping 100-ms bins. Within each bin, the proportion of correct trials was calculated across the subset of trials containing a microsaccade in that bin. As shown in Figures 3.3C and 3.3D, a dip in performance is apparent around $t = 0.3$ for both monkeys. Thus, poor performance is associated specifically with microsaccades during the stimulus plateau and not other times during the trial. The improvement in performance associated with microsaccades made late in the trial ($t > 0.6$ in Figures 3.3C and 3.3D) will be discussed in the section entitled, Relationship between microsaccade metrics and choices.

Influence of color and spatial frequency

Large amplitude saccades preferentially impair the detection of low spatial frequency, achromatic patterns (Burr et al. 1994). We asked whether microsaccadic suppression in our experiment had similar stimulus specificity. For each of the 6 conditions (2 colors x 3 spatial frequencies), we compared percent correct between no saccade and saccade trials. Both monkeys had a significantly higher percent correct on no saccade trials than on saccade trials when the stimulus was achromatic and had a spatial frequency ≥ 0.89 cpd (z-tests of differences in binomial proportions, $p < 0.05$; Figure 3.4A&B black bars). For Monkey K, but not Monkey S, this detrimental effect of microsaccades extended to lower spatial frequency achromatic stimuli (0.25 cpd). When the stimulus was red-green, performance on saccade and no saccade trials did not differ significantly for either monkey at any spatial frequency ($p > 0.05$; Figure 3.4A&B, red bars). Microsaccades are thus associated with poor task performance when the stimulus is achromatic but not when it is red-green.

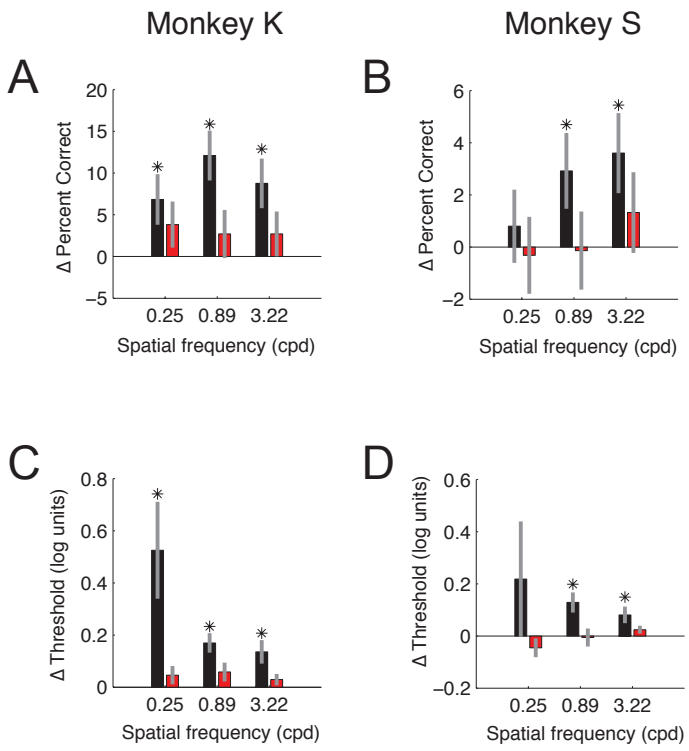

Figure 3.4 Summary of microsaccadic suppression. A, B: Effects of microsaccades during the stimulus plateau on percent correct. Δ Percent Correct is defined as the percentage of no saccade trials ending in a correct choice minus the percentage of saccade trials ending in a correct choice. Asterisks indicate significant differences in percentage of correct trials (z-tests for binomial proportions, $p < 0.05$). Error bars are ±1 standard error of the difference in binomial proportion. C, D: Effects of microsaccades during the stimulus plateau on detection thresholds assessed from psychometric function fits. Asterisks indicate significant differences in thresholds between saccade and no saccade trials (analysis of deviance, $p < 0.05$) (McCullagh and Nelder 1989). Error bars are ±1 standard error obtained by bootstrap resampling. Black bars show data from achromatic trials, red bars show data from red-green trials.

Detection thresholds, unlike percent correct, are unbounded and provide an intuitive measure of the magnitude of the change in visual sensitivity. Threshold changes, shown in Figures 3.4C and 3.4D, were significant in all achromatic conditions ($p < 0.05$) except for the 0.25 cpd condition for Monkey S ($p = 0.34$). The magnitudes of these effects were modest: across spatial frequencies, the median change in threshold was 0.17 log units for Monkey K and 0.13 log units for Monkey S. When the stimulus was red-green, threshold changes were not significant at any spatial frequency. Together, these analyses support the idea that microsaccades impair the detection of achromatic stimuli more than red-green stimuli across a range of spatial frequencies.

Relationship between microsaccade metrics and choices

Microsaccades vary in direction and amplitude, and the relationship between detection performance and microsaccade occurrence might depend on these metrics. For example, downward microsaccades increase the speed of the (upward moving) stimulus on the retina which in turn could make the stimulus easier or more difficult to detect. In this case, the vertical component of microsaccades would predict whether the monkey will make the correct choice at the end of the trial. Alternatively, microsaccades might invoke suppressive mechanisms when their amplitude exceeds a threshold, in which case microsaccade amplitude would be predictive of percent correct.

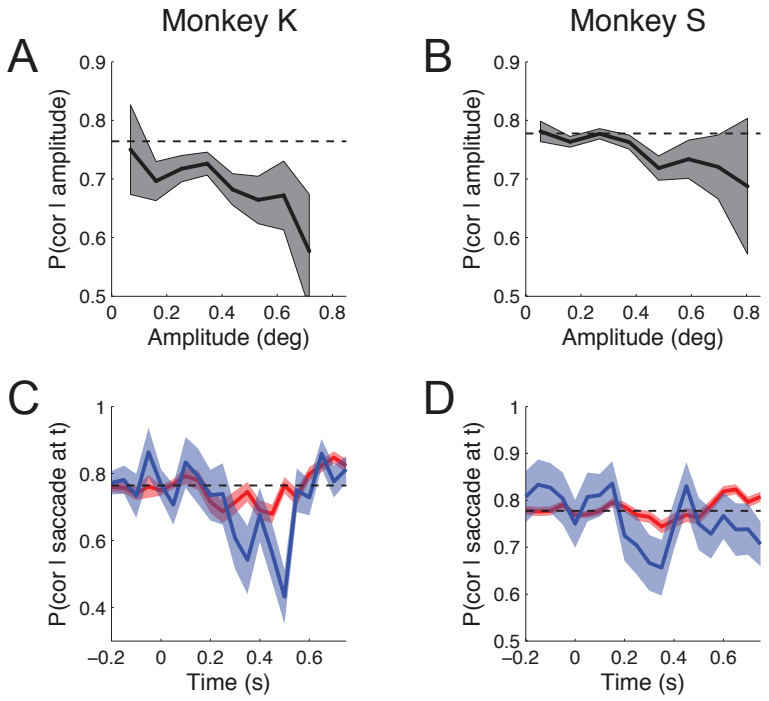

Figure 3.5 Effect of microsaccade amplitude on suppression. A, B: Proportion of correct choices as a function of microsaccade amplitude. C, D: Proportion of correct choices as a function of when a microsaccade occurred. Blue curve shows data from large (≥0.5°) amplitude microsaccades and red curve shows data from small (<0.5°) amplitude microsaccades. In all panels, dashed lines show the proportion of correct choices on no saccade trials, and shaded areas represents ±1 standard error of a binomial proportion.

We addressed these possibilities with two analyses. In the first, we binned microsaccades made during the stimulus plateau according to their amplitude and then computed percent correct across trials that contained a microsaccade in each bin. Bins containing fewer than 10 microsaccades were omitted from this analysis. As shown in

Figures 3.5A and 3.5B, percent correct decreased with microsaccade amplitude for both monkeys (Monkey K: weighted least-squares regression slope = -0.24, $p < 0.01$; Monkey S: slope = -0.11, $p < 0.001$). On trials containing a large microsaccade ($\geq 0.5°$) during the stimulus plateau, percent correct was lower than on trials containing a microsaccade of lower amplitude (Monkey K: 65 vs 71%, $p = 0.05$; Monkey S: 72 vs 78%, $p < 0.05$, z-tests for equality of binomial proportions). Consistent with this relationship, microsaccade amplitudes during the stimulus presentation were slightly larger on error trials than on correct trials (Monkey K: 0.35 vs 0.34°, $p = 0.08$, two-sample t-test, Monkey S: 0.27 vs 0.26°, $p < 0.05$). Figures 3.5C and 3.5D show the time course of microsaccadic suppression separated by saccade amplitude.

To probe the relationship between percent correct and microsaccade vector (amplitude and direction considered jointly), we plotted distributions of microsaccade vectors at different times during the trial and asked whether probability correct depended on microsaccade vector. In the top rows of panels in Figure 3.6 (labelled "p(correct)"), color represents the probability that the monkey makes a correct response at the end of the trial. Warm and cool colors represent a high and low probability that the trial will be answered correctly, respectively. Colors were assigned by binning microsaccade vectors, coding them according to trial outcome (correct or incorrect), and computing the proportion of correct trials in each bin. For visual clarity, bins with fewer than 10 vectors were omitted from the analysis.

These plots, which appear in the upper row of panels of Figure 3.6 for each monkey, lack clear spatial structure suggesting that microsaccade vectors are not strongly related to percent correct. Nevertheless, a bootstrap test on the centroids of microsaccade vectors preceding correct and incorrect choices uncovered a weak relationship that evolves late in the trial. Microsaccades with a large downward component tend to precede incorrect choices. In Figure 3.6, centroids of microsaccade vectors preceding correct and incorrect choices are represented by white and black dots respectively in panels for which the difference between them was significant. The distance between the white and black dots was increased by a factor of 10 to better illustrate their relative positions. The intercentroid distance was significant for Monkey K from $t \geq 0.55$ and for Monkey S from $t \geq 0.4$ (asterisks in Figure 3.6, $p < 0.05$) and the white dot lies

consistently above the black one. At first glance, this result is consistent with the idea that downward microsaccades induce stronger suppression than upward microsaccades, but the emergence of this effect late in the trial suggests a different interpretation.

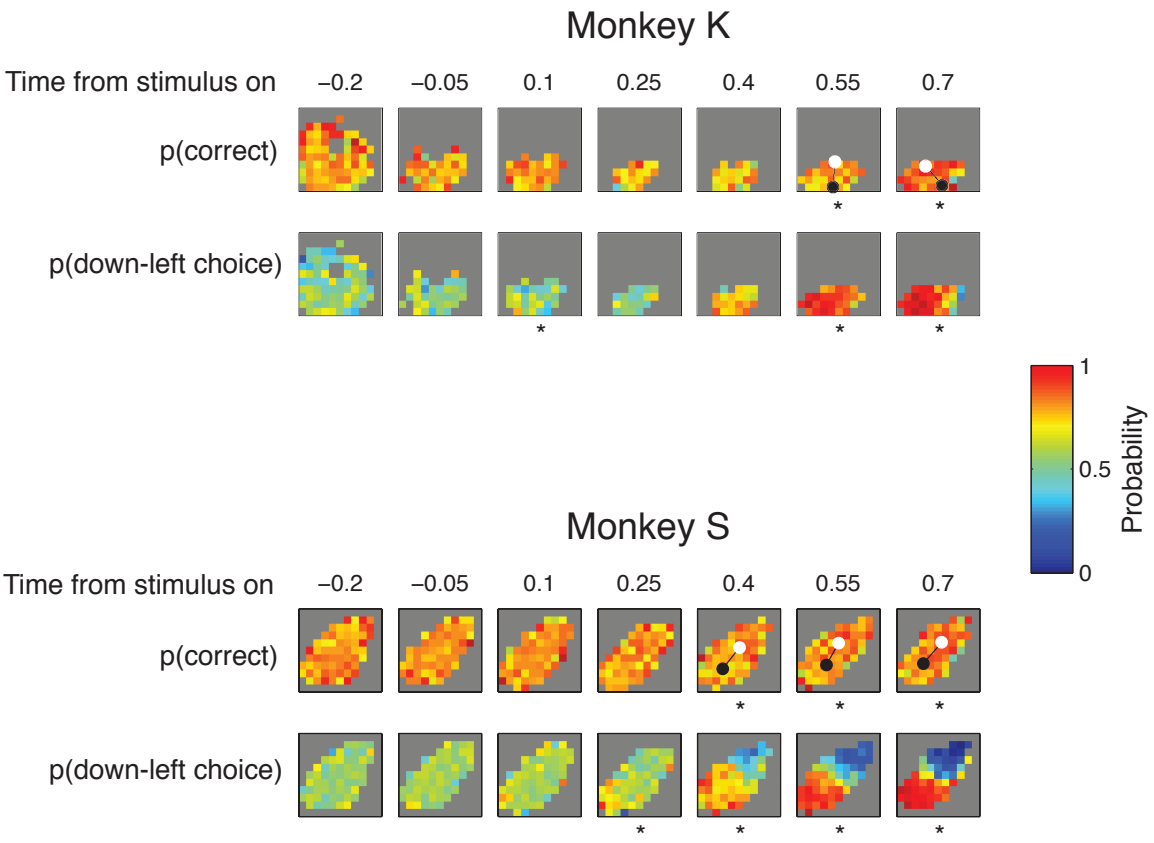

Figure 3.6 Probability of correct choices and down-leftward choices as a function of microsaccade vector and time. The center of each time bin (in seconds) appears above the upper panels (stimulus onset at time 0). Upper panels for each monkey: color represents probability correct. Lower panels for each monkey: color represents the probability of a choice to the lower-left hand target. Bins containing fewer than 10 trials were excluded from the analysis. Asterisks indicate epochs during which the mean microsaccade vector differed significantly ($p < 0.01$) between conditions (correct vs. incorrect in the upper panels or T1 vs. T2 choices in the lower panels) by a nonparametric bootstrap test. White and black dots in upper panels represent the mean vector of microsaccades preceding correct and incorrect choices, respectively. The distance between the white and black dots has been increased 10-fold to prevent overlap between the symbols.

The relationship between microsaccade direction and percent correct can be explained by a choice bias. Both monkeys made more choices (and more errors) to the lower-left target than the upper-right target (data not shown). Moreover, before making a

choice to the lower-left target, the monkeys tended to make more downward microsaccades than upward microsaccades (shown below). Together, these two effects account for the fact that downward microsaccades tended to precede incorrect choices (to the lower-left target).

An analysis of microsaccade vectors preceding upward and downward choices supports this interpretation. This analysis was identical to that shown in the upper panels of Figure 3.6 except that vectors were colored to reflect the probability that the monkey chose the lower-left target. Results from this analysis appear in the lower row of panels in Figure 3.6 (labelled "p(down-left choice)"). Using a bootstrap test analogous to the one described above, we found that microsaccade vectors predicted target choices ~550 ms after the onset of the visual stimulus for Monkey K and ~250 ms after the onset of the stimulus for Monkey S. Monkey K tended to make downward saccades preceding downward choices but rarely made upward microsaccades preceding upward choices. Monkey S tended to make microsaccades in the direction of the chosen target. These effects became stronger as the trial progressed; for Monkey S, an upward microsaccade following stimulus disappearance preceded an upward choice ~10 times more often than a downward choice.

The relationship between microsaccade vectors and percent correct can thus be explained as a consequence of the relationship between microsaccade vectors and target choice. Can we account for the relationship between microsaccade occurrence and percent correct (Figures 3.3, 3.4, and 3.5) this way also? We cannot; performance on achromatic saccade trials was worse than on achromatic no saccade trials even when the analysis was restricted to choices made to single targets (Monkey K: downward target 66 vs 74% correct, $p < 0.01$, upward target 70 vs 80% correct, $p < 0.01$; Monkey S: downward target 74 vs 77% correct, $p < 0.01$, upward target 82 vs 82% correct, $p = 0.81$). We conclude that microsaccades during the presentation of an achromatic stimulus are associated with elevated detection thresholds, and that this effect depends little on the target the monkey chooses or microsaccade vector.

Influence of microsaccades on V1 neuron responses

Microsaccades affect the firing rates of neurons at many stages of the visual system (Bair and O'Keefe 1998; Leopold and Logothetis 1998; Martinez-Conde et al. 2000; Snodderly et al. 2001; Kagan et al. 2008; Hafed and Krauzlis 2010). At least some of these modulations likely contribute to saccadic suppression. The fact that microsaccades affect chromatic and achromatic detection thresholds differently implies a differential modulation of achromatic and chromatic signals somewhere in the brain. Whether magnocellular neurons in the LGN are suppressed preferentially during saccades is controversial (Ramcharan et al. 2001; Reppas et al. 2002; Royal et al. 2006). We tested the idea that microsaccades preferentially suppress firing in cone-nonopponent neurons in area V1.

We recorded from 52 L-M opponent and 61 L+M nonopponent V1 neurons from Monkey K during random visual stimulation. Cone inputs were estimated and cells classified on the basis on an analysis of spike-triggered stimulus averages (STAs) (Horwitz et al. 2007). Neurons were stimulated with a 10 x 10 checkerboard stimulus in which the color of each 0.1 x 0.1° element changed independently at 75 Hz (details of the stimulus and analysis can be found in Horwitz et al. 2007). The mean receptive field location of the recorded neurons was at (-3.1, -4.8°), which is closely matched to the location of the lower-left Gabor stimulus in the contrast detection task. The sample of neurons was thus representative of those available for mediating performance on the detection task.

STAs are shown for 16 nonopponent neurons in Figure 3.7A and for 16 cone-opponent neurons in Figure 3.7C. For each cell, we aligned spike rasters to microsaccade initiations and averaged across them to derive a microsaccade-triggered spike-density function (SDF). SDFs are displayed in Figures 3.7B and 3.7D at the corresponding position of each STA. Some neurons were suppressed after microsaccades, others were excited, and others exhibited a suppression followed by an excitatory rebound. We found no clear relationship between SDFs and the spatial structure of STAs.

Nor did we find a clear relationship between SDFs and cone opponency. Figure 3.8A shows SDFs for each of the 113 neurons represented as a stack of vertically concatenated grayscale raster lines. To compensate for differences in firing rate across

cells, each SDF was normalized by division by its maximum. On average, microsaccades evoked a brief suppression and then a rebound in spiking activity in both cone-opponent or non-opponent neurons (Figure 3.8B). Comparison of normalized SDFs from the dip (50 - 100 ms postsaccade) or rebound (120 - 300 ms postsaccade) in activity did not differ significantly between opponent and non-opponent neurons (dip: $p = 0.17$, rebound: $p = 0.32$, unpaired t-tests).

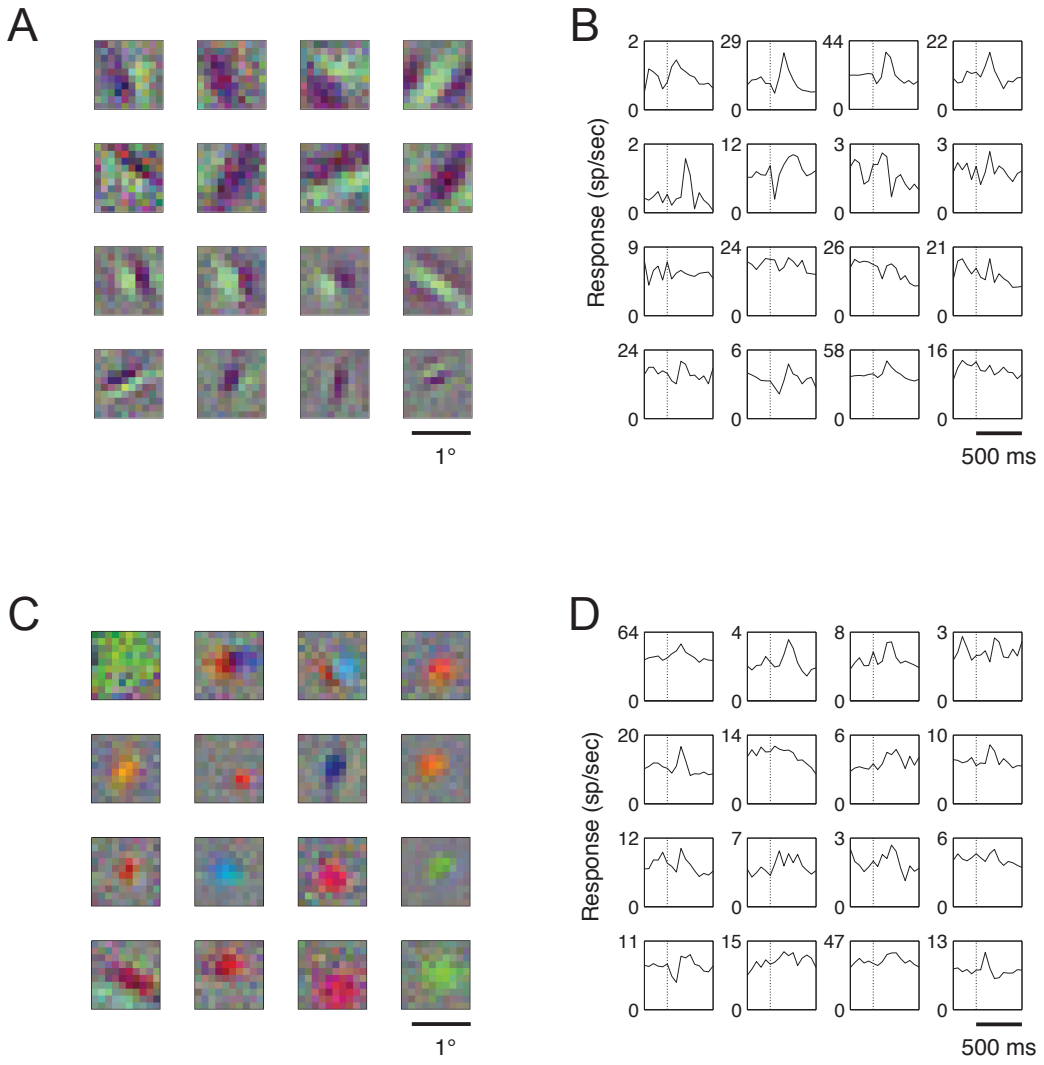

Figure 3.7 A,C: Spike-triggered averages (STA) for 16 neurons with non-opponent L and M cone weights (A) and for 16 neurons with opponent L and M cone weights (C). B, D: Microsaccade-triggered spike density functions. Dotted lines indicate the time of microsaccade initiation. Data from single neurons appear at corresponding locations in panels A and B (and similarly in panels C and D).

To express suppression in percent change in firing rate, we divided the firing rate during the dip by the maintained firing rate over the 250 ms preceding microsaccade initiation. Figure 3.8C shows how suppression quantified this way varies with maintained firing rate. The geometric mean suppression across all neurons (dashed line) was 0.83, implying a 17% reduction in firing rate ($p < 0.0001$, one-sample t-test). Suppression was not significantly related to the maintained firing rate (Pearson's $r = 0.028$, $p = 0.77$), but was significantly greater for non-opponent neurons (22%) than cone-opponent neurons (11%) (two-sample t-test, $p < 0.05$). This difference between cone-opponent and non-opponent neurons is consistent with the greater effect of microsaccades on the detection of achromatic relative to red-green stimuli, but was contingent on the inclusion of two cone-opponent neurons (circled in Figure 3.8C) that responded above baseline during the 50-100 ms following a microsaccade. Omitting these two neurons from the analysis eliminated the difference between cone-opponent and non-opponent neurons (two-sample t-test: $p = 0.17$).

To determine whether the suppression of V1 responses following microsaccades depended on saccade amplitude, as perceptual suppression does, we computed for each neuron the correlation between microsaccade amplitude and the firing rate during the 50-100 ms following a microsaccade. The average correlation coefficient was 0.003, which was not significantly different from 0 ($p = 0.57$ one-sample t-test). Our data thus provides no evidence that microsaccadic suppression of V1 responses depends on microsaccade amplitude.

The white noise stimulus had the same average luminance and chromaticity as the Gabor stimulus, but it differed in spatiotemporal contrast. The possibility therefore remains that microsaccades modulate the activity of V1 neurons when they are stimulated with white noise stimuli but not low contrast, red-green Gabor stimuli. To address this possibility, we recorded V1 responses during performance of the 2AFC detection task. In these experiments, the square frames were not shown, and the stimulus contrasts, which spanned psychophysical threshold, were determined by the Method of Constant Stimuli. Many of the neurons we screened responded weakly or not at all to these near-threshold red-green stimuli, but 21 neurons were sufficiently responsive to be included in this analysis (14 from Monkey K and 7 from Monkey S). As shown in Figure 3.8D,

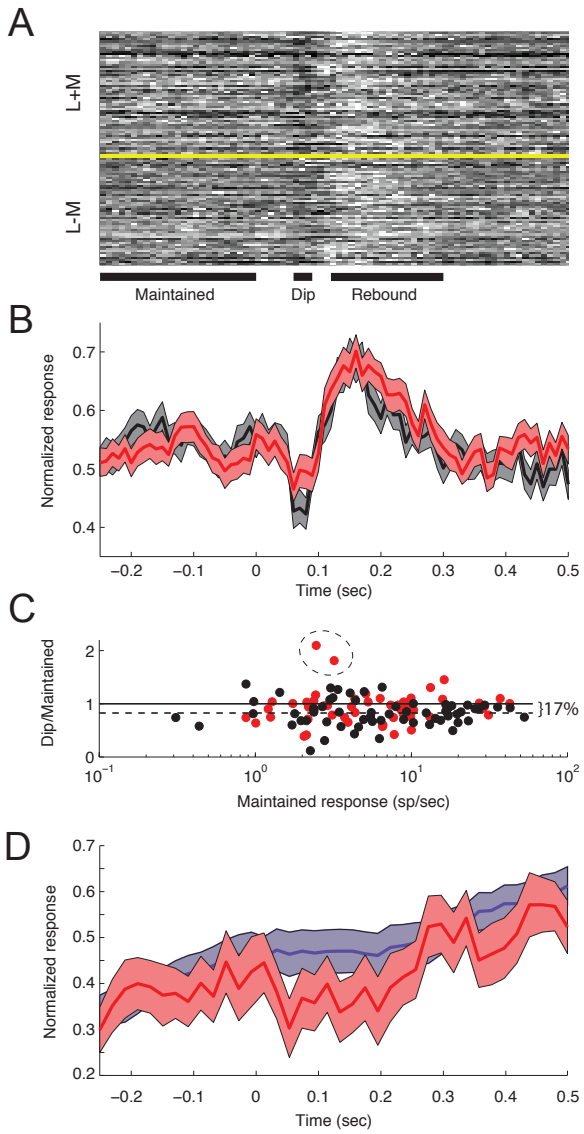

Figure 3.8 A: Normalized microsaccade-triggered spike density functions displayed as grayscale raster lines. Normalization was achieved by dividing each cell's spike-density function by the largest value of that function over the time domain shown. Data from 61 non-opponent L+M cells and 52 L-M opponent cells appear above and below the yellow line, respectively. Solid lines at the base of panel A delimit epochs over which spikes were counted for quantitative analyses. B: Normalized microsaccade-triggered spike density functions averaged across non-opponent neurons (black) and opponent neurons (red). C: Scatter plot of suppression (firing rate during dip divided by maintained firing rate) as a function of the maintained firing rate for non-opponent neurons (black) and opponent neurons (red). The dashed line shows the geometric mean of this ratio across neurons (0.83 = 17% suppression). The dashed ellipse encloses two cone-opponent neurons whose firing rate was above baseline during the dip interval. D: Normalized microsaccade-triggered spike density function (red) averaged across 21 V1 neurons that were responsive to near-threshold red-green modulations during the 2AFC detection task. The spike-density function shown in purple was computed from data in which microsaccade and spike times were randomly permuted across trials. Width of band in B and D indicates ±1 SEM across neurons.

microsaccades suppressed the responses of these neurons as well. The time course of the suppression was protracted relative to the time course observed with white noise stimulation (Figure 3.8B), and a clear rebound was not observed.

The normalized firing rate 500 ms after a microsaccade exceeded the normalized firing rate 250 ms before a microsaccade. This change in firing rate was not due to microsaccades but rather results from the fact that most microsaccades preceded visual responses to the Gabor stimulus. To isolate the effects of microsaccades from other influences on firing rate, we shuffled microsaccade times and spike times across trials. The purple curve in Figure 3.8D shows the average SDF calculated from randomly shuffled data across the 21 neurons. A gradual increase in firing rate is common to both the shuffled (purple) and unshuffled (red) SDFs and therefore is not time-locked to the occurrence of microsaccades. In contrast, a ~200 ms-long post-saccadic dip in activity is visible in the unshuffled (red) SDF only, indicating that this suppression is time-locked to microsaccades. We conclude that the differential effect of microsaccades on the detection of achromatic and red-green stimuli is not due to a privileged immunity of red-green responsive V1 neurons from microsaccadic suppression.

Discussion

We report that microsaccades increase luminance contrast detection thresholds, but not red-green contrast detection thresholds, in rhesus monkeys. We tested the hypothesis that this chromatic selectivity is manifest in a suppression of L+M, but not L-M, V1 neurons. Contrary to this hypothesis, microsaccadic modulation of spiking activity was similar in the two groups of neurons.

Below we consider and reject an alternative interpretation of the suppression effect: that detection of the stimulus inhibited microsaccade production. We then discuss the influence of color and spatial frequency and discuss clues that these effects provide regarding the mechanisms of microsaccadic suppression. We describe the microsaccadic behavior of our monkeys during task performance and compare our results to those obtained with human subjects. We conclude with the implications of our results for the neurophysiological investigation of contrast detection in monkeys.

Direction of causality

We found that microsaccades were correlated with increased detection thresholds. Logically, this correlation could be due to an elevation of detection thresholds by microsaccades or to an inhibition of microsaccades by the appearance of the stimulus (Cui et al. 2009; Rolfs 2009). We favor the former explanation for three reasons. First, the color specificity of the microsaccadic suppression we observed matched the color specificity of suppression observed in human subjects making large amplitude saccades (Burr et al. 1994; Burr and Morrone 1996; Diamond et al. 2000), whereas the inhibition of microsaccades by visual transients in humans is not color-specific (Rolfs 2009). Second, large amplitude saccades produce suppression in monkeys (Mohler and Cechner 1975) and it is likely that microsaccades do too, as they do in humans. Third, if stimulus visibility inhibited microsaccades, we would expect microsaccades to be suppressed strongly on high contrast trials and weakly on low contrast trials. This was not the case; mean stimulus contrast was higher on saccade trials than on no saccade trials on average.

Effects of color

Large amplitude saccades exert greater effects on the perception of achromatic than chromatic stimuli (Burr et al. 1994; Bridgeman and Macknik 1995; Uchikawa and Sato 1995; Diamond et al. 2000). Similarly, we found greater microsaccadic suppression for achromatic stimuli than for red-green chromatic stimuli. These observations suggest that saccadic and microsaccadic suppression invoke common mechanisms and may be related to the recent finding that large amplitude saccades and microsaccades are produced by largely overlapping neural circuits (Hafed et al. 2009).

One explanation for the chromatic specificity of saccadic suppression is that nonopponent neurons somewhere in the visual system are suppressed preferentially around the time of a saccade. We looked for, and failed to find, differences in peri-microsaccadic modulation of cone-opponent and nonopponent neurons in V1. Our results are consistent with those of Kleiser et al. (2004) who found comparable suppression in V1 BOLD response when subjects made saccades across luminance or isoluminant red-green gratings. We propose that the chromatic specificity of saccadic suppression occurs largely downstream of V1. The fact that V4 neurons are more strongly suppressed by

saccades when stimulated with achromatic than chromatic stimuli suggests that a critical locus for saccadic suppression may lie between V1 and V4 (Han et al. 2009). Transient visual neurons in the superficial superior colliculus, which are activated weakly by color (White et al. 2009) and suppressed by microsaccades (Hafed and Krauzlis 2010), may play a particularly important role.

Effects of spatial frequency

Microsaccades elevated detection thresholds for low spatial frequency stimuli more than for high spatial frequency stimuli, consistent with results from Burr, Morrone et al. (1994). Although this relationship has been reported before, seeing this trend in our data was surprising for two reasons. First, the range of spatial frequencies we tested was not optimal for observing this effect. Burr, Morrone et al., (1994) found that saccadic suppression was maximal at spatial frequencies below ~0.12 cpd. The lower end of our spatial frequency range, 0.25 cpd, was above this range. Second, retinal image blur, which affects high spatial frequencies more than low spatial frequencies, played a greater role in our study than in the study of Burr, Morrone et al. (1994). Burr, Morrone et al., (1994) instructed subjects to make saccades parallel to the bars of an extended grating, a configuration that minimizes the contributions of retinal blur to saccadic suppression. The saccades we studied had a variety of directions and amplitudes, some of which smeared the stimulus on the retina. For example, one half-cycle of the 3.2 cpd stimulus is 0.16°, so a vertical microsaccade of typical amplitude could reverse the spatial phase of this stimulus in ~14 ms (the duration of a microsaccade of 0.16°). Such a shift would cause individual photoreceptors to encounter both a stimulus peak and trough within one integration period thereby reducing or nulling the response (Schneeweis and Schnapf 1999). A microsaccade could not exert the same effect on the 0.25 cpd stimulus, one half-cycle of which is larger than the largest microsaccade in our study.

Microsaccades did not significantly impair the detection of 0.25 cpd, achromatic stimuli for Monkey S, but did for Monkey K. We considered the possibility that Monkey S performed the task poorly in this condition as poor behavior could have caused subtle effects of microsaccades on stimulus detectability to go unnoticed. Instead, we found that Monkey S's performance in this condition was similar to that of Monkey K, and when we

analyzed only those sessions from Monkey S in which detection thresholds were lowest, the suppression effect changed minimally and remained insignificant. The absence of a saccadic suppression effect in this condition is therefore unlikely a product of poor task performance.

Another possibility is that this difference between monkeys may result from differences in their microsaccadic behavior. Monkey K made more large amplitude microsaccades than Monkey S, and large amplitude microsaccades increased detection thresholds more than small amplitude microsaccades. These observations are consistent with the larger microsaccadic suppression in Monkey K than Monkey S. On the other hand, microsaccades exerted a greater effect on detection for Monkey K than for Monkey S even when matched for amplitude (Figure 3.5). We are thus unable to explain this difference between monkeys on the basis of microsaccade amplitudes. Data from additional animals could help resolve this issue.

Dynamics in microsaccade frequency

The variations in microsaccade frequency over the course of the trial (Figure 3.3A and 3.3B) can be understood in terms of the influences of visual stimulation and task demands on microsaccades. Our monkeys exhibited a biphasic modulation of microsaccade rate following the presentation of the stimulus frames. This modulation may be related to the transient suppression and rebound of microsaccades made by human observers following a flash in the retinal periphery (Engbert and Kliegl 2003). The monkeys made relatively few microsaccades during the Gabor stimulus presentation which may be related to the temporary allocation of resources to a demanding visual task (Winterson and Collewijn 1976; Bridgeman and Palca 1980). The increase in saccade frequency at the end of the trial may be related to the allocation of covert spatial attention or the preparation of the saccade to a peripheral target (Hafed and Clark 2002; Engbert and Kliegl 2003; Horowitz et al. 2007). The effect was greater on correct trials, consistent with the idea that these movements represent a (barely) suppressed urge to make the saccade to the identified correct target.

The magnitude of microsaccadic suppression

Large amplitude saccades increase detection thresholds by 0.5 to 1 log unit (Mohler and Cechner 1975; Volkmann et al. 1978; Burr et al. 1994; Diamond et al. 2000). Spontaneous microsaccades (of unreported amplitude) increase detection threshold by ~0.3 log units (Beeler 1967). The changes in threshold that we observed (0.1-0.5 log units) span this benchmark.

Our stimulus was on the screen for 667 ms, which is much longer than the typical microsaccade duration (10-30 ms), the subsequent perceptual suppression (<100 ms) (Beeler 1967), or stimulus presentations used in previous studies (<1-32 ms, Krauskopf et al. 1966; Zuber and Stark 1966; Volkmann et al. 1978; Uchikawa and Sato 1995; Diamond et al. 2000; Kleiser et al. 2004; Schütz et al. 2007). Given this long stimulus duration, the fact that suppression was modest in some of the conditions we studied is perhaps less surprising than the fact that it was detectable at all. For many purposes, microsaccadic suppression in monkeys may be sufficiently small as to be negligible. One context in which it might not be negligible is in the interpretation of neurophysiological experiments of contrast detection in monkeys, which is discussed below.

Microsaccades and choice probability

Choice probability is a metric that quantifies the covariation between neuronal activity and behavioral performance during psychophysical tasks (for a review see: Parker and Newsome 1998). Significant choice probabilities have been taken as evidence that a sensory neuron's spiking activity contributes causally to the animal's perceptual judgements (Shadlen et al. 1996), but microsaccades may contribute to choice probability in the absence of a causal relationship.

Herrington et al., (2009) found that microsaccades contribute to choice probability in some tasks. Monkeys more readily detect changes in visual motion when the change modulates the activity of motion-selective neurons in visual cortex strongly. Part of this relationship can be attributed to the fact that microsaccades increase detection thresholds for changes in visual motion and suppress the responses of motion-sensitive visual neurons. A correlation between task performance and neuronal responses thus follows.

Our study extends the findings of Herrington et al., (2009) to luminance contrast detection. We found that microsaccades impair contrast detection and modulate the spiking activity of V1 neurons (see also: Leopold and Logothetis 1998; Martinez-Conde et al. 2000; Snodderly et al. 2001; Kagan et al. 2008). A monkeys' ability to detect a near-threshold, achromatic stimulus is therefore expected to be correlated with V1 response to that stimulus. On trials without a microsaccade during the stimulus presentation, we would expect low behavioral thresholds and vigorous stimulus-locked neural responses. On trials including a microsaccade during the stimulus presentation, we would expect elevated behavioral thresholds and diminished neural responses. In the absence of a visual stimulus, we would expect no relationship between perceptual reports and neural responses. These effects have been reported in monkeys performing a seen/not seen contrast detection task (Palmer et al. 2007).

Our study shows that microsaccades play a small but potentially important role in determining contrast detection thresholds of rhesus monkeys. We found clear evidence for microsaccadic suppression when the animal was detecting achromatic but not red-green stimuli. We found that microsaccadic modulation of L-M and L+M V1 neurons was similar in amplitude and time course, suggesting that the locus of chromatic specificity is downstream of V1. Our study does not address whether microsaccade-induced modulation of V1 activity is causally related to detection performance. It remains possible that activity modulations in V1 are unrelated to behavioral microsaccadic suppression. An important future direction is to determine at what stage of the visual system microsaccade-related changes in activity can account quantitatively for changes in visual performance.

Chromatic detection from cone photoreceptors to V1 neurons to behavior

Color vision begins with the absorption of photons by photopigment in the outer segments of the cone photoreceptors. Each absorption triggers a complex phototransduction cascade that ultimately generates an electrical signal across the cone's cell membrane. These signals are further transformed, and potentially corrupted, by processing downstream of the cones (Donner 1992; Borghuis et al. 2009; Ala-Laurila et al. 2011). Nevertheless, noise in the phototransduction cascade places an upper bound on the sensitivity of an observer; downstream processing may add additional noise or filter the cone signals, but cannot eliminate noise that is introduced during phototransduction.

To determine whether noise in cone outer segments is a bottleneck for chromatic sensitivity, we developed a computational model of stimulus encoding in the monkey outer retina, and we compared performance of the model to the behavior of monkeys performing a chromatic detection task. The model simulated responses of a realistic mosaic of cones using a temporal impulse response function, a contrast gain function, and a noise power-spectrum derived from in vitro recordings of cone photoreceptors from the macaque monkey (Angueyra and Rieke 2013).

Our results indicate that the temporal frequency dependence of the monkey's contrast sensitivity followed closely that of the cones. Specifically, the shape of the temporal contrast sensitivity function can be explained almost entirely by the deterministic component of the modeled cone responses; decreases in noise at higher temporal frequencies could lower behavioral thresholds, but under the range of stimulus conditions we tested, the temporal frequency dependence of the noise process influenced detection thresholds minimally.

In a previous study, we showed that the psychophysical chromatic sensitivity of monkeys was well matched to the average chromatic sensitivity of individual color-responsive neurons in their primary visual cortex (V1). A single scale factor served to equate the sensitivity of V1 neurons and the monkey across four isoluminant color directions. The model provided an extension of this result: a different scale factor related the sensitivity of the modeled cone mosaic to the sensitivity of recorded V1 neurons. This

result implies that, for low spatiotemporal frequency modulations, the downstream processing of cone signals is similar across chromatic color directions from the cones all the way to behavioral performance on a detection task despite the fact that these signals are carried by different neural pathways.

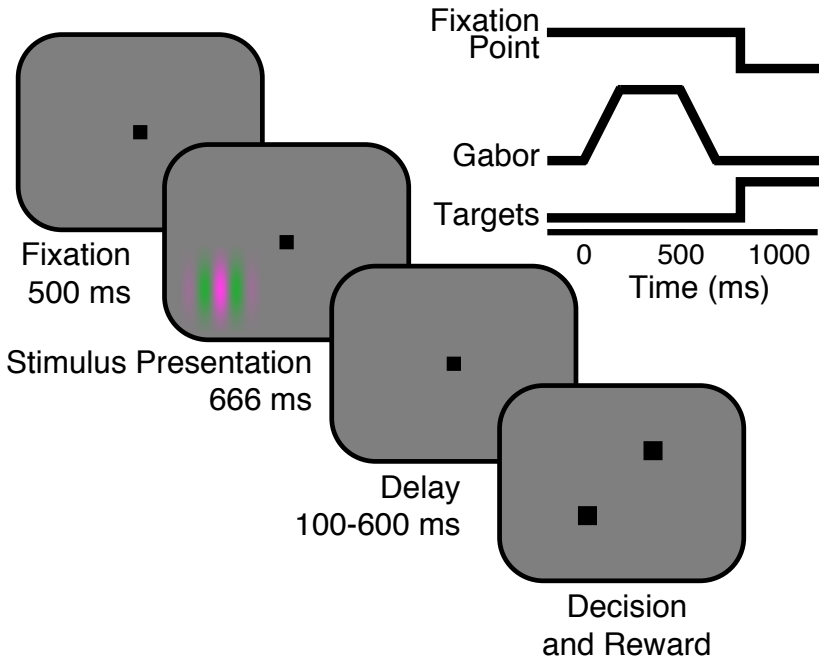

Figure 4.1 Display geometry and event timing of the chromatic detection task. See Methods for details.

Table 4.1

Description of symbols:

Table 1: Description of symbols

Symbol	Units	Descripton
A_{ret}	μm^2	Area of the retina subtended by a single pixel
θ	degrees	Angle of elevation subtended by a single pixel
F_{post}	mm	Posterior focal length of the eye
x	degrees	Eccentricity
$\mathrm{F}_{(\lambda)}$	μm^2	Cone absorbtance function
$\mathrm{A}_{(\lambda)}$		Cone action spectra
λ	nm	Wavelength
$t_{(\lambda)}$		Lens transmittance
$\mathrm{R}_{(\lambda)}$	$\mathrm{W} \cdot \mathrm{str}^{-1} \cdot \mathrm{m}^{-2}$	Spectral radiance
$\mathrm{I}_{(\lambda)}$	$\mathrm{W} \cdot \mu\mathrm{m}^{-2}$	Spectral irradiance
$m_{(\lambda)}$		Macular pigment transmittance function
h	$\mathrm{W} \cdot \mathrm{sec}^2$	Planck's constant
c	$\mathrm{m} \cdot \mathrm{sec}^{-1}$	Speed of light
ϕ	μm^2	Cone collecting area
γ		Gain of the cone response
L	pA	Linear response of a cone
PR	pA	Pooled response
IRF	$\mathrm{pA} \cdot (\mathrm{R}^* \cdot \mathrm{sec}^{-1})^{-1}$	Cone temporal impulse response function
G	$\mathrm{R}^* \cdot \mathrm{sec}^{-1}$	Gabor stimulus
wt		Spatiotemporal weighting function
ϵ	pA	Time series of zero-mean cone noise
$\lvert\mathrm{WT}_f\rvert$		Fourier magnitudes of the spatiotemporal weight function
$\lvert\boldsymbol{E}_f\rvert$	$\mathrm{pA} \cdot \mathrm{Hz}^{-1}$	Fourier magnitudes of the cone noise
$\mathbf{W}$		Within class scatter matrix
$\mathbf{B}$		Between class scatter matrix
μ		Mean of the decision variable distribution
σ		Standard deviation of decision variable distribution
ν		LDA discriminant vector
cc		Cone contrast of the Gabor
α		Contrast at detection threshold
β		Slope of the psychometric function
ψ		Interaction exponent for isodetection surface

Methods

Subjects and behavioral training

4 *Macaca mulatta* monkeys (3 female) were used in this study. All procedures conformed to the guidelines provided by the US National Institutes of Health and the University of Washington's Animal Care and Use Committee. Monkeys were surgically implanted with a titanium head post to minimize head movements and a monocular scleral search coil to measure eye position. 2 monkeys were implanted with a recording chamber above opercular V1 (Crist Instrument, Md).

Chromatic contrast detection task

We defined chromatic sensitivity in terms of performance on a contrast detection task that we have described previously (Figure 4.1, and see Hass and Horwitz 2013). Each trial began when the monkey fixed their gaze on a 0.1º black square located at the center of the monitor. Five hundred milliseconds later, a Gabor stimulus appeared in one of two mirror symmetric locations about the fixation point and disappeared after 666 ms. Contrast increased and decreased linearly during the first and last quarters of the stimulus interval to smooth out onset and offset transients (Figure 4.1). Following a brief delay (100 to 600 ms), the fixation point disappeared and two choice targets appeared. An eye movement to the choice target located in the direction of the Gabor stimulus triggered a juice reward. No feedback was given for incorrect choices.

Stimulus event timing and eye-position monitoring was controlled by a computer (Dell Dimension 4800) running REX (US National Institutes of Health). Monkeys were required to maintain fixation within a 1º electronic electronic around the fixation point. Trials were aborted if the monkey's eye position exited this window at any time prior to the onset of the choice targets. Stimulus presentation was controlled using an Apple Mac Pro computer running custom routines in Matlab (MathWorks) and the Psychophysics Toolbox (Brainard 1997).

Stimuli were displayed on a cathode ray tube computer monitor (Sony Trinitron, 760x1400 pixels, 75 Hz refresh rate) whose phosphor emission spectra were characterized with a spectroradiometer (PR650, Photo Research Inc, CA). The color depth of each channel of the monitor was increased from 8 to 14 bits using a digital video signal processor (Bits++, Cambridge Research) at the expense of spatial resolution: each pixel was twice as wide as it was tall. Gamma correction was performed in software. All stimuli were presented on a uniform gray background (CIE coordinates: x = 0.33, y = 0.33, Y = 100 cd/m2).

Stimuli were generated using the method of silent substitution (Estévez and Spekreijse 1982) and were based on the Stockman, McLeod, and Johnson 1993 cone fundamentals (Stockman et al. 1993). Contrast was defined as the vector norm of the stimulus in L, M, S cone-contrast space:

$$\text{Cone Contrast} = \sqrt{\left(\frac{\Delta L}{L_b}\right)^2 + \left(\frac{\Delta M}{M_b}\right)^2 + \left(\frac{\Delta S}{S_b}\right)^2} \qquad \text{(Eq. 4.1)}$$

Adaptive estimation of iso-detection surfaces in 3-D color space

Iso-detection surfaces were measured using an iterative process. Each iteration had two phases: The first phase consisted of estimating detection thresholds in three interleaved color directions. The second phase consisted of selecting new color directions to probe during the subsequent iteration. Detection threshold was measured using the QUEST adaptive procedure (Watson and Pelli 1983) and defined as the contrast necessary to support 82% correct performance, which was estimated as the modal value of the QUEST function at the end of the procedure (40 trials per condition for Monkey K, $\geq$ 20 trials for Monkey S).

During the second phase of each iteration, new color directions were selected for later iterations using a technique that we described previously (Horwitz and Hass 2012). Briefly, each threshold was represented as a point in a 3-dimensional color space spanned by the L-, M-, and S-cone contrast axes. The points corresponding to three neighboring color directions form a triangle. A ray from the origin through the midpoint of this triangle specified a direction in color space to be probed. Once measured, the detection threshold in this direction was represented as a point along this ray. This point was then joined to each pair of vertices from the original triangle, splitting the original triangle into three sub-triangles. In later iterations, color directions were selected to pass through the mid-points of these sub-triangles.

Not every sub-triangle was tested. If the threshold measured at the mid-point of a triangle was close to the plane of the triangle (within a tolerance of 27% of the distance to the plane), then the triangle was not subdivided. This technique has the advantage of preferentially testing color directions corresponding to locations on the iso-detection surface that are most curved.

To compare datasets across stimulus conditions or observers, we fit the raw data with an isodetection surface according to the following equation:

$$\sum_{i=1}^{3}\left(l_i\frac{\Delta \mathrm{L}}{\mathrm{L}}+m_i\frac{\Delta \mathrm{M}}{\mathrm{M}}+s_i\frac{\Delta \mathrm{S}}{\mathrm{S}}\right)^{\psi}=1 \qquad \text{(Eq. 4.2)}$$

This model assumes detection is subserved by three statistically independent visual channels that interact via probability summation (Cole et al. 1993). The coefficients l_i, m_i, and s_i specify the cone weights to the i_{th} visual mechanism, and $\left[\frac{\Delta \mathrm{L}}{\mathrm{L}}, \frac{\Delta \mathrm{M}}{\mathrm{M}}, \frac{\Delta \mathrm{S}}{\mathrm{S}}\right]$ are the coordinates of a Gabor stimulus at detection threshold. The parameter ψ determines the degree of interaction between the three mechanisms.

To fit the isodetection surface to the monkey's psychophysical detection thresholds, we selected a set of mechanism cone weights that minimized the difference between the predicted and actual detection thresholds as follows. Since $\left[\frac{\Delta \mathrm{L}}{\mathrm{L}}, \frac{\Delta \mathrm{M}}{\mathrm{M}}, \frac{\Delta \mathrm{S}}{\mathrm{S}}\right]$ corresponds to the *coordinates* of a stimulus at threshold, its vector norm corresponds to the *threshold* in cone contrast units. We can thus rewrite Eq. 4.2 as follows, were a is the predicted detection threshold and $\left[\frac{\Delta \mathrm{L}}{\mathrm{L}}, \frac{\Delta \mathrm{M}}{\mathrm{M}}, \frac{\Delta \mathrm{S}}{\mathrm{S}}\right]$ is a unit vector:

$$\sum_{i=1}^{3}\left(l_i a\frac{\Delta \mathrm{L}}{\mathrm{L}}+m_i a\frac{\Delta \mathrm{M}}{\mathrm{M}}+s_i a\frac{\Delta \mathrm{S}}{\mathrm{S}}\right)^{\psi}=1 \qquad \text{(Eq. 4.3)}$$

Solving for a yields the following:

$$a=\frac{1}{\left[\sum_{i=1}^{3}\left(l_i\frac{\Delta \mathrm{L}}{\mathrm{L}}+m_i\frac{\Delta \mathrm{M}}{\mathrm{M}}+s_i\frac{\Delta \mathrm{S}}{\mathrm{S}}\right)^{\psi}\right]^{\left(\frac{1}{\psi}\right)}} \qquad \text{(Eq. 4.4)}$$

We fit cone weights to the three visual mechanisms by minimizing the squared radial distance between the predicted thresholds (a) and the measured thresholds (i.e., $[\log(a) - \log(\text{threshold})]^2$) using function-minimization routines in Matlab.

To compare detection thresholds between the monkey and model we computed the ratio of the distances to their isodetection surfaces (threshold ratio, or TR) as a function of color direction. We used a bootstrap approach to test for significant

differences in TRs between pairs of color directions. First, we calculated the log residuals of the fit and then re-assigned them across tested color directions randomly and with replacement. We then fit a new isodetection surface to the bootstrapped data. To test for significant differences in TR between two color directions, we computed 4000 bootstrap TRs by dividing the bootstrapped behavioral thresholds by the threshold of the model. We then calculated the 95% confidence interval of the distribution of paired differences between bootstrapped TRs. If the confidence interval did not contain the value of zero, then we rejected the null hypothesis of no difference in the TR measured for two color directions at the $\alpha = 0.05$ level.

Neurophysiological recordings from V1

Neurons in V1 were recorded previously, and details for the neurophysiological procedure can found elsewhere (Hass and Horwitz 2013). Briefly, recordings from individual V1 neurons were attained via glass-tipped transdural tungsten microelectrodes (FHC Inc.). The raw voltage signal was amplified, bandpass filtered (100 Hz to 8 kHz), and digitized using the Multichannel Acquisition Processor (Plexon Inc.). Single unit isolation was assessed by stability in the action potential waveform over the duration of the recording and by the absence of inter-spike-intervals < 1 ms.

Neurophysiological recordings from cone photoreceptors

The cone impulse response function and noise power spectrum were derived from previously published data. Details of the recording procedures can be found in Angueyra et al., (2013). Briefly, photocurrents were recorded in the whole-cell voltage-clamp configuration from cone photoreceptors of macaque monkeys obtained through the Tissue Distribution Program of the Washington National Primate Research Center. All procedures conformed to the guidelines set by University of Washington's Institutional Animal Care and Use Committee. Small sections of retina were mounted to a recording chamber and perfused with oxygenated Ames solution (32º C). The recording pipet internal solution contained (in mM): 133 potassium aspartate, 10 KCl, 10 HEPES, 1 MgCl2, 4 ATP, 0.5 GTP; pH was adjusted to 7.2 with NMG-OH and osmolarity was ~280

mOSM. The recorded photocurrent was low-pass filtered at 3 kHz and digitized at 20 kHz.

The cone impulse response function (IRF) was derived by reverse correlation of photocurrent in response to visual, Gaussian white-noise stimuli. Measuring the IRF from a variety of mean light levels allowed us to quantify the relationship between cone gain and background illumination, which was parameterized by a Weber-Fechner relationship (Schnapf et al. 1990; Schneeweis and Schnapf 1999). The cone-noise power spectrum was obtained through Fourier analysis of the photocurrent in response to steady light pulses and subtracting off the spectrum of noise from the recording equipment.

Constructing the artificial cone mosaic

The model cone mosaic was constructed by subdividing the area of the retina stimulated by the Gabor stimulus into subregions corresponding to each stimulus pixel. We calculated the area of each retinal subregion using a reduced-eye model with one nodal point:

$$\mathrm{A_{ret}} = (\tan\theta \times \mathrm{F_{post}})^2 \qquad \text{(Eq. 4.5)}$$

Where A_{ret} is the area of a retinal subregion and θ is the angle of elevation subtended by a single pixel of the Gabor stimulus. When a ray from the bottom edge of a stimulus pixel is collinear with the lens's axis, and a ray from the top of the pixel passes through the nodal point of the lens, then θ is the angle of elevation subtended by the retinal (or real) image measured at the lens's nodal point (Figure 4.2 A; Katz and Kruger 1994). F_{post} is the distance between the nodal point and the retina, and was set to 12.75 mm (Lapuerta and Schein 1995; Qiao-Grider et al. 2007). This calculation assumes that the retina is locally planar for small images, and assumes that the eye's refracting elements (i.e., cornea, lens, aqueous, vitreous) can be combined into an optical system with a single nodal point. We also assume that each pixel of the Gabor stimulates the same retinal area regardless of the pixels' eccentricity from the center of gaze. We do not take into account blurring of the visual image as it passes through the eye's optics.

We allocated cone photoreceptors to each retinal subregion according to its eccentricity following measurements of cone density on the macaque retina (Packer et al. 1989; Goodchild et al. 1996):

$$\frac{\text{Cones}}{\mu\text{m}^2} = 150.9\, e^{(-1.2x)} + 36\, e^{(-0.16x)} + 10\, e^{(-0.03x)} \quad \text{(Eq. 4.6)}$$

Where x is the eccentricity at the center of each retinal subregion. The product of A_{ret} with the cone density determines the number of cone photoreceptors in each retinal subregion.

After determining the number of cones in each retinal subregion, we determined their identity (i.e., L-, M-, or S-cones) using the following proceedure. The number of S-cones was determined using published estimates of S-cone density on the macaque temporal retina for eccentricities greater than 1º (De Monasterio et al. 1985):

$$\frac{\text{S–cones}}{\text{deg}^2} = 121.9\, e^{(-0.2x)} + 90\, e^{(-0.05x)} \quad \text{(Eq. 4.7)}$$

We converted the units of retinal area from deg^2 to μm^2 by multiplying by the square of the modeled eye's magnification factor (220 $\mu m \bullet deg^{-1}$, calculated on the basis of A_{ret} and the size of a single stimulus pixel). The number of S-cones in each retinal subdivision was then calculated as the product of the S-cone density with A_{ret}. The remaining cones were allocated equally to the L- and M-cone classes (Figure 4.2 B, and see: Jacobs and Deegan 1999). This simplification allows fractional numbers of cones per pixel, but this mathematical convenience is inconsequential for our ideal observer model which pools cone signals across many pixels.

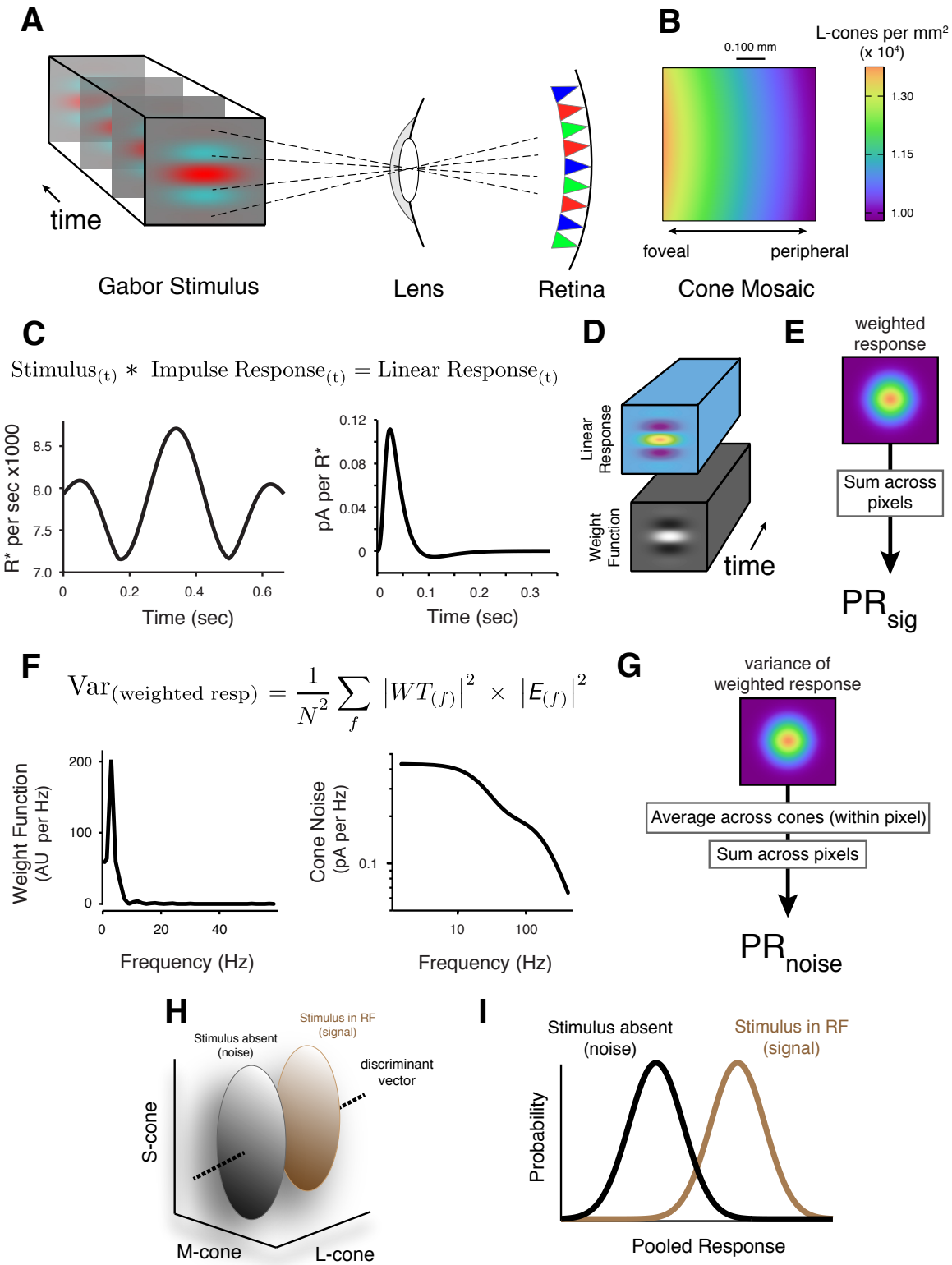
A
time
Gabor Stimulus
Lens
Retina
B
0.100 mm
L-cones per mm²
(x 10⁴)
1.30
1.15
1.00
foveal
peripheral
Cone Mosaic
C
Stimulus(t) * Impulse Response(t) = Linear Response(t)
R* per sec x1000
8.5
8.0
7.5
7.0
0
0.2
0.4
0.6
Time (sec)
pA per R*
0.12
0.08
0.04
0
0
0.1
0.2
0.3
Time (sec)
D
Linear Response
Weight Function
time
E
weighted response
Sum across pixels
PRsig
F
Var(weighted resp) = 1/N² Σf |WT(f)|² × |E(f)|²
Weight Function (AU per Hz)
200
100
0
0
20
40
Frequency (Hz)
Cone Noise (pA per Hz)
0.1
10
100
Frequency (Hz)
G
variance of weighted response
Average across cones (within pixel)
Sum across pixels
PRnoise
H
Stimulus absent (noise)
Stimulus in RF (signal)
discriminant vector
S-cone
M-cone
L-cone
I
Stimulus absent (noise)
Stimulus in RF (signal)
Probability
Pooled Response

Converting the physical stimulus into cone photoisomerizations

The number of photoisomerizations induced by the Gabor stimulus was quantified in a multi-step process. First, we calculated the spectral power distribution of the stimulus incident on the retina. Second, we adjusted the spectral irradiance to account for the eye's pre-retinal filters. Third, we converted the irradiance values into photon flux incident on individual cones. Fourth, we derive a set cone fundamentals that determines the wavelength dependence of the photon absorption. Each of these steps is detailed as follows.

For each monitor phosphor, we converted spectral radiance (in units of Watts steradian^{-1} • m^{-2}) into spectral *irradiance* (Watts • μm^{-2}) using the number of steradians subtended by the pupil:

$$I_{(\lambda)} = R_{(\lambda)} \times \frac{\text{pupil area}}{(\text{eye diameter})^2} \times 10^{-12} \quad \text{(Eq. 4.8)}$$

$R_{(\lambda)}$ is the emission spectrum for one of the monitor's three phosphors measured at its maximum intensity. The surface area equal to 1 steradian is equal to the square of the eye's diameter, which was set to 19 mm (Lapuerta and Schein 1995; Qiao-Grider et al. 2007). Dividing the pupil area by the square of the eye diameter determines the number of steradians subtended by the pupil. Pupil area (12.6 mm^2) was measured using an

---

Figure 4.2 (previous page): Overview of the cone-mosaic model illustrated for a single cone type. *A:* The spectral power distribution of the Gabor stimulus was filtered through the optics of the eye and converted into photoisomerizations for each cone type at each retinal subregion. *B:* The artificial L-cone mosaic for a patch of retina located at 5º eccentricity along the horizontal meridian. *C:* Example stimulus time series for a single pixel (left) and the cone temporal impulse response function (IRF; right). The linear response portion of the model-cone output was calculated as the convolution of the stimulus with the IRF. *D:* The linear response of the L-cone mosaic (top; represented an X by Y by Time volume) was multiplied by the spatiotemporal weighting function (bottom). *E:* The weighted responses were pooled across retinal subregions to derive the signal portion of the pooled response (PR_{sig}). *F:* The spatiotemporal weighting function (left) and the cone-noise (right) represented in the Fourier domain. The variance of the weighted cone noise was calculated from the dot product of the two power spectra. *G:* The weighted cone-noise was then pooled across retinal subregions to derive the noise component of the pooled response (PR_{noise}). *H:* The PR distributions for Gabor-present (brown) and Gabor-absent (black) trial types in a 3D cone-response space. The discriminant vector was found using linear discriminant analysis. *I:* The 1D decision variables used by the ideal observer for the detection task were derived by projecting the 3D distributions onto the discriminant vector. The performance of the model on the detection task was defined by the discriminability between the two distributions of decision variables (area under the ROC).

optical eye tracker (SensoMotoric Instruments). Multiplying by 10^{-12} converts m^2 into μm^2.

The spectral irradiance of the stimulus was adjusted for pre-retinal filtering by multiplying the irradiance values with the lens and macular-pigment transmittance functions:

$$\hat{\mathrm{I}}_{(\lambda)} = \mathrm{I}_{(\lambda)} \times m_{(\lambda, x)} \times t_{(\lambda)} \quad \text{(Eq. 4.9)}$$

The macular pigment transmittance function, $m_{(\lambda, x)}$, was calculated by converting the Wyszecki and Styles (1982) absorbance functions into transmittance values and by taking into account the eccentricity dependence of macular pigment density:

$$m_{(\lambda,\, x)} = \frac{1}{10^{\left[m_{(\lambda)}\, e^{\left(\frac{x}{1.03}\right)}\right]}} \quad \text{(Eq. 4.10)}$$

$m_{(\lambda)}$ is the macular-pigment absorbance spectrum in log units, which was scaled to have a value of 0.35 at 460 nm and 0º of eccentricity (Stockman et al. 1993; Snodderly et al. 1984; Wooten and Hammond 2005). Notice that the macular pigment density decays exponentially with eccentricity (Snodderly et al. 1984; Wooten and Hammond 2005). We calculated $m_{(\lambda, x)}$ at a single eccentricity (x) defined by the center of the Gabor stimulus. The lens transmittance function, $t_{(\lambda)}$, was based on published estimates (Stockman et al. 1993), and was scaled to have a value of 1 at 400 nm (van Norren 1972).

We converted the spectral irradiance of the stimulus (Watts • μm^{-2}) into photon flux using the relationship between the energy of a photon and its wavelength:

$$\mathrm{Photons}_{(\lambda)} = \hat{\mathrm{I}}_{(\lambda)} \times \frac{\lambda}{hc} \quad \text{(Eq. 4.11)}$$

The second term in this equation describes the energy of a photon (in Watts • sec) at a wavelength equal to λ. Planck's constant (h) is in units of Watts • sec^2, and c is the speed of light. The resulting photon spectrum is in units of photons • μm^{-2} • sec^{-1}.

We constructed an absorptance function for each cone type by multiplying the Baylor et al., (1987) cone action spectra ($A_{(\lambda)}$) by the photopigment optical density (0.3, see Stockman et al. 1993) and then converting from logarithmic to linear units:

$$F_{(\lambda)} = 1 - 10^{(-0.3A_{(\lambda)})}$$

(Eq. 4.12)

The cone absorptance functions were then normalized to have a peak value equal to the cone collecting area (0.6 μm2, see Schnapf et al. 1990; Schneeweis and Schnapf 1999). Thus, the absorptance functions have units of μm^2.

The last step is to create a 3x3 transformation matrix that converts the photon spectrum into cone photoisomerizations. This matrix is obtained by computing the inner product between the cone absorptance functions and the photon spectra. The transformation matrix was then used to convert the monitor phosphor intensities of the neutral gray background into R* sec^{-1} for each of the cone types. At 5º of eccentricity, the R* sec^{-1} due to the neutral gray background were L=7131, M=6017, S=1973, rods=8200. The activity of rod photoreceptors due to the neutral gray background was 8200 R* sec^{-1}, which was estimated using the rod action spectrum (Baylor et al. 1984) and published estimates of rod optical density (0.45) and collecting area (1 μm^2) (Schneeweis and Schnapf 1999; Baylor et al. 1984).

Calculating the linear response of the cone mosaic

The Gabor stimulus is composed of spatial and temporal modulations of the CRT phosphors which can be converted in to units of R* sec^{-1} using the transformation matrix described above. The Gabor stimulus can be conceptualized as a 3D matrix for each cone type (x by y by time, Figure 4.2 A) where each element describes the cone photoisomerization rate.

The linear response of a single cone was calculated as the discrete time convolution between the cone's empirically derived temporal impulse response function and the stimulus time-series for the corresponding pixel:

$$L_{(x,y,t)} = \gamma \sum_{\tau} IRF_{(\tau)} \times G_{(x,y,t-\tau)}$$

(Eq. 4.13)

Where $L_{(x,y,t)}$ represents the linear response of a single cone in the retinal subregion defined by the stimulus pixel at location [x,y] and has units of pA. $G_{(x,y,t)}$ is the Gabor stimulus represented in R* sec^{-1} (Figure 4.2 D). γ is a scale factor that is unique to each

cone type and scales the linear response to reflect the gain of each cone type at their specific background adaptation state. The gain of the cone response follows a Weber-Fechner relationship with a half-desensitization constant of 4500 R* and a dark-adapted cone impulse response function that peaks at 0.15 pA/R* (Angueyra and Rieke 2013). We assume that adaptation is identical for the three cone types, and that the shape of the IRF is separable with the background intensity.

Pooling the responses of the cone mosaic

Signals from the model's cone photoreceptors were pooled and then transformed into a decision variable used by the ideal observer to detect the stimulus. We calculate a pooled response (PR), by applying a spatiotemporal weighting function (*wt*) to the modeled photocurrent of each cone. The weighting function had the same spatiotemporal profile as the Gabor stimulus but differed from the Gabor stimulus in two ways. First, the weight function was constrained to have a mean of zero and range of ± 1 (Figure 4.2 E). Second, the weight function was delayed in time by an amount that was equal to the latency of the cone's linear response. We applied the same weighting function to each of the L-, M-, and S-cone mosaics.

The pooled response was modeled as the sum of independent signal and noise components (Angueyra and Rieke 2013), which were computed separately. We calculated the signal component of the pooled response (PR_{sig}) by taking the dot product between the model's baseline-subtracted linear response and the spatiotemporal weighting function. We then averaged the weighted responses across cones of the same type within each retinal subregion and added the pooled signals across retinal subregions (Figure 4.2 E&F). Because cones of the same type produce an identical response if they are located in the same retinal subregion, the average response across cones in each subregion is identical to the response produced by a single cone. The entire process can be described by the following equation:

$$\mathrm{PR}_{\mathrm{sig}} = \sum_{x,y,t} \left[\mathrm{L}_{(x,y,t)} - \mathrm{L}_{\mathrm{O}}\right] \times wt_{(x,y,t)} \qquad \text{(Eq. 4.14)}$$

This process was repeated for each cone type and yields a 3 element vector which quantifies the signal component of the pooled response of the artificial cone mosaic.

The noise component of the pooled response (PR_{noise}) is the dot-product between the weighting function (*wt*) and a noise vector ($\mathcal{E}$) whose temporal statistics are given by the empirically derived cone-noise power spectrum. We are primarily interested in the sensitivity of the ideal observer across many repeated trials, so instead of computing PR_{noise} on individual trials, we compute the variance of this quantity across trials. The variance of the dot product of the noise ($\mathcal{E}$) onto the weight function (*wt*) can be written:

$$\mathrm{Var}\left(\epsilon \cdot wt\right) = wt^{\top} \sum_{\epsilon} wt \tag{Eq. 4.15}$$

Where $\Sigma_{\mathcal{E}}$ is the covariance of the noise , and the mean of the dot product is zero because both $\mathcal{E}$ and *wt* are assumed to have mean zero. In the time domain, calculating the variance of the dot product is difficult due to temporal correlations in the cone noise that manifest as non-zero entries in the off-diagonal elements of the covariance matrix. On the other hand, assuming the cone noise is wide sense stationary, then in the Fourier domain, the power in each frequency band is uncorrelated, and we can calculate the variance of the dot product in the Fourier domain without regard to correlations that exist in the time domain. To begin, we note that Plancherel's theorem states that dot products in the time domain are equivalent to dot products in the Fourier domain. Here we use lowercase symbols to denote time domain values, and uppercase symbols for Fourier coefficients. The * operator denotes complex conjugation. For a discrete Fourier transform, the two dot products are related as follows:

$$\epsilon_{(t)} \cdot wt_{(t)} = \frac{1}{N} \left(E_{(f)} \cdot WT^{*}_{(f)}\right) \tag{Eq. 4.16}$$

The variance of a dot product in the Fourier domain can then be calculated on the basis of the Fourier coefficients and their covariance.

$$\mathrm{Var}\left(\epsilon_{(t)} \cdot wt_{(t)}\right) = \frac{1}{N^2} \mathrm{Var}\left(E_{(f)} \cdot WT^{*}_{(f)}\right)$$

$$= \frac{1}{N^2}\left(WT_{(f)}^{\top} \sum_{E} WT_{(f)}^{*}\right)$$

(Eq. 4.17)

Because the covariance matrix of the Fourier coefficients is a diagonal matrix whose elements correspond to the cone noise power spectrum (Leon-Garcia 1994), we can rewrite this expression as the sum over element-wise products:

$$= \frac{1}{N^2}\sum_{f} WT_{(f)} \times \left|E_{(f)}\right|^2 \times WT_{(f)}^{*}$$

Rearranging terms, and noticing that *WT* x *WT** corresponds to the square of the Fourier magnitudes, we arrive at the following expression which states that the variance of the dot product of two time domain signals can be derived as the dot product of their power spectra. For a wide sense stationary stochastic process, this expression holds true regardless of correlations that may be present in the time domain.

$$= \frac{1}{N^2}\sum_{f} \left|WT_{(f)}\right|^2 \times \left|E_{(f)}\right|^2$$

(Eq. 4.18)

This operation defines the variance of a single cone's response after weighting the response by the spatiotemporal weight function. Because the noise is assumed to be independent between cones, we derived the noise component of the pooled response (PR_{noise}) by pooling the variance across cones of the same type within each retinal subregion, and then summing across pixels (Figure 4.2 H):

$$\mathrm{PR}_{\mathrm{noise}} = \sum_{x,y}\left[\frac{1}{N^2 n_{(x,y)}}\sum_{f}\left(\left|\mathrm{WT}_{(x,y,f)}\right|^2 \times \left|E_{(f)}\right|^2\right)\right]$$

(Eq. 4.19)

where $n_{(x,y)}$ is the number of cones of a specific type in the retinal subregion at *(x,y)*. Repeating this process for each cone type results in a three element vector describing the variance of the model's pooled response. Assuming Gaussian cone noise gives the three elements of the pooled response a jointly Gaussian distribution that is completely specified by its mean, PR_{sig}, and variance, PR_{noise} (Figure 4.2 I).

Ideal observer analysis on the pooled responses

The performance of the model on the chromatic detection task was calculated using the distribution of pooled responses for Gabor-present and Gabor-absent trial types (Figure 4.2 I). There are two components of the pooled response for Gabor present trials at a single intensity, GAB_{sig} and GAB_{noise}, each of which is a three element vector. Similarly, there are two components of the pooled response for Gabor absent trials: $BLANK_{sig}$ and $BLANK_{noise}$.

This analysis begins by reducing the 3D pooled-response distributions (GAB and BLANK) to 1D distributions using linear discriminant analysis:

$$\mathbf{W} = \begin{bmatrix} \mathrm{GAB}_{\mathrm{noise},\,l} & & \\ & \mathrm{GAB}_{\mathrm{noise},\,m} & \\ & & \mathrm{GAB}_{\mathrm{noise},\,s} \end{bmatrix} + \begin{bmatrix} \mathrm{BLANK}_{\mathrm{noise},\,l} & & \\ & \mathrm{BLANK}_{\mathrm{noise},\,m} & \\ & & \mathrm{BLANK}_{\mathrm{noise},\,s} \end{bmatrix}$$

(Eq. 4.20)

Where **W**, the within-class scatter matrix, is the sum of the covariance matrices for each of the 3D distributions. Because the stimulus modulations to each of the cone types are assumed to be independent, the covariance matrices are diagonal with elements equal to PR_{noise} for each cone type.

The between-class scatter matrix (**B** in the equation below) can be calculated as the outer product of a vector of differences in PR_{sig} for Gabor present and absent trials:

$$\mathrm{b} = \mathrm{GAB}_{\mathrm{sig}} - \mathrm{BLANK}_{\mathrm{sig}}$$

$$\mathbf{B} = \mathrm{b}^{\top}\mathrm{b}$$

(Eq. 4.21)

The discriminant vector (v) was defined as the largest eigenvector of the matrix $\mathbf{W}^{-1}\mathbf{B}$. We then projected the 3D pooled response distributions (GAB and BLANK) onto the discriminant vector to yield 1D probability densities which were the decision variables used by the ideal observer (Figure 4.2 I&J). The mean and standard deviation for each 1D probability density can be calculated using the discriminant vector (v) as a set of coefficients to weight the mean (μ) and variance (σ^2) of the 3D pooled response distribution:

$$\mu = \mathrm{PR}_{\mathrm{sig}} \cdot v \tag{Eq. 4.22}$$

$$\sigma^2 = \begin{bmatrix} \mathrm{PR}_{\mathrm{noise},\,l} & \mathrm{PR}_{\mathrm{noise},\,m} & \mathrm{PR}_{\mathrm{noise},\,s} \end{bmatrix} \begin{bmatrix} v_l^2 \\ v_m^2 \\ v_s^2 \end{bmatrix} \tag{Eq. 4.23}$$

The performance of the model on the detection task was determined by the discriminability between the 1D distributions for Gabor-present and Gabor-absent trials, which was calculated using a well established signal detection theory framework (Green and Swets 1966; Britten et al. 1992; Hass and Horwitz 2013). Implicit in our model is the existence of an ideal observer that performs the detection task using only the pooled responses of the cone mosaic. On a single trial, the ideal observer receives a draw from both of the 1D decision variable distributions and must decide which draw came from the Gabor-present distribution. The task of the ideal observer is thus analogous to the monkey's decision regarding the location of the Gabor stimulus. The probability of a hit can be obtained from the cumulative density of the 1D Gabor-present and Gabor-absent distributions:

$$p(\mathrm{Hit}) = 1 - \left(\frac{1}{2}\left[1 + \mathrm{erf}\left(\frac{criterion - \mu_{\mathrm{GAB}}}{\sigma_{\mathrm{GAB}}\sqrt{2}}\right)\right]\right) \tag{Eq. 4.24}$$

The probability of a false alarm can be derived similarly using μ_{BLANK} and σ_{BLANK}. Lastly, the percent correct for the ideal observer can be calculated as the integral of the receiver operator characteristic defined by the p(Hit) and p(false alarm) (Green and Swets 1966). We repeated this process for multiple stimulus intensities to derive a neurometric function, and we defined the detection threshold for the model on the basis of the best fitting cumulative Weibull function:

$$p(\mathrm{Correct}) = 1 - 0.5e^{\left(-\frac{cc}{\alpha}\right)^{\beta}} \tag{Eq. 4.25}$$

Where *cc* is the cone contrast of the stimulus, α is the contrast at detection threshold and β defines the slope of the neurometric function.

Results

Testing the model

To test the model, we compared the photocurrent of modeled cones to that of real cones recorded in vitro in response to a brief pulse of light. Real and modeled cones were adapted to a 4000 R*/sec background light level and then stimulated with a 4000 R*/sec pulse of light for 10 ms. The amplitude of the photocurrent measured in vitro was well predicted by the model (Figure 4.3 A) but the variability of real-cone photocurrents had high temporal frequency components that were absent in the model's response (Figure 4.3 A). This discrepancy is due to the fact that modeled-cones sampled time at a finite rate. As we increased the sampling rate of the cones (equivalently, decreased the Δt of the simulation), the power of high-temporal frequency noise in the model's response increased (Figure 4.3 right panels). The coarse temporal quantization of the model excludes temporal frequency components that exist in real cones, but ideal observer that reads out the models cones responses uses a temporal weighting function filters out these high temporal-frequency components anyway (Figure 4.2 G). Unless otherwise noted, the sampling rate of the model was set to 825 Hz.

Human observers can detect a stimulus that delivers 2-5 R* to each of approximately 14 cones subtended by a foveally presented stimulus (Koenig and Hofer 2011). We verified that such a stimulus resulted in a just-detectable output of our model. An individual modeled-cone could detect a stimulus that induced 18 R*. A group of 14 modeled cones could detect a stimulus that induced 5 R* per cone (Figure 4.3 B). Importantly, the congruence between our model and the results of Koenig and Hofer (2011) are dependent on the adaptation state of the cones (γ in Eq. 4.13). Koenig and Hofer's (2011) subjects were dark adapted, and their data are well aligned to the model's result when the gain term reflects dark adapted cones measured in vitro. On the other hand, the model's thresholds make a prediction about how detection thresholds should depend on mean light level: increases in the background light level cause decreases in the gain of the cone signals and resulted in slightly higher detection thresholds for the model. Overall, these findings suggest that our choice for the ideal-observer readout of modeled cone responses is supported by existing physiological and psychophysical measurements.

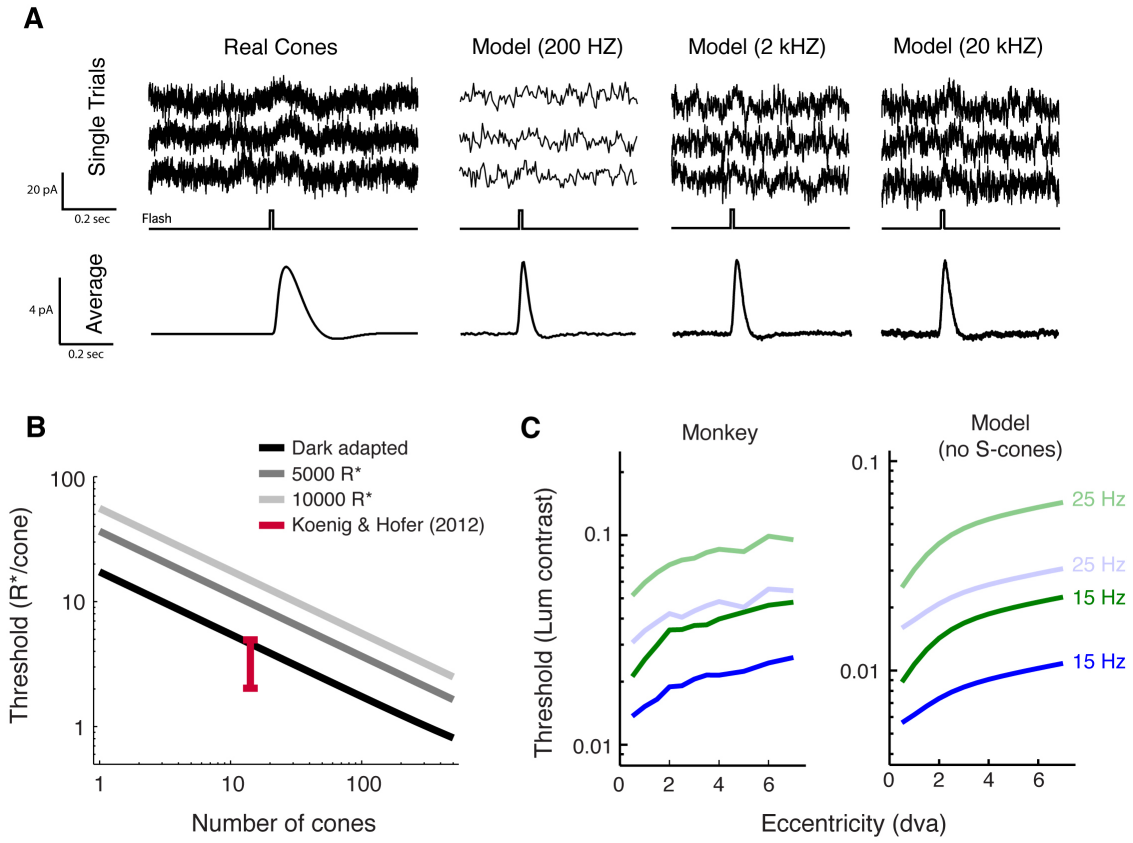

Figure 4.3 Comparing model predictions to physiological and psychophysical data. *A*: The responses of real (left column) and model cones (right three columns) to a 10 ms 100% contrast pulse delivered on a 4000 R*/sec background. Single trial responses (upper panels) and average responses (lower panels) demonstrate similar response dynamics of real and modeled cones. High-frequency noise is less pronounced when the model used a low sampling rate, but was more prevalent when the model's sampling rate approached the data acquisition rate used in vitro. *B:* Absolute detection threshold (measured in R*/sec) as a function of number of cones in the artificial mosaic, modeled at 3 different adaptation states. Thresholds for the dark-adapted case match the range of detection thresholds (red bar) of dark-adapted human observers (Koenig and Hofer 2011). *C:* Eccentricity and temporal frequency dependence of thresholds for 15 and 25 Hz luminance flicker. Stimuli were Gabor patterns with a SD=0.15º truncated at 2SD and spatial frequency of 3 cyc/deg. Stimuli were presented along the horizontal midline. Threshold is expressed in terms of luminance contrast defined by the human photopic luminance efficiency function. Green and blue curves correspond to green and blue monitor phosphor modulations respectively.

Effects of eccentricity and temporal frequency

The visual sensitivity of primates depends on the eccentricity and temporal frequency of stimulation. This is also true of the model. In the model, eccentricity dependence comes from macular pigment and cone density, and the temporal frequency

sensitivity comes from the dynamics of the cone's temporal impulse response and noise power spectrum.

To compare the model's eccentricity dependence to psychophysical data, we measured a monkey's detection threshold for a 15 Hz drifting Gabor stimulus that varied in retinal eccentricity. In interleaved trials, the Gabor was defined by modulations of either the blue or green monitor phosphor. Using two phosphors allowed us to dissociate the influence of macular pigment and cone density. Sensitivity to blue is impaired specifically where macular pigment density is highest because macular pigment absorbs light from the blue phosphor more efficiently than it does light from the green phosphor. Outside of the central 2°, macular pigment density is negligible, and sensitivity to both of blue and green decreases in a nearly fixed ratio due to decreasing cone density. As shown in Figure 4.3 C, the model cone mosaic qualitatively matched the monkeys' psychophysical data. Thresholds for the ideal observer were consistently lower than the monkey's, but the eccentricity dependence of thresholds was similar between the model and the monkey for both blue and green modulations. S-cones were omitted from the model for this analysis because they are not thought to contribute strongly to the detection of high temporal frequency luminance flicker (Eisner and MacLeod 1980). This suggests that the eccentricity dependence of thresholds for these stimuli is well predicted by signals present in the cone outer segments.

The model does not include any interactions between temporal frequency and eccentricity. It therefore predicts that detection thresholds measured at two different temporal frequencies should be related to each other by a scale factor that does not change with eccentricity. This prediction was confirmed by comparing detection thresholds for the model and the monkey in response to a 15 and 25 Hz stimulation. Across both temporal frequencies, the model was ~2.5 more sensitive than the monkey.

Temporal contrast sensitivity for L- and M-cone modulations

Contrast detection thresholds for modulations of the L- and M-cones depend on their relative phase and temporal frequency. Sensitivity is low-pass for out-of-phase modulations (L–M) but band-pass for in-phase modulations (L+M) (Kelly 1974; Kelly and van Norren 1977; Swanson et al. 1987). Despite this difference in stimulus

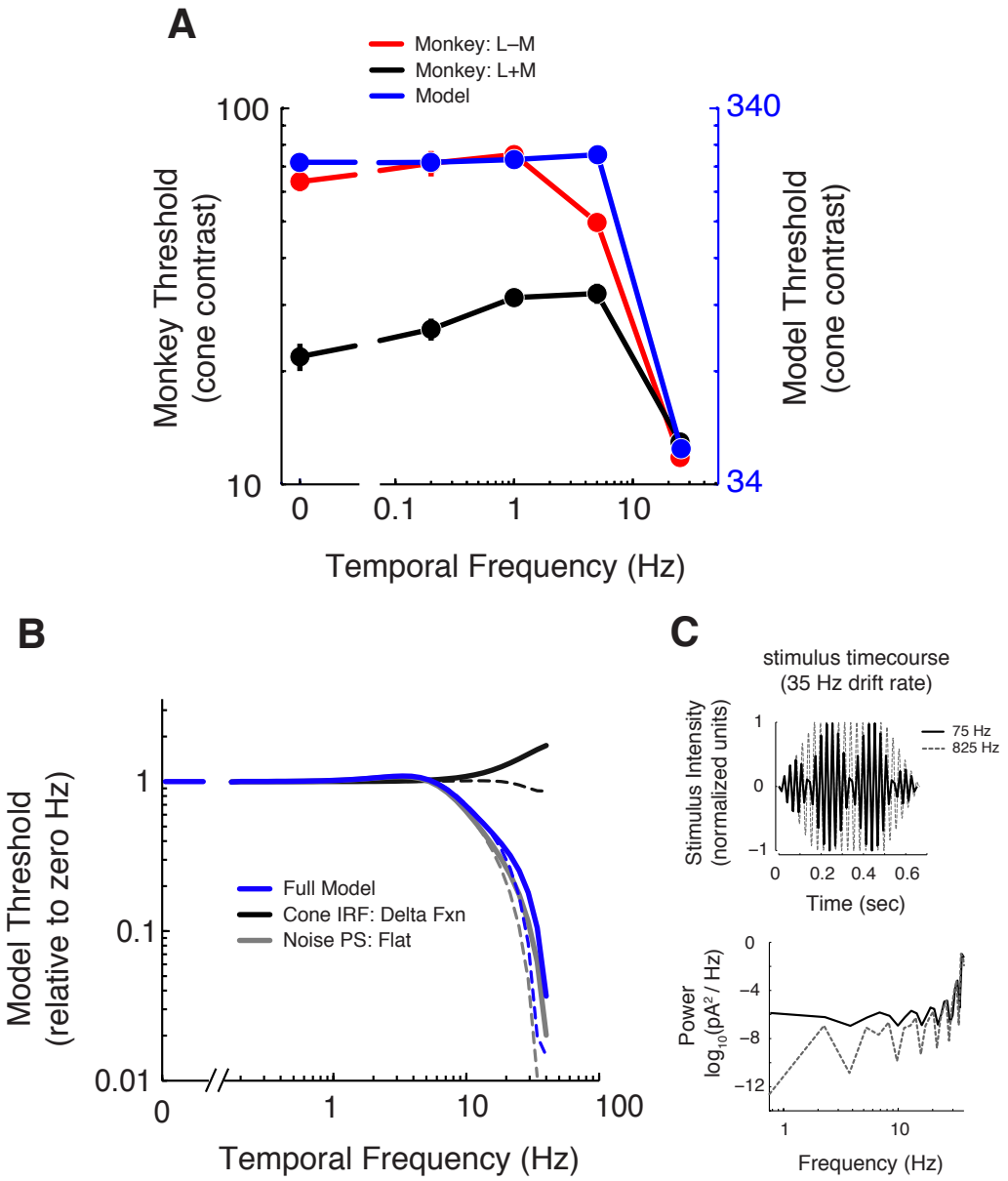

Figure 4.4 Temporal contrast sensitivity functions. *A:* L–M and L+M contrast sensitivity (1/threshold) as a function of temporal frequency for the model (blue) and for Monkey N (black and red). The model's sensitivity function has been shifted vertically to aid in comparison to the monkey's data. Gabor stimuli had a SD=0.4º truncated at 3SD and a spatial frequency of 3 cyc/deg. *B*: Contrast sensitivity of the full model (blue), a model that has a flat cone-noise power spectrum (black), or a model that uses a delta function for the cone IRF (gray). Solid lines correspond to a modeled monitor refresh rate of 825 Hz, dashed lines correspond to a modeled monitor refresh rate of 75 Hz (the rate actually used in all experiments). *C:* Normalized stimulus intensity as a function of time as displayed using a modeled monitor refresh rate of 825 Hz (dotted line) or using a modeled refresh rate of 75 Hz (black). The bottom panel illustrates the power spectra of the stimuli in the top panel. Notice that the different monitor refresh rates produce stimuli with different power spectra.

detectability, the information available at the level of the cone mosaic is invariant to the temporal phase of the L- and M-cone modulations. Clearly, signals from the cones are not used equally efficiently to detect L+M and L-M modulations.

To determine the extent to which the temporal dependence of behavioral sensitivity to L+M and L–M modulations are inherited from the cone photoreceptors, we calculated detection thresholds for the model in response to modulations of the L- and M-cones and compared them to thresholds of one monkey. The model's sensitivity (1/ threshold) was temporally low-pass with a high-cutoff frequency of approximately 10 Hz (drift rate at 70% of maximal sensitivity; Figure 4.4 A). Behavioral sensitivity for the monkey is plotted on the same set of axes for in-phase (L+M) and out-of-phase (L–M) modulations. Consistent with previous studies, the monkey's behavioral sensitivity is low-pass for chromatic (L–M) stimuli but band-pass for luminance (L+M) stimuli (Hass and Horwitz 2013) .

The shape of the monkey's sensitivity function to the L–M stimulus follows closely the temporal-frequency dependence of the model: both of the functions are temporally low-pass and have similar cutoff frequencies. The model was roughly a factor of three more sensitive than the monkey for high temporal frequency modulations (L+M or L-M) and for low temporal frequency modulations (L-M only). The high-frequency cutoff for the model was roughly matched to that of the monkey over the range of frequencies we tested. This suggests that, up to 25 Hz, behavioral sensitivity for chromatic stimuli follows the limits imposed by stimulus transduction in the cone outer segments. The discrepancy between the model and monkey for low temporal frequency L +M modulations suggest that the visual system attenuates these signals and corrupts them, either with higher frequency transduction noise or with noise in post-receptoral processing.

Stimulus detection depends on the signal and noise characteristics of neural responses. An advantage of the model is that we can isolate these two components in a way that would be experimentally impossible. By using a cone-noise power spectrum that is spectrally flat, we can run the model to determine how the temporal contrast sensitivity function would look if it were determined only by the characteristics of the cone's impulse response function. Likewise, by using a delta function for the cone's impulse

response (which corresponds to a flat frequency response), we can determine how the temporal contrast sensitivity function would look if it were only determined by the spectral properties of the noise.

The temporal contrast sensitivity of the model was almost entirely determined by the temporal dynamics of the cone's impulse response function (Figure 4.4 B). The sharp decrease in the cone's frequency response above 10 Hz (gray line) is opposed by a slight decrease in cone noise (black line) which serves to improve the model's sensitivity for frequencies between 10 and 40 Hz (Figure 4.4 B). Overall, the temporal statistics of noise in the phototransduction cascade make only minor contributions to the shape of the temporal contrast sensitivity function.

The model also reveals an unexpected relationship among the sensitivity of the observer, the *nominal* temporal drift rate of the stimulus, and the refresh rate of the display device. When drifting Gabor stimuli are displayed on a CRT computer monitor, the temporal dynamics of the intended stimulus are sampled at the monitor's refresh rate. As a consequence, the pattern of light *actually* displayed has a component at the difference frequency between the stimulus frequency and half the monitor refresh rate. For example, when the sinusoidal component of the Gabor drifts at 35 Hz, the actual stimulus will be amplitude modulated at 5 Hz (when displayed on a 75 Hz refresh rate monitor, see Figure 4.4 C). This changes the spectral power distribution for the stimulus. Differences in the monitor refresh rate can also affect the noise in the decision variable used by the ideal observer: the raw cone noise is filtered by the spatiotemporal weighting function, whose temporal statistics are tied to the Gabor stimulus. The net effect is that the model's temporal contrast sensitivity function changes as a function of the monitor's refresh rate (compare solid and dashed curves in Figure 4.4 B). Furthermore, the model makes the prediction that the behavioral sensitivity should also depend on the monitor's refresh rate. For a stimulus drift rate of 30 Hz, the model predicts a factor of 2 improvement when using a high refresh rate monitor.

Chromatic contrast detection and comparison with V1 sensitivity

The temporal contrast sensitivity function for L–M (but not L+M) modulations followed closely the limits imposed by the cones. These two stimuli are physically

similar (they differ only in the relative phase of L- and M-cone modulation), but are perceptually quite different. L+M modulations are closely aligned to the luminance color direction. L–M modulations are therefore nearly orthogonal to the luminance direction and can be considered a purely chromatic modulation. We can recast the difference between L+M and L–M processing as a difference between luminance and color processing. Viewed this way, our results indicate that color sensitivity is more closely tied to signals in the cones than luminance sensitivity, at least at low spatial and temporal frequencies.

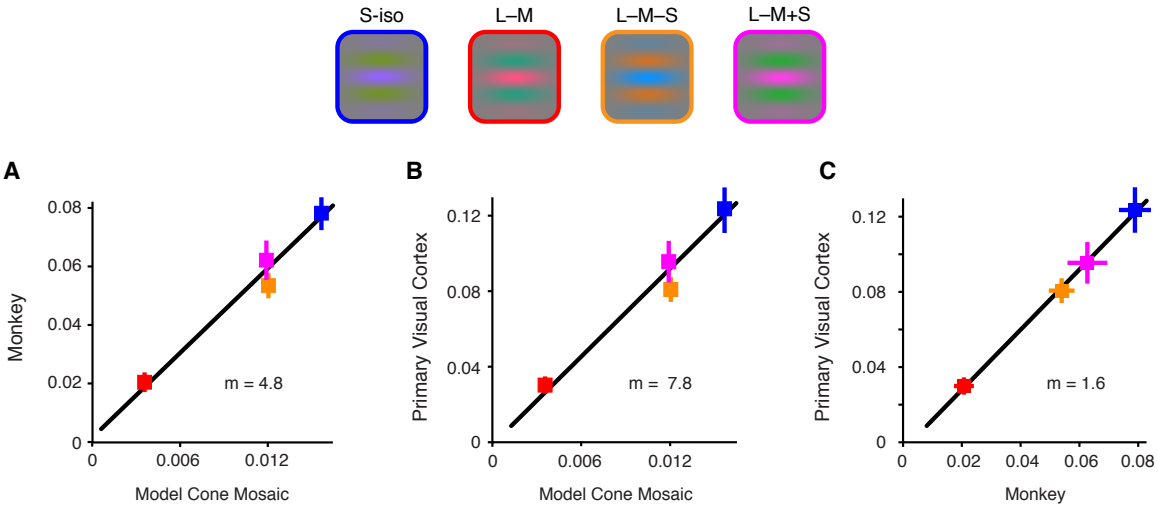

Figure 4.5 Sensitivity of the cone mosaic model, individual V1 neurons, and behaving monkeys on the contrast detection task. Upper panel: four color directions in the isoluminant plane defined by the following unit vectors S-iso (blue symbols) = [0 0 1], L–M (red) = [0.71, –0.71, 0], L–M–S (orange) = [0.14, –0.14, –0.98], L–M+S (magenta) = [0.14, –0.14, 0.98]. The Gabor stimulus had a SD=0.4º truncated at 3SD and drifted at 3 Hz. The other parameters of the Gabor were optimized eachV1 neuron. *A:* Average behavioral thresholds for the monkey vs. detection thresholds for the model, and the best fitting line (black) derived with orthogonal regression. Error bars represent 1 s.e.m. *B:* Neurometric thresholds of individual V1 neurons (recorded at the same time as the monkey's behavior) plotted against the detection thresholds of the cone-mosaic model. Conventions as for A. *C:* V1 neurometric thresholds plotted against behavioral detection thresholds. Conventions as for A.

To test the generality of this result we took advantage of the fact that color signals in the retina are mediated by at least two separate pathways: one pathway that mediates L–M signals and another that mediates S-cone signals. We tested the sensitivity of the model and the monkey to four different chromatic modulations: S-cone isolating, L–M, L–M–S, and L–M+S. The first two are expected to isolate the retinal cone-opponent

pathways, and the remaining two are expected to co-activate them. These color directions do not produce in-phase modulations of the L-cones and M-cones, and we consider these color directions to be approximately isoluminant. The spatial and temporal parameters for the Gabor stimulus were identical to those we used in a previous study (Hass and Horwitz 2013) which allows us to make direct comparisons between the model's thresholds and those of behaving monkeys and individual V1 neurons.

Detection thresholds for the monkey and for the model varied considerably across the four isoluminant colors. Thresholds were the lowest for the L–M color direction and were the highest for the S-cone isolating color direction. Nevertheless, thresholds for the monkeys and the model were related by a single scale factor across color directions (Figure 4.5 A). We estimated the scale factor using orthogonal regression on the mean detection thresholds and found that behavioral thresholds were 4.8 times larger than those of the model.

This result is particularly interesting when cast in terms of the neural mechanisms that mediate chromatic signal-processing. These colors are processed in parallel by at least two post-receptoral neural channels. The fact that behavioral sensitivity is related to the cone signals by a single scale factor across colors implies that the net output of these post-receptoral mechanisms operates similarly on their incoming signals from the cones. If one visual channel attenuates the cone signals or adds noise then the other visual channel must do the same. This gives rise to the possibility that, for each level of the visual hierarchy (retina, LGN, cortex, etc), there could be a single scale factor that relates the sensitivity of that visual area to the sensitivity of the cone mosaic across the four colors we tested.

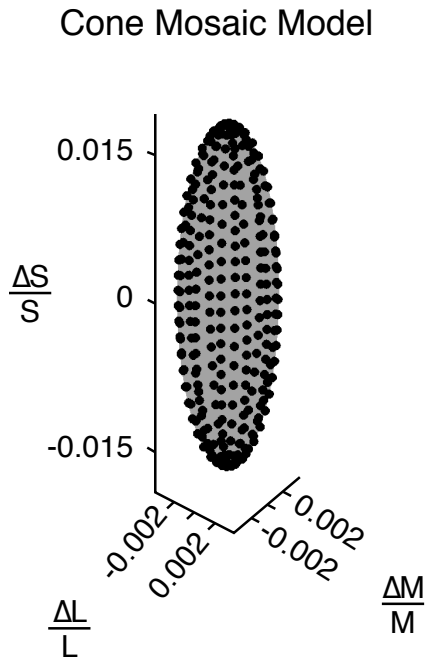

Figure 4.6 Isodetection surface in a 3D color space for the cone mosaic model. Detection thresholds (black points) and the isodetection surface (gray) for a Gabor stimulus located at 5º eccentricity along the horizontal meridian. SD = 0.4º truncated at 3SD. Temporal frequency = 3 Hz. The model responds identically for all spatial frequencies.

We probed this possibility by measuring neurometric thresholds for individual V1 neurons recorded from two monkeys performing the chromatic detection task (Hass and Horwitz 2013). Average neurometric thresholds for V1 neurons spanned nearly an order of magnitude across color directions (Figure 4.5 B), yet for each color, the average V1 neurometric threshold was a factor of 7.8 larger than the model's threshold (orthogonal regression on the mean thresholds). Likewise, there was a single scale factor that related the sensitivity of individual V1 neurons to the psychophysical thresholds of the monkey (slope = 1.6; Figure 4.5 C). The ratio of thresholds calculated for each data set in Figure 4.5 was not statistically different across colors (oneway anova on log(TR) $p > 0.05$). Together, these results suggest that processing of chromatic stimuli follows the limits imposed by the cones: thresholds for the model, individual V1 neurons, and the monkey depend on color, but across each level of the visual system there is a single scale factor that relates their sensitivity.

Comparison of 3D iso-detection surfaces for monkey and model

Our V1 neurophysiology experiments were well suited to precisely measure the neurometric thresholds for individual neurons, but this precision came at a cost: due to experimental time constraints we were only able to measure thresholds in four color directions (two per neuron). Our finding that behavioral thresholds were similarly related to those of the cone-mosaic across four isoluminant stimuli does not provide strong evidence that this result holds more generally for all of the colors we could have chosen (of which there are an infinite number). In order to quantify psychophysical thresholds in the context of the limits imposed by the cones for all stimuli in color space, we began by estimating the locus of points that are equally detectable to the model. We measured detection thresholds for 150 color directions in a 3D cone contrast space, and then fit the threshold values with an isodetection surface (Figure 4.6; see Methods). The isodetection surface represents the locus of points that are equally detectable to the model. It is elongated along the S-cone isolating color direction but is symmetric in the plane of L- and M-cone modulations.

Estimating the isodetection surface for the monkey is more challenging. We don't know a priori what the shape of the surface will be, and measuring a threshold in every color direction is not feasible. We approached this challenge by measuring isodetection surfaces of two monkeys using an adaptive technique (see Methods). After several iterations of the adaptive procedure we had identified a constellation of Gabor stimuli that were equally detectable to the monkey (Figure 4.7 A-G). These data sets are elongated along color directions that were difficult for the monkey to detect, and narrow for color directions that were easy to detect. We fit the raw data of each observer with an isodetection surface (Figure 4.7; see Methods) using a theoretical framework (Cole et al. 1993; Cole et al. 1994) that assumes that detection is mediated by three visual mechanisms that receive linear combinations of cone contrast inputs and interact via probability summation. The best fitting mechanisms for the two monkeys in this study are given in Table 4.2.

Table 4.2 Mechanism directions for the best fitting isodetection surface

	Mech 1	Mech 2	Mech 3	ψ	N
Monkey K					
0.5 cpd	0.76, -0.64, -0.09	0.36, -0.87, 0.33	0.84, -0.32, 0.43	1.2	168
1 cpd	0.81, -0.57, 0.01	0.67, -0.54, -0.50	0.33, -0.94, 0.07	1.0	135
2 cpd	0.76, -0.65, 0.04	0.97, -0.13, -0.22	0.18, -0.95, -0.27	2.5	119
4 cpd	0.99, 0.08, -0.14	0.13, 0.99, 0.03	0.96, -0.27, 0.02	1.4	87
Monkey S					
0.5 cpd	0.77, -0.63, -0.09	0.77, -0.47, 0.43	0.12, -0.98, 0.17	1.4	171
1 cpd	0.86, -0.50, -0.11	0.08, 0.96, 0.28	0.45, -0.88, 0.13	3.4	292
2 cpd	0.98, -0.16, 0.14	0.96, 0.08, -0.27	0.40, -0.90, -0.14	1.5	246
4 cpd	0.64, -0.76, -0.08	0.76, -0.54, -0.36	0.81, 0.59, 0.03	6.3	78

The three best fitting mechanism directions for isodetection surfaces of two monkeys at four different spatial frequencies. N = number of colors tested. ψ = exponent parameter of the best fitting surface. The shading corresponds to mechanisms that approximate the following cone combinations: L–M (red), S–(L+M) (blue), L–M–S (orange), L–M+S (magenta), L+M (black).

To identify the color directions that elicited behavioral sensitivity closest or farthest from the limits imposed by the cones, we computed the ratio between the monkey and model detection thresholds as specified by their isodetection surfaces. We then plotted threshold ratios (TR) as a heat map on a sphere (Figure 4.7 A-G). When the TR is one, then the monkeys match the limits imposed by phototransduction in the cones. When the TR is >>1, then the monkeys are particularly insensitive relative to the idea observer.

For the lowest spatial frequency stimulus (0.5 cyc • deg^{-1}), TRs ranged from 1.7 to 15 in Monkey K and from 1.6 to 7.2 in Monkey S. The low end of this range suggests that for some conditions, behavioral sensitivity is within a factor of two of the limits set by the cones. For both monkeys, TRs were consistent across a large portion of color space near the isoluminant plane (as evidenced by cool colors along the great-circle connecting the S-iso and L–M axes). Monkeys were most sensitive (relative to the cones) to stimuli near the L–M+S color direction (coordinates for Monkey K: [0.4, -0.46, 0.79] and Monkey S: [0.58, -0.7, 0.43]) although the TRs measured in these preferred

directions were not significantly different than the TRs for the L–M or S-iso color directions (bootstrap test, see methods). This suggests that TRs are relatively constant across isoluminant stimuli.

Adding an L+M component to the stimulus decreased the sensitivity of the monkey, and thus *increased* the TR values for those color directions. Although TRs were high for the L+M color direction, the lowest sensitivity was in response to achromatic stimuli (i.e., L+M+S). By definition, achromatic stimuli do not contain a chromatic component, and are not thought to modulate the neural mechanisms involved in color processing. The difference in sensitivity to L+M+S and L+M modulations was significant for Monkey K ($TR_{(L+M)} = 8.7$, $TR_{(L+M+S)} = 12.8$; bootstrap test, $p < 0.05$), but not for Monkey S ($TR_{(L+M)} = 6.4$, $TR_{(L+M+S)} = 7.0$; bootstrap test, $p > 0.05$) although the same trend was observed.

At higher spatial frequencies, monkeys continued to be maximally sensitive to modulations near the isoluminant plane (Figure 4.7 C-H). The color direction of minimal sensitivity transitioned from L+M+S (at low spatial frequency), to L+M (at intermediate spatial frequencies, to S-iso (at the highest spatial frequency). The relative insensitivity to high spatial frequency S-cone isolating stimuli can not be explained by the low numerosity of S-cones on the retina or by the distance between S-cones on the mosaic. A single cone in our model produces a sinusoidal photocurrent in response to drifting Gabor stimuli, and for a fixed temporal frequency, the temporal dynamics of the photocurrent are the same irrespective of spatial frequency. Thus, the information provided by the S-cone mosaic to the ideal observer does not depend on the spatial frequency of the stimulus.

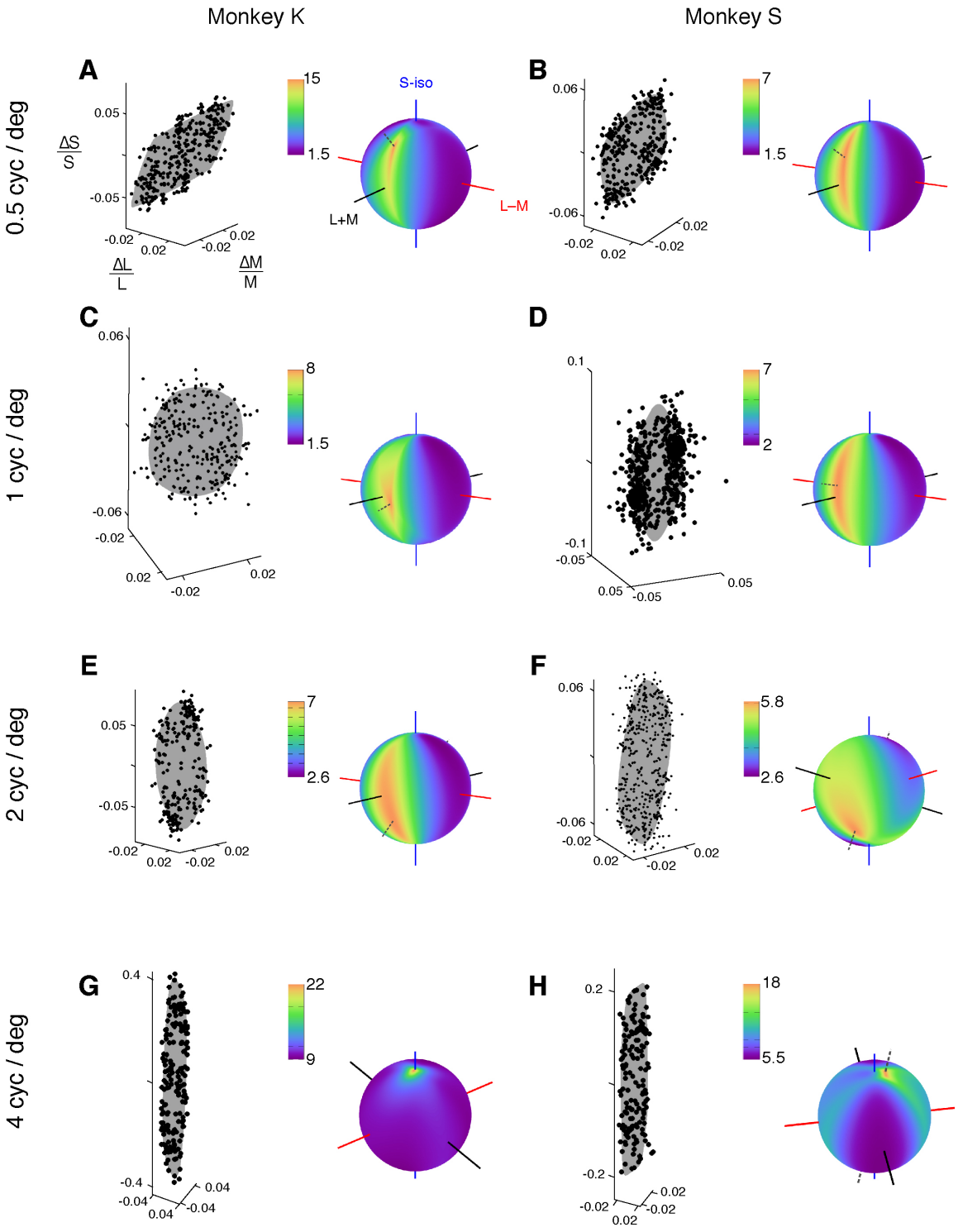
Monkey K
Monkey S
0.5 cyc / deg
1 cyc / deg
2 cyc / deg
4 cyc / deg
A
B
C
D
E
F
G
H
ΔS/S
ΔL/L
ΔM/M
S-iso
L+M
L−M

The isodetection surfaces illustrated in Figure 4.7 are conditional functions of a 4 dimensional stimulus space (3 dimensions for color plus one for spatial frequency), each of which permits the comparison of thresholds across many different color directions for a single spatial frequency. To facilitate comparisons across spatial frequency, we plotted TRs as a function of spatial frequency for 6 color directions (Figure 4.8). Four of these color directions are the identical isoluminant colors used in the V1 neurophysiology experiment, one is the L+M stimulus, and one is the achromatic stimulus. This representation forms a different conditional through the 4D stimulus space that highlights facets of the data that are otherwise hard to see.

Threshold ratios for isoluminant stimuli increased with spatial frequency but were relatively constant for luminance or achromatic modulations. At low spatial frequency, TRs were statistically indistinguishable across the four isoluminant color directions, but at higher spatial frequencies, detection performance for L–M+S color direction became increasingly impoverished relative to the others. The difference in TRs between the L–M +S and the L–M–S color directions was significant for spatial frequencies above 1 cyc/ deg for Monkey K, and above 0.5 cyc/deg for Monkey S (bootstrap test). This difference is surprising because both stimuli modulate the cones identically (but with a different phase relationship). Chromatic aberrations are negligible at such low spatial frequencies (Marimont and Wandell 1994), suggesting that they do not account for the asymmetry in the visibility of these stimuli.

Figure 4.7 (previous page): Isodetection surfaces two monkeys and comparisons with the model. *A:* detection thresholds (left panel, black points) for Monkey K at 0.5 cyc/deg. Color directions were selected using an adaptive sampling procedure. The isodetection surface (left panel, gray surface) was fit by assuming that detection is mediated by three independent visual channels (see Methods). The ratio of the monkey to the model isodetection surfaces plotted as a heat map on a sphere (right panel). Cool colors on the heat map show areas of color space for which the monkey's performance is close to the limits imposed by the phototransduction cascade. The basis vectors of the color space are shown as axes through the globe. Red = L–M, blue = S-cone isolating, black = L+M. The dashed line indicates the color direction associated with the largest TR. *C-J:* raw detection thresholds (left panel) and ratio of isodetection surfaces (right panel) for Monkey K and Monkey S across 4 spatial frequencies. Stimulus details for *A-H* as for Figure 4.6.

Discussion

Stimulus transduction by the mosaic of cone photoreceptors places an upper bound on the photopic visual sensitivity of the observer. Our experiments demonstrate that this fundamental limit is manifested in the chromatic contrast detection of macaque monkeys in various ways. The eccentricity dependence of detection thresholds for luminance flicker is well explained by the cone density at different retinal eccentricities, and the absolute detection thresholds of dark-adapted human observers is predicted by modeled cones that operate at the same adaptation state. The temporal frequency dependence of behavioral thresholds for a chromatic stimulus (but not luminance) follows the temporal frequency limits imposed by the cones. The shape of the temporal contrast sensitivity function up to 25 Hz is predictable on the basis of the impulse response of the cones and is essentially unaffected by the temporal statistics of noise in the phototransduction cascade.

Detection performance of the model was related by a single scale factor to detection thresholds of the monkey across a wide array of isoluminant color directions. For the four of these isoluminant color directions that we used to study V1 responses, signal-to-noise measurements of single neurons were similarly well matched to the monkey's behavioral sensitivity. This suggests that the neural circuits that underlie low spatiotemporal frequency contrast detection are equally noisy irrespective of color direction in the isoluminant plane. Lastly, a comparison of isodetection surfaces for the model and monkey identified spatiotemporal chromatic conditions for which behavioral sensitivity was within a factor of two of the limits set by the cones. This suggests that the post-receptoral circuitry adds only modest amounts of noise to the processing of low spatiotemporal frequency isoluminant modulations.

Model thresholds as a benchmark for comparison across stimulus space

The geometric configuration of data points in a stimulus space is often interpreted in terms of potential underlying biological mechanisms, but this interpretation can be misleading because the geometric configuration of the data points depends on the parameterization of the stimuli. Different, equally reasonable, parameterizations can change the apparent structure of the data. Our cone-mosaic model provides a benchmark

that can be used to create a metric (TR) that is immune to the space in which stimuli are represented. Using this approach we demonstrated that behavioral sensitivity to low spatiotemporal achromatic stimuli is acutely impoverished in absolute terms – not relative to other low spatiotemporal frequency stimuli or other achromatic stimuli, but relative to an ideal observer with access to the cones. This type of stimulus filtering may be ethological important: Shadows, which are achromatic and have low spatial frequencies, are generally less behaviorally relevant than changes in reflectance, which are usually indicated by chromatic and high spatial frequency luminance components.

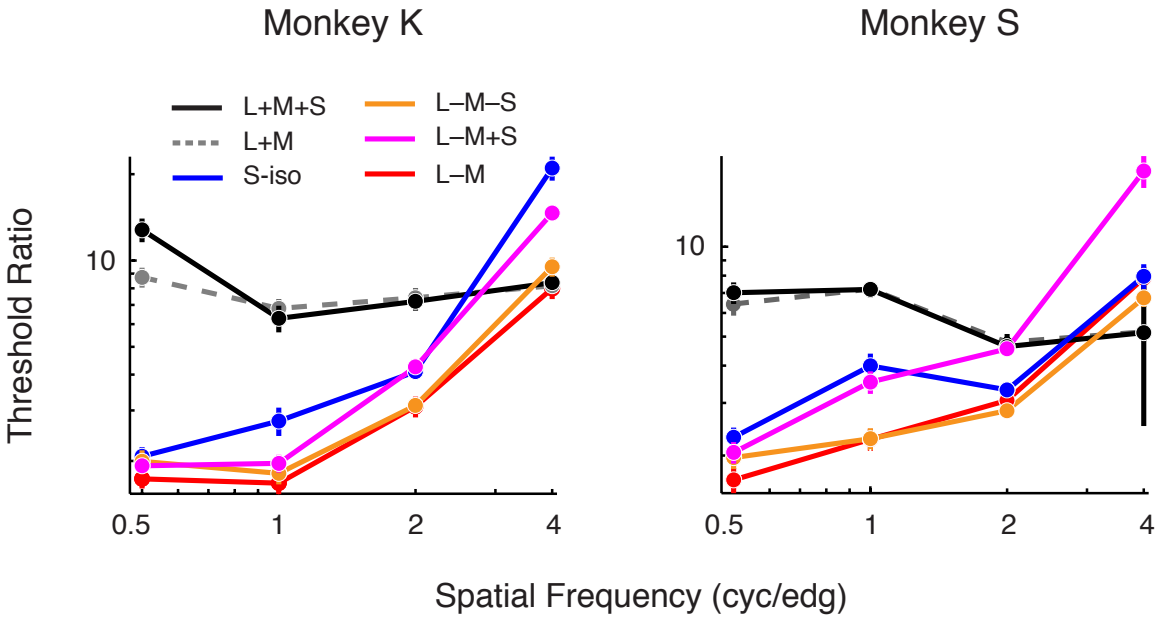

Figure 4.8 Comparison of threshold ratios across spatial frequency for 6 representative color directions across 4 spatial frequencies for Monkey K (*A*) and Monkey S (*B*). Data points were taken from the TR heat maps of Figure 4.7. Error bars represent 1 s.e.m and were estimated using a bootstrap procedure (see Methods).

Model assumptions and parameter uncertainty

A strength of our approach is that the responses of synthetic cones were modeled with no free parameters using biophysical values that were either measured directly or identified from existing studies. This simple approach yielded good qualitative and quantitative agreement with established measures of neurophysiology and detection behavior (Figure 4.3). On the other hand, not all the parameters were equally constrained

by the data, and an important question is how changes to each of the parameters affects the output of the model.

Many of the parameters affect the absolute sensitivity of the model without affecting its spatiotemporal chromatic tuning. Examples of these parameters include the dimensions of the eye (which affect the number of cones and the spectral irradiance), the cone collecting area (which affects the conversion of photons into photoisomerizations), and the eccentricity dependence of cone density. Other parameters affect the chromatic tuning of the model without influencing its spatiotemporal tuning. For example, the chromaticity of the background adapting field affects the relative gain of the cone responses across cone types: a short-wavelength adapting field would decrease the gain of the S-cones while holding the L- and M-cones in a higher gain state, and would necessarily change the aspect ratio of the model's isodetection surface. Importantly, we chose an adapting field that was identical to that used in our behavioral and neurophysiological studies.

The ideal observer had access to the cone photocurrents only through their projection onto a spatiotemporal weighting function. We chose a weighting function that would not selectively filter signals based on color direction but that would give the ideal observer essentially perfect access to the stimulus spatiotemporal profile. This means that the only noise allowed to degrade the quality of cone signals is in the pass band of the stimulus. It is unlikely that our monkeys filter the temporal dynamics of the real cone signals as selectively as our ideal observer, and a fruitful extension of our model would be to quantify the decrement in the model's performance when non-optimal weighting functions are used. On the other hand, our model assumes that the noise is additive with, and independent of, the mean responses. This implies that permitting cone-noise outside the pass band of the stimulus to intrude on the decision variable would only change the absolute sensitivity of the model without affecting its stimulus tuning. In summary, most of the uncertainty regarding the exact values of the model's parameters translates to uncertainty in our estimate of the ideal observer's absolute sensitivity. Nevertheless, the *relative* sensitivity across temporal and chromatic stimulus conditions is less sensitive to uncertainty in parameter estimates, and our results focus primarily on these comparisons.

We assumed that the noise component of the cone photocurrent was additive with, and independent of the mean response. This approximation is valid for low contrast stimuli (< 20%) typically used in contrast detection experiments. Additional considerations would be required to extend our model to a high-contrast regime. We also assumed that the cone IRF was separable with background illumination. This assumption forced the L-, M-, and S-cones to filter stimuli identically despite the fact that they were adapted to different levels by our background field. This assumption is not strictly true (Schneeweis and Schnapf 1999; Angueyra and Rieke 2013), but the difference in temporal filtering by the cone IRF across background light levels is modest over the range of background illuminiants we probed (2000 to 8000 R*/sec).

Comparisons with individual V1 neurons

One of our main findings was that a single scale factor relates detection thresholds of our model to those of individual V1 neurons and to behaving monkeys. We found that cone-mosaic model was roughly 5 times more sensitive than the monkey and 8 times more sensitive than individual V1 neurons. One asymmetry in our model is that the ideal observer bases its decisions on the pooled output of the cone mosaic (when analyzing signals from the retina), but only considers individual V1 neurons (when analyzing signals from the visual cortex). Pooling the responses of V1 neurons would improve the performance of an ideal observer and decrease the superiority of the cone-mosaic, but estimating the pooling rule for V1 neurons is non-trivial: the joint distribution of spiking responses among multiple V1 neurons is unknown and number of V1 neurons that could meaningfully contribute to the decision is poorly constrained by available data.

Discrepancies between human and monkey isodetection surfaces

The isodetection surfaces we measured for monkeys differ from those measured for humans under similar conditions (Cole et al. 1993; Sankeralli and Mullen 1996). Human isodetection surfaces for low spatial-frequency patterns are well predicted by three visual mechanisms: one that receives antagonistic inputs from the L- and M-cones (L–M), a second that sums the input from L- and M-cones (L+M) and a third that receives inputs from the S-cones opposed to the L- and M-cones (S-[L+M]) (Cole et al.

1993; Sankeralli and Mullen 1996). The best fitting mechanisms for monkey isodetection surfaces measured at low spatial frequency included three with opposed L- and M-cone inputs. One of these mechanisms typically lacked an S-cone component, but the other two had strong S-cone inputs in-phase with the L-cones (i.e., L–M+S). At higher spatial frequencies the cone inputs were often idiosyncratic. The S–(L+M) cone combination was rare among best fitting mechanisms.

The superficial interpretation of this result is that the post-receptoral channels that mediate contrast detection in humans receive different combinations of cone inputs than those in macaques, but several other explanations exist. Whereas our adaptive procedure selected color directions based on the local curvature of the surface, the isodetection surfaces of Cole et al., (1993) were constructed using colors from three principal planes in the color space. One possibility is that the full 3D isoresponse surface is poorly predicted from a subset of the points and that measuring the human surfaces in the full 3D color space would bring their measurements in closer agreement with the monkey's. An alternative explanation is that our use of the human corneal cone fundamentals (Stockman et al. 1993) produces inadequate stimulus control for experiments in non-human primates. Although photopigments for humans and monkeys are quite similar (Baylor et al. 1987; Schnapf et al. 1987), differences in the pre-retinal filtering between the two species could manifest as an aberrant S-cone input to psychophysical estimates of visual channels (Horwitz and Hass 2011; Hall and Colby 2013).

Future directions

Our model computes the output of a realistic cone mosaic to any arbitrary spatiotemporal chromatic stimulus and provides a benchmark that can be used to compare fairly the sensitivity to visual patterns across a wide range of conditions. In this study we probed low temporal frequency stimuli (< 25 Hz) and found that sensitivity to chromatic stimuli was superior. Future studies could investigate higher temporal frequencies where achromatic sensitivity is thought to be superior (Kelly 1974; Kelly and van Norren 1977; Swanson et al. 1987). Importantly, the model allows us to determine whether sensitivity to low frequency chromatic modulation is higher than to high frequency achromatic modulations in an absolute sense. Lastly, the orientation and shape of color

discrimination ellipses depends on the chromaticity of the background adapting field (LeGrand 1949; Krauskopf and Gegenfurtner 1992). Our model, which controls the gain of the cone signals according to their adaption state, provides a point of leverage to understand the contribution of phototransduction to the shape and orientation of these discrimination ellipses.

Discussion

This research has advanced our understanding of the role of primary visual cortex (V1) in chromatic contrast detection in three regards. First, the responses of individual V1 neurons at detection threshold are inconsistent with the cardinal mechanisms model. Second, the decrease in detectability of achromatic (but not red-green isoluminant) stimuli due to fixational saccades is not caused by a differential modulation of L/M cone opponent and non-opponent V1 neurons. Third, detection of low spatial and temporal frequency isoluminant modulations follow the limits imposed by signal transduction in the cone photoreceptors. Noise in the phototransduction cascade appears to play only a minor role in shaping the temporal passband of chromatic detection over the range we tested. Despite these advances there are several outstanding questions with regard to the role of V1 in chromatic detection. In this section, I will attempt to place our results in the broader context color vision and cortical neurophysiology.

The success of the cardinal mechanisms model at describing detection thresholds in cone contrast space, and the fact neurons in the early visual system (LGN and RGC) are well tuned to the cardinal colors, is seemingly at odds with our finding that V1 neurons do not behave as cardinal mechanisms at detection threshold. On the other hand, many studies have found evidence for 'higher-order' mechanisms that may also mediate chromatic contrast detection. Using a habituation task, Krauskopf et al., (1982) found a dominant role for the cardinal mechanisms but found additional evidence for higher-order mechanisms: threshold elevations were more tightly clustered for habituation to intermediate color directions than would be predicted by the cardinal mechanisms model (Krauskopf et al. 1986). This finding has been replicated using noise masking (Hansen and Gegenfurtner 2006) and is consistent with studies of motion coherence judgements (Krauskopf and Farell 1990; Krauskopf et al. 1996) and chromatic discrimination from non-neutral adaptation points (Krauskopf and Gegenfurtner 1992).

Many of the studies that revealed higher-order chromatic mechanisms used exogenous stimulus manipulations that may preferentially affect cortical neurons, but not neurons in the early visual pathway. Habituation paradigms are known to induce contrast adaptation in the retina and LGN when using achromatic stimuli (Chander and

Chichilnisky 2001; Baccus and Meister 2002; Solomon et al. 2004a), but the ability of chromatic stimuli to induce contrast adaptation in these neurons appears to be minimal (Solomon et al. 2004a). In primate V1, chromatic contrast can strongly adapt the responses of individual neurons (Tailby et al. 2008a). This suggests that the higher-order mechanisms identified psychophysically could be a result of contrast adaptation in the visual cortex. This possibility is supported by the observation that the habituation effect of Krauskopf et al., (1982) demonstrates intraocular transfer, which suggests that the neural locus of the effect receives inputs from both eyes. A parsimonious explanation may be that the bottleneck for chromatic detection is located in the retina, which causes psychophysical detection contours to be oriented along 'retinal' color coordinates. Psychophysical tasks that recruit cortical-specific physiological effects such as contrast adaptation expose the higher-order mechanisms, which are otherwise not evident in traditional detection experiments.

V1 is the gateway to extrastriate visual areas. As such, V1 is populated by neurons that support all aspects of vision. Color is multiplexed with signals for other visual functions, but the extent to which color-selective V1 neurons support these other sub-modalities remains unknown. We showed that some V1 neurons are very broadly tuned to color even at detection threshold. This gives rise to the possibility that one role for V1 is to broaden the color tuning of some neurons while sharpening the tuning of others. In a separate set of experiments, we recently demonstrated non-linear color tuning among V1 neurons (Horwitz and Hass 2012). Some neurons responded to all colors in cone contrast space and had ellipsoidal isoresponse surfaces, whereas other neurons were more tightly tuned and responded only to a subset of colors. An interesting possibility is that the broadly tuned neurons act as generalized contrast detectors whereas the tightly tuned neurons are important for color discrimination.

A second important role for V1 in color perception may be to rotate the principal axes of color space from "retinal" to "perceptual" coordinates (De Valois and De Valois 1993). Although the cardinal color directions are often referred to as "red-green" and "blue-yellow", there are important differences between the "retinal" axes and the perceptually defined unique hues (Derrington et al. 1984; Tailby et al. 2008b). For example, Krauskopf et al., (1982) noted that their S-cone isolating axis is inconsistent

with the Blue-Yellow unique hue axis. However, mixing S-cone signals with L–M signals could produce neurons sensitive to unique blue (–L+M+S), unique yellow (L–M–S), unique green (–L+M–S), and unique red (L–M+S) (Krauskopf et al. 1982; Wuerger et al. 2005; Stoughton and Conway 2008). This observation is supported by fitting the cone spectra to Jameson and Hurvich's (1955) hue cancelation data, which suggests that the neural mechanisms underlying the unique hues require the mixing of information from the two cardinal channels (Stockman and Brainard 2009). V1 is the first neural structure where signals from the parvo- and koniocellular pathways converge suggesting that the transition from retinal to perceptual color space may begin here. Consistent with this hypothesis, many neurons in V1 respond maximally to stimuli in the L–M–S color direction (Conway and Livingstone 2006; Solomon and Lennie 2005; Johnson et al. 2004; Horwitz et al. 2007). Taken together, these observations suggest a role for V1 in reshaping the primary color directions inherited from the LGN.

The experiments that contribute to this dissertation are by no means exhaustive, but they do point towards potentially fruitful future investigations. Measuring the width of color tuning and the chromatic contrast sensitivity for each neuron may provide clues to their functional significance to different aspects of color vision. Specifically, neurons that are tightly tuned to color are well equipped to mediate chromatic discrimination whereas neurons that are highly sensitive to contrast are well equipped to mediate visual detection. The experiments presented in Chapter 2 were constructed to test a specific hypothesis but were poorly suited to measure neurometric thresholds in many color directions simultaneously. This limitation made it challenging to measure the width of color tuning at detection threshold. An alternative approach would be to measure the activity of individual V1 neurons in response to Gabor stimuli located on the isodetection surfaces we identified in Chapter 3, which would extend the findings of our previous research (Horwitz and Hass 2012) to stimuli at detection threshold.

Intracellular recordings from V1 neurons could also elucidate some of the biophysical mechanisms involved in the color tuning we observed at detection threshold. For example, we found that some neurons were very broadly tuned at detection threshold. Because color-tuning and contrast are not generally separable (Solomon and Lennie 2005), one possibility is that neurons are broadly tuned at threshold but more narrowly

tuned to high contrast stimuli. This might be the case if the color tuning of excitatory and inhibitory inputs are differentially affected by contrast.

In conclusion, color vision remains an excellent model system to investigate the neural basis of perception. Future studies will hopefully continue to use a combined approach of psychophysics and neurophysiology at the level of V1 and beyond.

References

Ala-Laurila P, Greschner M, Chichilnisky EJ, Rieke F, (2011). Cone photoreceptor contributions to noise and correlations in the retinal output. *Nat Neurosci* 14: 1309-1316.

Andersen CF, Finlayson GD, (2010). Estimation of an individuals Human Cone Fundamentals from their Color Matching Functions. *Conference on Colour in Graphics, Imaging, and Vision* 2010: 138-142.

Angueyra JM, Rieke F, (2013). Origin and Impact of Phototransduction Noise in Primate Cone Photoreceptors. *In submission* .

Anzai A, Ohzawa I, Freeman RD, (1999). Neural mechanisms for processing binocular information I. Simple cells. *J Neurophysiol* 82: 891-908.

Baccus SA, Meister M, (2002). Fast and slow contrast adaptation in retinal circuitry. *Neuron* 36: 909-919.

Bair W, O'Keefe LP, (1998). The influence of fixational eye movements on the response of neurons in area MT of the macaque. *Vis Neurosci* 15: 779-786.

Baylor DA, Nunn BJ, Schnapf JL, (1984). The photocurrent, noise and spectral sensitivity of rods of the monkey Macaca fascicularis. *J Physiol* 357: 575-607.

Baylor DA, Nunn BJ, Schnapf JL, (1987). Spectral sensitivity of cones of the monkey Macaca fascicularis. *J Physiol* 390: 145-160.

Beeler GW, (1967). Visual threshold changes resulting from spontaneous saccadic eye movements. *Vision Res* 7: 769-775.

Billock VA, (1995). Cortical simple cells can extract achromatic information from the multiplexed chromatic and achromatic signals in the parvocellular pathway. *Vision Res* 35: 2359-2369.

Blakemore C, Campbell FW, (1969). On the existence of neurones in the human visual system selectively sensitive to the orientation and size of retinal images. *J Physiol* 203: 237-260.

Borghuis BG, Sterling P, Smith RG, (2009). Loss of sensitivity in an analog neural circuit. *J Neurosci* 29: 3045-3058.

Boynton GM, Demb JB, Glover GH, Heeger DJ, (1999). Neuronal basis of contrast discrimination. *Vision Res* 39: 257-269.

Bradley A, Switkes E, De Valois K, (1988). Orientation and spatial frequency selectivity of adaptation to color and luminance gratings. *Vision Res* 28: 841-856.

Brainard DH, (1997). The Psychophysics Toolbox. *Spat Vis* 10: 433-436.

Bridgeman B, Macknik SL, (1995). Saccadic suppression relies on luminance information. *Psychol Res* 58: 163-168.

Bridgeman B, Palca J, (1980). The role of microsaccades in high acuity observational tasks. *Vision Res* 20: 813-817.

Britten KH, Newsome WT, Shadlen MN, Celebrini S, Movshon JA, (1996). A relationship between behavioral choice and the visual responses of neurons in macaque MT. *Vis Neurosci* 13: 87-100.

Britten KH, Shadlen MN, Newsome WT, Movshon JA, (1992). The analysis of visual motion: a comparison of neuronal and psychophysical performance. *J Neurosci* 12: 4745-4765.

Burr DC, Morrone MC, (1996). Temporal impulse response functions for luminance and colour during saccades. *Vision Res* 36: 2069-2078.

Burr DC, Morrone MC, Ross J, (1994). Selective suppression of the magnocellular visual pathway during saccadic eye movements. *Nature* 371: 511-513.

Cavanaugh JR, Bair W, Movshon JA, (2002). Nature and interaction of signals from the receptive field center and surround in macaque V1 neurons. *J Neurophysiol* 88: 2530-2546.

Chander D, Chichilnisky EJ, (2001). Adaptation to temporal contrast in primate and salamander retina. *J Neurosci* 21: 9904-9916.

Chatterjee S, Callaway EM, (2003). Parallel colour-opponent pathways to primary visual cortex. *Nature* 426: 668-671.

Chatterjee S, Ohki K, Reid C, (2008). Functional micro-architecture of color selectivity in macaque primary visual cortex. *Society for neuroscience abstract [666 15/ LL15]* .

Chen Y, Geisler WS, Seidemann E, (2006). Optimal decoding of correlated neural population responses in the primate visual cortex. *Nat Neurosci* 9: 1412-1420.

Chen Y, Geisler WS, Seidemann E, (2008). Optimal temporal decoding of neural population responses in a reaction-time visual detection task. *J Neurophysiol* 99: 1366-1379.

Cole GR, Hine T, McIlhagga W, (1993). Detection mechanisms in L-, M-, and S-cone contrast space. *J Opt Soc Am A* 10: 38-51.

Cole GR, Hine TJ, McIlhagga W, (1994). Estimation of linear detection mechanisms for stimuli of medium spatial frequency. *Vision Res* 34: 1267-1278.

Conway BR, (2001). Spatial Structure of Cone Inputs to Color Cells in Alert Macaque Primary Visual Cortex (V-1). *The Journal of Neuroscience* 8: .

Conway BR, Livingstone MS, (2006). Spatial and temporal properties of cone signals in alert macaque primary visual cortex. *The Journal of neuroscience* 26: 10826-10846.

Cottaris NP, (2003). Artifacts in spatiochromatic stimuli due to variations in preretinal absorption and axial chromatic aberration: implications for color physiology. *J Opt Soc Am A Opt Image Sci Vis* 20: 1694-1713.

Crook JD, Davenport CM, Peterson BB, Packer OS, Detwiler PB, Dacey DM, (2009). Parallel ON and OFF cone bipolar inputs establish spatially coextensive receptive field structure of blue-yellow ganglion cells in primate retina. *J Neurosci* 29: 8372-8387.

Crook JD, Manookin MB, Packer OS, Dacey DM, (2011). Horizontal cell feedback without cone type-selective inhibition mediates "red-green" color opponency in midget ganglion cells of the primate retina. *J Neurosci* 31: 1762-1772.

Cui J, Wilke M, Logothetis NK, Leopold DA, Liang H, (2009). Visibility states modulate microsaccade rate and direction. *Vision Res* 49: 228-236.

Dacey DM, Lee BB, (1994). The 'blue-on' opponent pathway in primate retina originates from a distinct bistratified ganglion cell type. *Nature* 367: 731-735.

De Monasterio FM, Gouras P, (1975). Functional properties of ganglion cells of the rhesus monkey retina. *J Physiol* 251: 167-195.

De Monasterio FM, McCrane EP, Newlander JK, Schein SJ, (1985). Density profile of blue-sensitive cones along the horizontal meridian of macaque retina. *Invest Ophthalmol Vis Sci* 26: 289-302.

De Valois RL, Abramov IA, Jacobs GH, (1966). Analysis of response patterns of LGN cells. *JOSA* 56: 966-977.

De Valois RL, Cottaris NP, Elfar SD, Mahon LE, Wilson JA, (2000). Some transformations of color information from lateral geniculate nucleus to striate cortex. *Proc Natl Acad Sci U S A* 97: 4997-5002.

De Valois RL, De Valois KK, (1993). A multi-stage color model. *Vision Res* 33: 1053-1065.

De Vries HL, (1948). The fundamental response curves of normal and abnormal dichromatic and trichromatic eyes. *Physica* 14: 367-380.

Derrington AM, Krauskopf J, Lennie P, (1984). Chromatic mechanisms in the lateral geniculate nucleus of macaque. *Journal of Physiology* 357: 241-265.

Deubel H, Elsner T, (1986). Threshold perception and saccadic eye movements. *Biol Cybern* 54: 351-358.

Diamond MR, Ross J, Morrone MC, (2000). Extraretinal control of saccadic suppression. *J Neurosci* 20: 3449-3455.

Ditchburn RW, (1955). Eye movements in relation to retinal action. *Optica acta* 1: 171-176.

Donner K, (1992). Noise and the absolute thresholds of cone and rod vision. *Vision Res* 32: 853 - 866.

D'Zmura M, Knoblauch K, (1998). Spectral bandwidths for the detection of color. *Vision Res* 38: 3117-3128.

Economides JR, Sincich LC, Adams DL, Horton JC, (2011). Orientation tuning of cytochrome oxidase patches in macaque primary visual cortex. *Nat Neurosci* 14: 1574-1580.

Edwards DP, Purpura KP, Kaplan E, (1995). Contrast sensitivity and spatial frequency response of primate cortical neurons in and around the cytochrome oxidase blobs. *Vision Res* 35: 1501-1523.

Eisner A, MacLeod DI, (1980). Blue-sensitive cones do not contribute to luminance. *J Opt Soc Am* 70: 121-123.

Engbert R, Kliegl R, (2003). Microsaccades uncover the orientation of covert attention. *Vision Res* 43: 1035-1045.

Eskew RT, (2009). Higher order color mechanisms: a critical review. *Vision Res* 49: 2686-2704.

Eskew RT, Newton JR, Giulianini F, (2001). Chromatic detection and discrimination analyzed by a Bayesian classifier. *Vision Res* 41: 893-909.

Estévez O, Spekreijse H, (1982). The "silent substitution" method in visual research. *Vision Res* 22: 681-691.

Field GD, Gauthier JL, Sher A, Greschner M, Machado TA, Jepson LH, Shlens J, Gunning DE, Mathieson K, Dabrowski W, Paninski L, Litke AM, Chichilnisky EJ, (2010). Functional connectivity in the retina at the resolution of photoreceptors. *Nature* 467: 673-677.

Field GD, Sher A, Gauthier JL, Greschner M, Shlens J, Litke AM, Chichilnisky EJ, (2007). Spatial properties and functional organization of small bistratified ganglion cells in primate retina. *J Neurosci* 27: 13261-13272.

Gegenfurtner KR, Kiper DC, (1992). Contrast detection in luminance and chromatic noise. *JOSA A* 9: 1880-1888.

Gegenfurtner KR, Kiper DC, Beusmans JMH, Carandini M, Zaidi Q, Movshon JA, (1994). Chromatic properties of neurons in macaque MT. *Vis Neurosci* 11: 455-455.

Geisler WS, Albrecht DG, (1997). Visual cortex neurons in monkeys and cats: Detection, discrimination, and identification. *Vis Neurosci* 14: 897 - 919.

Giulianini F, Eskew RTJ, (1998). Chromatic masking in the (delta L/L, delta M/M) plane of cone-contrast space reveals only two detection mechanisms. *Vision Res* 38: 3913-3926.

Goodchild AK, Ghosh KK, Martin PR, (1996). Comparison of photoreceptor spatial density and ganglion cell morphology in the retina of human, macaque monkey, cat, and the marmoset Callithrix jacchus. *J Comp Neurol* 366: 55-75.

Gouras P, (1974). Opponent-colour cells in different layers of foveal striate cortex. *J Physiol* 238: 583-602.

Graham N, (1977). Visual detection of aperiodic spatial stimuli by probability summation among narrowband channels. *Vision Res* 17: 637-652.

Green DM, and Swets JA, (1966). *Signal detection theory and psychophysics*. New York: Wiley.

Hafed ZM, Clark JJ, (2002). Microsaccades as an overt measure of covert attention shifts. *Vision Res* 42: 2533-2545.

Hafed ZM, Goffart L, Krauzlis RJ, (2009). A neural mechanism for microsaccade generation in the primate superior colliculus. *Science* 323: 940-943.

Hafed ZM, Krauzlis RJ, (2010). Microsaccadic suppression of visual bursts in the primate superior colliculus. *J Neurosci* 30: 9542-9547.

Hall N, Colby C, (2013). Psychophysical definition of S-cone stimuli in the macaque. *J Vis* 13: .

Hanazawa A, Komatsu H, Murakami I, (2000). Neural selectivity for hue and saturation of colour in the primary visual cortex of the monkey. *Eur J Neurosci* 12: 1753-1763.

Hansen T, Gegenfurtner KR, (2006). Higher level chromatic mechanisms for image segmentation. *J Vis* 6: 239-259.

Han X, Xian SX, Moore T, (2009). Dynamic sensitivity of area V4 neurons during saccade preparation. *Proc Natl Acad Sci U S A* 106: 13046-13051.

Harwerth RS, Smith EL, DeSantis L, (1993). Behavioral perimetry in monkeys. *Invest Ophthalmol Vis Sci* 34: 31-40.

Hass C, Horwitz G, (2010). Chromatic Detection in Non-Human Primates: Neurophysiology and Comparison with Human Chromatic Sensitivity. *J Vis* 10: 937-937.

Hass CA, Horwitz GD, (2013). V1 mechanisms underlying chromatic contrast detection. *J Neurophysiol* 109: 2483-2494.

Hawken MJ, Parker AJ, (1990). Detection and discrimination mechanisms in the striate cortex of the old-world monkey. *Vision: Coding and efficiency* 103-116.

Heeger DJ, (1992). Half-squaring in responses of cat striate cells. *Vis Neurosci* 9: 427-443.

Helmholtz HV, (1852). LXXXI. On the theory of compound colours. *Philosophical Magazine Series 4* 4: 519-534.

Hendry SH, Reid RC, (2000). The koniocellular pathway in primate vision. *Annu Rev Neurosci* 23: 127-153.

Hendry SH, Yoshioka T, (1994). A neurochemically distinct third channel in the macaque dorsal lateral geniculate nucleus. *Science* 264: 575-577.

Henry CA, Joshi S, Xing D, Shapley RM, Hawken MJ, (2013). Functional Characterization of the Extraclassical Receptive Field in Macaque V1: Contrast, Orientation, and Temporal Dynamics. *The Journal of Neuroscience* 33: 6230-6242.

Herrington TM, Masse NY, Hachmeh KJ, Smith JET, Assad JA, Cook EP, (2009). The effect of microsaccades on the correlation between neural activity and behavior in middle temporal, ventral intraparietal, and lateral intraparietal areas. *J Neurosci* 29: 5793-5805.

Hornstein EP, Verweij J, Schnapf JL, (2004). Electrical coupling between red and green cones in primate retina. *Nat Neurosci* 7: 745-750.

Horowitz TS, Fine EM, Fencsik DE, Yurgenson S, Wolfe JM, (2007). Fixational eye movements are not an index of covert attention. *Psychological Science* 18: 356-363.

Horwitz GD, Albright TD, (2003). Short-latency fixational saccades induced by luminance increments. *J Neurophysiol* 90: 1333-1339.

Horwitz GD, Chichilnisky EJ, Albright TD, (2005). Blue-Yellow Signals Are Enhanced by Spatiotemporal Luminance Contrast in Macaque V1. *J Neurophysiol* 93: 2263-2278.

Horwitz GD, Chichilnisky EJ, Albright TD, (2007). Cone inputs to simple and complex cells in V1 of awake macaque. *J Neurophysiol* 97: 3070-3081.

Horwitz GD, Hass CA, (2011). Misestimates of preretinal filters can manifest as spurious S-cone signals in LM non-opponent macaque V1 neurons. *Program No. 799.12. 2011 Neuroscience Meeting Planner. Wasington. DC: Society For Neuroscience* .

Horwitz GD, Hass CA, (2012). Nonlinear analysis of macaque V1 color tuning reveals cardinal directions for cortical color processing. *Nat Neurosci* .

Hubel DH, Livingstone MS, (1990). Color and contrast sensitivity in the lateral geniculate body and primary visual cortex of the macaque monkey. *J Neurosci* 10: 2223-2237.

Hubel DH, Wiesel TN, (1962). Receptive fields, binocular interaction and functional architecture in the cat's visual cortex. *Journal of Physiology* 160: 106-154.

Hubel DH, Wiesel TN, (1968). Receptive fields and functional architecture of monkey striate cortex. *J Physiol* 195: 215-243.

Jacobs GH, Deegan JF, (1999). Uniformity of colour vision in Old World monkeys. *Proceedings of the Royal Society of London. Series B: Biological Sciences* 266: 2023-2028.

Jameson D, Hurvich LM, (1955). Some quantitative aspects of an opponent-colors theory. I. Chromatic responses and spectral saturation. *JOSA* 45: 546-552.

Johnson EN, Hawken MJ, Shapley R, (2001). The spatial transformation of color in the primary visual cortex of the macaque monkey. *Nat Neurosci* 4: 409-416.

Johnson EN, Hawken MJ, Shapley R, (2004). Cone Inputs in Macaque Primary Visual Cortex. *J Neurophysiol* 91: 2501-2514.

Johnson EN, Hawken MJ, Shapley R, (2008). The Orientation Selectivity of Color-Responsive Neurons in Macaque V1. *The Journal of Neuroscience* 28: 8096-8106.

Judge SJ, Richmond BJ, Chu FC, (1980). Implantation of magnetic search coils for measurement of eye position: an improved method. *Vision Res* 20: 535-538.

Kaas JH, Huerta MF, Weber JT, Harting JK, (1978). Patterns of retinal terminations and laminar organization of the lateral geniculate nucleus of primates. *Journal of Comparative Neurology* 182: 517-553.

Kagan I, Gur M, Snodderly DM, (2008). Saccades and drifts differentially modulate neuronal activity in V1: effects of retinal image motion, position, and extraretinal influences. *J Vis* 8: 19.1-1925.

Kang IK, Maunsell JM, (2012). Potential confounds in estimating trial-to-trial correlations between neuronal response and behavior using choice probabilities. *J Neurophysiol* .

Katz M, and Kruger PB, (1994). The human eye as an optical system, In: *Duane's Clinical Ophthalmology*. J.B. Lippincott Co..

Kelly DH, (1974). Spatio-temporal frequency characteristics of color-vision mechanisms. *JOSA* 64: 983-990.

Kelly DH, (1990). Moving gratings and microsaccades. *J Opt Soc Am A* 7: 2237-2244.

Kelly DH, van Norren D, (1977). Two-band model of heterochromatic flicker. *J Opt Soc Am* 67: 1081-1091.

Kleiser R, Seitz RJ, Krekelberg B, (2004). Neural correlates of saccadic suppression in humans. *Curr Biol* 14: 386-390.

Koenig D, Hofer H, (2011). The absolute threshold of cone vision. *J Vis* 11(1): 1-24 .

Krauskopf J, Farell B, (1990). Influence of colour on the perception of coherent motion. *Nature* 348: 328-331.

Krauskopf J, Gegenfurtner K, (1992). Color discrimination and adaptation. *Vision Res* 32: 2165-2175.

Krauskopf J, Graf V, Gaarder K, (1966). Lack of inhibition during involuntary saccades. *The American Journal of Psychology* 79: 73-81.

Krauskopf J, Williams DR, Heeley DW, (1982). Cardinal directions of color space. *Vision Res* 22: 1123-1131.

Krauskopf J, Williams DR, Mandler MB, Brown AM, (1986). Higher order color mechanisms. *Vision Res* 26: 23-32.

Krauskopf J, Wu HJ, Farell B, (1996). Coherence, cardinal directions and higher-order mechanisms. *Vision Res* 36: 1235-1245.

Lapuerta P, Schein SJ, (1995). A four-surface schematic eye of macaque monkey obtained by an optical method. *Vision Res* 35: 2245-2254.

LeGrand Y, (1949). Les seuils différentiels de couleurs dans la théorie de Young. *Revue d'Optique* 28: 261-278.

Lennie P, Krauskopf J, Sclar G, (1990). Chromatic Mechanisms in Striate Cortex of Macaque. *The Journal of Neuroscience* 10: 649-669.

Leon-Garcia A, (1994). *Probability and random processes for electrical engineering*. Addison-Wesley Reading.

Leopold DA, Logothetis NK, (1998). Microsaccades differentially modulate neural activity in the striate and extrastriate visual cortex. *Exp Brain Res* 123: 341-345.

Livingstone MS, Hubel DH, (1984). Anatomy and physiology of a color system in the primate visual cortex. *The Journal of neuroscience* 4: 309.

Livingstone MS, Hubel DH, (1988). Segregation of form, color, movement, and depth: anatomy, physiology, and perception. *Science* 240: 740-749.

Losada MA, Mullen KT, (1994). The spatial tuning of chromatic mechanisms identified by simultaneous masking. *Vision Res* 34: 331-341.

Malpeli JG, Schiller PH, Colby CL, (1981). Response properties of single cells in monkey striate cortex during reversible inactivation of individual lateral geniculate laminae. *J Neurophysiol* 46: 1102-1119.

Marimont DM, Wandell BA, (1994). Matching color images: the effects of axial chromatic aberration. *J Opt Soc Am A* 11: 3113 - 3122.

Martinez-Conde S, Macknik SL, Hubel DH, (2000). Microsaccadic eye movements and firing of single cells in the striate cortex of macaque monkeys. *Nat Neurosci* 3: 251-258.

Martinez-Conde S, Macknik SL, Troncoso XG, Dyar TA, (2006). Microsaccades counteract visual fading during fixation. *Neuron* 49: 297-305.

Martin PR, White AJR, Goodchild AK, Wilder HD, Sefton AE, (1997). Evidence that Blue-on Cells are Part of the Third Geniculocortical Pathway in Primates. *European Journal of Neuroscience* 9: 1536-1541.

Matin E, (1974). Saccadic suppression: a review and an analysis. *Psychol Bull* 81: 899-917.

Maxwell JC, (1860). On the Theory of Compound Colours, and the Relations of the Colours of the Spectrum. *Philosophical Transactions of the Royal Society of London* 150: 57-84.

McCullagh P, and Nelder JA, (1989). *Generalized linear models*. Boca Raton, FL: Chapman & Hall/CRC.

Mohler CW, Cechner R, (1975). Saccadic suppression in the monkey. *Vision Res* 15: 1157-1160.

Motokawa K, Taira N, Okuda J, (1962). Spectral responses of single units in the primate visual cortex. *The Tohoku journal of experimental medicine* 78: 320.

Movshon JA, Thompson ID, Tolhurst DJ, (1978a). Receptive Field Organization of Complex Cells in the Cat's Striate Cortex. *Journal of Physiology* 283: 79-99.

Movshon JA, Thompson ID, Tolhurst DJ, (1978b). Spatial Summation in the Receptive Fields of Simple Cells in the Cat's Striate Cortex. *Journal of Physiology* 283: 53-77.

Mullen KT, (1985). The contrast sensitivity of human colour vision to red-green and blue-yellow chromatic gratings. *J Physiol* 359: 381-400.

Mullen KT, Kingdom FA, (1996). Losses in peripheral colour sensitivity predicted from "hit and miss" post-receptoral cone connections. *Vision Res* 36: 1995-2000.

Mullen KT, Kingdom FA, (2002). Differential distributions of red--green and blue--yellow cone opponency across the visual field. *Vis Neurosci* 19: 109-118.

Mullen KT, Kulikowski JJ, (1990). Wavelength discrimination at detection threshold. *J Opt Soc Am A* 7: 733-742.

Mullen KT, Losada MA, (1999). The spatial tuning of color and luminance peripheral vision measured with notch filtered noise masking. *Vision Res* 39: 721-731.

Nagy AL, Eskew RTJ, Boynton RM, (1987). Analysis of color-matching ellipses in a cone-excitation space. *J Opt Soc Am A* 4: 756-768.

Newton JR, Eskew RT, (2003). Chromatic detection and discrimination in the periphery: a postreceptoral loss of color sensitivity. *Vis Neurosci* 20: 511-521.

Nienborg H, Cumming BG, (2006). Macaque V2 neurons, but not V1 neurons, show choice-related activity. *J Neurosci* 26: 9567-9578.

Nienborg H, Cumming BG, (2009). Decision-related activity in sensory neurons reflects more than a neuron's causal effect. *Nature* 459: 89-92.

O'Keefe LP, Levitt JB, Kiper DC, Shapley RM, Movshon JA, (1998). Functional organization of owl monkey lateral geniculate nucleus and visual cortex. *J Neurophysiol* 80: 594-609.

Packer O, Hendrickson AE, Curcio CA, (1989). Photoreceptor topography of the retina in the adult pigtail macaque (Macaca nemestrina). *J Comp Neurol* 288: 165-183.

Palmer C, Cheng S-Y, Seidemann E, (2007). Linking Neuronal and Behavioral Performance in a Reaction-Time Visual Detection Task. *The Journal of Neuroscience* 27: 8122 - 8137.

Parker AJ, Newsome WT, (1998). Sense and the single neuron: probing the physiology of perception. *Annu Rev Neurosci* 21: 227-277.

Poirson AB, Wandell BA, Varner DC, Brainard DH, (1990). Surface characterizations of color thresholds. *J Opt Soc Am A* 7: 783-789.

Qiao-Grider Y, Hung LF, Kee CS, Ramamirtham R, Smith EL, (2007). Normal ocular development in young rhesus monkeys (Macaca mulatta). *Vision Res* 47: 1424-1444.

Ramcharan EJ, Gnadt JW, Sherman SM, (2001). The effects of saccadic eye movements on the activity of geniculate relay neurons in the monkey. *Vis Neurosci* 18: 253-258.

Reid RC, Shapley RM, (2002). Space and time maps of cone photoreceptor signals in macaque lateral geniculate nucleus. *J Neurosci* 22: 6158-6175.

Reppas JB, Usrey WM, Reid RC, (2002). Saccadic eye movements modulate visual responses in the lateral geniculate nucleus. *Neuron* 35: 961-974.

Riggs LA, Ratliff F, Cornsweet JC, Cornsweet TN, (1953). The disappearance of steadily fixated visual test objects. *J Opt Soc Am* 43: 495-501.

Rinberg D, Koulakov A, Gelperin A, (2006). Speed-Accuracy Tradeoff in Olfaction. *Neuron* 51: 351 - 358.

Rolfs M, (2009). Microsaccades: small steps on a long way. *Vision Res* 49: 2415-2441.

Rolfs M, Kliegl R, Engbert R, (2008). Toward a model of microsaccade generation: the case of microsaccadic inhibition. *J Vis* 8: 5.1-523.

Rollman GB, Nachmias J, (1972). Simultaneous detection and recognition of chromatic flashes. *Perception and Psychophysics* 12: 309-314.

Romo R, Hernández A, Zainos A, Lemus L, Brody CD, (2002). Neuronal correlates of decision-making in secondary somatosensory cortex. *Nat Neurosci* 5: 1217-1225.

Royal DW, Sáry G, Schall JD, Casagrande VA, (2006). Correlates of motor planning and postsaccadic fixation in the macaque monkey lateral geniculate nucleus. *Exp Brain Res* 168: 62-75.

Rucci M, Desbordes G, (2003). Contributions of fixational eye movements to the discrimination of briefly presented stimuli. *J Vis* 3: 852-864.

Rule M, Stoffregen M, Ermentrout B, (2011). A model for the origin and properties of flicker-induced geometric phosphenes. *PLoS computational biology* 7: e1002158.

Rushton WA, (1972). Pigments and signals in colour vision. *J Physiol* 220: 1P-1P.

Rust NC, Schwartz O, Movshon JA, Simoncelli EP, (2005). Spatiotemporal elements of macaque v1 receptive fields. *Neuron* 46: 945-956.

Sachs MB, Nachmias J, Robson JG, (1971). Spatial-frequency channels in human vision. *J Opt Soc Am* 61: 1176-1186.

Sankeralli MJ, Mullen KM, (1996). Estimation of the L-, M-, and S-cone weights of the postreceptoral detection mechanisms. *J Opt Soc Am A* 13: 906-915.

Sankeralli MJ, Mullen KT, (1997). Postreceptoral chromatic detection mechanisms revealed by noise masking in three-dimensional cone contrast space. *J Opt Soc Am A Opt Image Sci Vis* 14: 2633-2646.

Schiller PH, Malpeli JG, (1978). Functional specificity of lateral geniculate nucleus laminae of the rhesus monkey. *J Neurophysiol* 41: 788-797.

Schnapf JL, Kraft TW, Baylor DA, (1987). Spectral sensitivity of human cone photoreceptors. .

Schnapf JL, Nunn BJ, Meister M, Baylor DA, (1990). Visual transduction in cones of the monkey Macaca fascicularis. *J Physiol* 427: 681-713.

Schneeweis DM, Schnapf JL, (1999). The photovoltage of macaque cone photoreceptors: adaptation, noise, and kinetics. *The Journal of neuroscience* 19: 1203-1216.

Schütz AC, Braun DI, Gegenfurtner KR, (2007). Contrast sensitivity during the initiation of smooth pursuit eye movements. *Vision Res* 47: 2767-2777.

Shadlen MN, Britten KH, Newsome WT, Movshon JA, (1996). A Computational Analysis of the Relationship between Neuronal and Behavioral Responses to Visual Motion. *The Journal of Neuroscience* 16: 1486-1510.

Shushruth S, Mangapathy P, Ichida JM, Bressloff PC, Schwabe L, Angelucci A, (2012). Strong recurrent networks compute the orientation tuning of surround modulation in the primate primary visual cortex. *The Journal of Neuroscience* 32: 308-321.

Sigel C, Pugh Jr EN, (1980). Stiles"s W_5 color mechanism: Tests of field displacement and field additivity properties. *JOSA* 70: 71-81.

Smith VC, Pokorny J, (1975). Spectral sensitivity of the foveal cone photopigments between 400 and 500 nm. *Vision Res* 15: 161-171.

Snodderly DM, Auran JD, Delori FC, (1984). The macular pigment. II. Spatial distribution in primate retinas. *Invest Ophthalmol Vis Sci* 25: 674-685.

Snodderly DM, Kagan I, Gur M, (2001). Selective activation of visual cortex neurons by fixational eye movements: implications for neural coding. *Vis Neurosci* 18: 259-277.

Solomon SG, Lennie P, (2005). Chromatic Gain Controls in Visual Cortical Neurons. *The Journal of Neuroscience* 25: 4779-4792.

Solomon SG, Peirce JW, Dhruv NT, Lennie P, (2004a). Profound contrast adaptation early in the visual pathway. *Neuron* 42: 155-162.

Solomon SG, Peirce JW, Lennie P, (2004b). The impact of suppressive surrounds on chromatic properties of cortical neurons. *J Neurosci* 24: 148-160.

Soltani A, Wang X-J, (2009). Synaptic computation underlying probabilistic inference. *Nat Neurosci* 13: 112-119.

Stockman A, and Brainard DH, (2009). Color Vision Mechanims, In: *The Optical Society Of America Handbook Of Optics*, edited by Bass M, DeCusatis C, Enoch J, Lakshminarayanan V, Li G, Macdonald C, Mahajan V, and Stryland EV. New York: McGraw Hill.

Stockman A, MacLeod DI, Johnson NE, (1993). Spectral sensitivities of the human cones. *J Opt Soc Am A Opt Image Sci Vis* 10: 2491-2521.

Stoughton CM, Conway BR, (2008). Neural basis for unique hues. *Curr Biol* 18: R698-R699.

Stoughton CM, Lafer-Sousa R, Gagin G, Conway BR, (2012). Psychophysical chromatic mechanisms in macaque monkey. *J Neurosci* 32: 15216-15226.

Sun H, Smithson HE, Zaidi Q, Lee BB, (2006). Specificity of cone inputs to macaque retinal ganglion cells. *J Neurophysiol* 95: 837-849.

Svaetichin G, (1956). Spectral response curves from single cones. *Acta physiologica Scandinavica. Supplementum* 39: 17.

Swanson WH, Ueno T, Smith VC, Pokorny J, (1987). Temporal modulation sensitivity and pulse-detection thresholds for chromatic and luminance perturbations. *J Opt Soc Am A* 4: 1992-2005.

Tailby C, Solomon SG, Dhruv NT, Lennie P, (2008a). Habituation reveals fundamental chromatic mechanisms in striate cortex of macaque. *J Neurosci* 28: 1131-1139.

Tailby C, Solomon SG, Lennie P, (2008b). Functional asymmetries in visual pathways carrying S-cone signals in macaque. *J Neurosci* 28: 4078-4087.

Tolhurst DJ, Movshon JA, Dean AF, (1983). The statistical reliability of signals in single neurons in cat and monkey visual cortex. *Vision Res* 23: 775-785.

Touryan J, Lau B, Dan Y, (2002). Isolation of Relevant Visual Features from Random Stimuli for Cortical Complex Cells. *The Journal of Neuroscience* 22: 10811-10818.

Ts'o DY, Gilbert CD, (1988). The organization of chromatic and spatial interactions in the primate striate cortex. *J Neurosci* 8: 1712-1727.

Uchikawa K, Sato M, (1995). Saccadic suppression of achromatic and chromatic responses measured by increment-threshold spectral sensitivity. *J Opt Soc Am A Opt Image Sci Vis* 12: 661-666.

Van Norren D, (1972). Macaque lens absorption in vivo. *Invest Ophthalmol Vis Sci* 11: 177-181.

Verweij J, Hornstein EP, Schnapf JL, (2003). Surround antagonism in macaque cone photoreceptors. *The Journal of neuroscience* 23: 10249-10257.

Volkmann FC, Riggs LA, White KD, Moore RK, (1978). Contrast sensitivity during saccadic eye movements. *Vision Res* 18: 1193-1199.

Vos JJ, Walraven PL, (1971). On the derivation of the foveal receptor primaries. *Vision Res* 11: 799-818.

Wandell BA, (1985). Color measurement and discrimination. *J Opt Soc Am A* 2: 62-71.

Watson AB, Pelli DG, (1983). QUEST: a Bayesian adaptive psychometric method. *Percept Psychophys* 33: 113-120.

Webster MA, De Valois KK, Switkes E, (1990). Orientation and spatial-frequency discrimination for luminance and chromatic gratings. *J Opt Soc Am A* 7: 1034-1049.

Webster MA, Mollon JD, (1994). The influence of contrast adaptation on color appearance. *Vision Res* 34: 1993-2020.

White BJ, Boehnke SE, Marino RA, Itti L, Munoz DP, (2009). Color-related signals in the primate superior colliculus. *J Neurosci* 29: 12159-12166.

Whittle P, Challands PDC, (1969). The effect of background luminance on the brightness of flashes. *Vision Res* 9: 1095-1110.

Wiesel TN, Hubel DH, (1966). Spatial and chromatic interactions in the lateral geniculate body of the rhesus monkey. *J Neurophysiol* 29: 1115-1156.

Winterson BJ, Collewijn H, (1976). Microsaccades during finely guided visuomotor tasks. *Vision Res* 16: 1387-1390.

Wooten BR, Hammond BR, (2005). Spectral absorbance and spatial distribution of macular pigment using heterochromatic flicker photometry. *Optometry & Vision Science* 82: 378-386.

Wright TM, Calabrese RL, (2011). Patterns of presynaptic activity and synaptic strength interact to produce motor output. *The Journal of Neuroscience* 31: 17555-17571.

Wuerger SM, Atkinson P, Cropper S, (2005). The cone inputs to the unique-hue mechanisms. *Vision Res* 45: 3210-3223.

Wyszecki G, and Stiles WS, (1982). *Color science*. Wiley New York.

Yang T, Shadlen MN, (2007). Probabilistic reasoning by neurons. *Nature* 447: 1075-1080.

Yoshioka T, Dow BM, (1996). Color, orientation and cytochrome oxidase reactivity in areas V1, V2 and V4 of macaque monkey visual cortex. *Behav Brain Res* 76: 71-88.

Young T, (1802). The Bakerian lecture: On the theory of light and colours. *Philosophical transactions of the Royal Society of London* 92: 12-48.

Zeki S, (1983). The distribution of wavelength and orientation selective cells in different areas of monkey visual cortex. *Proceedings of the Royal Society of London. Series B. Biological Sciences* 217: 449-470.

Zuber BL, Stark L, (1966). Saccadic suppression: elevation of visual threshold associated with saccadic eye movements. *Exp Neurol* 16: 65-79.

Zuber BL, Stark L, Cook G, (1965). Microsaccades and the velocity-amplitude relationship for saccadic eye movements. *Science* 150: 1459-1460.